Role of Magnesium on Mineralization and Periosteal Differentiation

by

Dandan Hong

BS Bioengineering, University of Pittsburgh, 2010

Submitted to the Graduate Faculty of

Swanson School of Engineering in partial fulfillment

of the requirements for the degree of

Doctor of Philosophy

University of Pittsburgh

2019

UNIVERSITY OF PITTSBURGH

SWANSON SCHOOL OF ENGINEERING

This dissertation was presented

by

Dandan Hong

It was defended on

April 15, 2019

and approved by

Elia Beniash, Ph.D., Professor
Department of Oral Biology

Tracy Cui, Ph.D., Professor
Department of Bioengineering

Frank Witte, MD, PhD, Professor
Julius Wolff Institute for Biomechanics and Musculoskeletal Regeneration
Charité Universitätsmedizin Berlin

Dissertation Director: Charles Sfeir, DDS, PhD, Associate Dean for Research
Department of Periodontics and Preventive Dentistry

Role of Magnesium on Mineralization and Periosteal Differentiation

Dandan Hong, PhD

University of Pittsburgh, 2019

Magnesium-based alloys have been fabricated into implants including the orthopedic fixation devices and endovascular stents. These metals not only fulfill the mechanical requirement in load bearing applications, they also degrade safely upon tissue healing. Their biocompatibility and osteoinductive potential have been evaluated in numerous studies. Our present study covers two topics involving magnesium, investigating 1) its osteogenic effect on periosteum and 2) surface mineralization triggered by its degradation process.

Our previous work showed that implantation of a magnesium-based device was associated with subperiosteal bone regeneration. In the present study, we harvested mouse and human periosteal cells, and exposed them to increased Mg^{2+} concentration. We found that the expression of osteogenic genes and proteins was cell- and concentration-dependent. We then electrospan magnesium metal nanopowder into PLGA nanofibers, and implanted in female and male rat calvaria defect with or without periosteum for one month. MicroCT and histology analyses showed greater new bone volume in magnesium+ periosteum group.

Magnesium degradation triggers calcium phosphate deposition on the metal surface. The mineral layer can potentially lead to ectopic calcification if the metal device is implanted in the soft tissue. We tested the feasibility of matrix Gla protein (MGP) to locally inhibit the mineralization. A secretory protein, MGP was shown to inhibit soft tissue calcification, especially in the vascular environment. To begin, we transfected MGP into mammalian cells, then exposed magnesium metals in medium containing MGP secreted by transfected cells. Results showed that

significantly less minerals were deposited on metal surface when MGP was present. We then implanted magnesium rod, embedded in collagen scaffold seeded with stably transfected cells, intramuscularly in mouse. Analyses supported our in vitro results. Moreover, higher magnesium corrosion rate was observed from MGP group, indicating a protective role of the mineral layer.

The present study proves the direct osteogenic effect of Mg^{2+} on periosteal cells, and demonstrates the efficacy of a biomolecule to reduce mineralization on magnesium surface. Taken together, these findings suggest therapeutic potential of Mg-releasing scaffolds for cranial injury repair, and open a frontier for the design of medical devices.

Table of Contents

List of Tables

List of Figures

Preface

This dissertation is dedicated to my mother (Dr. Lili Zhang), whom kept ensuring me that I will graduate someday since I have doubted about that constantly, and my loving family and lovely friends, whom pushed me to hang on just a little more every time when the tunnel of graduation seemed to be endless. Special thanks to the animals whom sacrificed their lives for me. The animals have always sacrificed for the human advancement today.

All work presented in this dissertation would never have been possible without the support of countless individuals. Especially, I would like to thank Dr. Elia Beniash and Dr. Tracy Cui for their continuous guidance to move my project forward and make my graduation possible. Great thanks to every member in the Center for Craniofacial Regeneration. We have always been and will always be a big warm family that take care of each other. Many thanks to the National Science Foundation for funding this project. Funding is what we cannot live without in the research world. Finally, I would like to thank and give a huge hug to Dr. Frank Witte (Danke Schön) and Dr. Charles Sfeir (Merci beaucoup), whom brought me to the world of graduate school and have never given up on me when my preliminary exam was a disaster and the data just pieces of baffling mystery. You have been truly wonderful mentors, the lighthouse in the tunnel. Thank you for bringing me all the happy memories in the graduate school. I will remember your jolly laughter forever.

Please do not wake me up even if this dissertation is just a dream.

1.0 Introduction

1.1 Degradable Materials for Biomedical Implants

The global implant market continues to grow in concordance with a large demand, primarily due to a growing geriatric population and advanced technology. According to a report from the consulting firm the Global Market Insights, in 2016, global orthopedic device market was valued around $40 billion, and is expected to reach $53 billion by 2024. In addition, global cardiovascular device market has reached $33 billion in 2015, and estimated to reach $69.3 billion by 2023. Market demands usually create enthusiastic researchers to satisfy the public needs. Traditionally, implants are fabricated from bioinert materials, such as titanium, stainless steel, or cobalt-chromium based alloys [1-5]. These materials are supposed to remain permanently in the body and interact minimally with the surrounding tissue. However, years of clinical applications using devices made of these materials have shown many limitations. Due to wear and fatigue, toxic metallic particles may be detached from the whole device, which may start an inflammatory cascade and cause further tissue damage [6-10]. For an orthopedic device, the mechanical properties, such as the density and elastic moduli, of these materials are much higher compared to the natural bone, bringing higher risk for stress shielding, which can lead to reduction in bone density and osteoporosis [11]. Metallic implants interfere with imaging modalities such as x-ray and MRI [12], so an additional invasive surgery will be followed to remove the implant, which not only increases the healthcare cost, but also decreases patients' welfare and quality of life [13]. Therefore, a new generation of implant material has emerged: replacing the functions of the traditional implant materials, and more advanced in solving the existing problems, with the

characteristics of biodegradability and biocompatibility. One of such materials is the magnesium (Mg) and its alloys.

The first attempt to use Mg as an implant material happened in 1878, when physician Huse took a Mg wire to stop a bleeding vessel in human patient [14, 15]. However, not until the late 1960s, Kulkarni and colleagues introduced the concept of biodegradable implants [16]. Biodegradable implants can be categorized into degradable metals and polymers.

1.1.1 Degradable Metals

One major advantage for using metals to fabricate degradable implants is the strength, which is strong enough for load bearing applications. Degradable metals that are currently being studied the most as implantable materials included magnesium (Mg) and iron (Fe) alloys. In recently years, some research groups have also started to investigate the use of strontium (Sr) as biomaterials [17-20]. A recent study by Naruphontjirakul and colleagues have shown that Sr released from nanoparticles were able to stimulate the differentiation of human bone marrow derived stem cells towards an osteogenic pathway [21]. This finding may attract more researchers to study Sr as a biomaterial for orthopedic application.

Fe and its alloys have similar mechanical properties as stainless steel [22]. Fe degradation in the body is very slow [23, 24]. A study found that the alloy remained intact for more than 12 months in contact with blood *in vivo*, which caused a similar reaction as those from permanent metal implants [25, 26]. Moreover, a large volume of its degradation product, iron oxide, is usually remained in the body and may not be safely metabolized [27]. Due to its ferromagnetism, Fe also interferes with radiological imaging [25]. Material modification, such as alloying and heat treatment, has been common to improve the properties of Fe-based materials [28]. Despite the

efforts in improving their properties, still much are to be done to prepare Fe-based materials to meet the requirements for clinical trials.

In the present dissertation, we will focus our attention on Mg. Because of its advantages over other materials, Mg has been fabricated into bone plates, screws, and pins to stabilize the fracture sites [29-31]. On the other hand, Mg also has been made into devices to be implanted in soft tissues [32-35]. The cardiovascular stent “Magmaris”, made of Mg alloy WE43, has received its CE mark in 2016 and is now commercially available [36]. Advantages of using biodegradable Mg alloys as cardiovascular stent materials will be introduced in more details at the later section.

1.1.2 Degradable Polymers

Some polymers have also been used for biomedical implant applications for many years. Both synthetic or natural polymers degrade by the process of either hydrolysis or enzymatic reactions [37]. Polyglycolide (PGA) was the first synthetic biodegradable polymer used in the field of biomedical devices. It was fabricated into surgical sutures, known under the tradename Dexon. As the need for temporary implantable scaffold increased, PGA was further produced into orthopedic rings, screws, and plates [38].

Poly-L-lactic acid (PLLA) is also a biodegradable and biocompatible polymer that is often used as a biomaterial. It has been approved by the FDA on 2004 as an injectable material for cosmetic enhancement [39]. After which, the research on PLLA has been extended to screws, plate, pins, and soft tissue implants, including the endovascular stents [40]. Stents made of PLLA fulfill the mechanical need to support the vessel temporarily before healing. However, there are still problems associated with PLLA. For example, a two-year clinical trial of a commercially available absorbable polymeric stent observed multiple adverse events, with a high rate of device

thrombosis and target vessel-related myocardial infarction [41]. Ultimately, this polymer stent was retracted from the market and under FDA investigation. The adverse outcomes associated with absorbable polymer stents are thought to be due to the fact that these stents require an increased strut thickness to compensate for weaker radial force. During absorption, polymer can induce an inflammatory response which then can lead to severe intimal hyperplasia [42].

Poly (lactic-co-glycolic acid), or PLGA, is another commonly used synthetic polymer in the biomedical field. Not only its degradation rate and mechanical properties can be easily tuned by selecting its molecular weight and the ratio between polylactide and polyglycolide, this material has been approved by the FDA to be used in human [43]. Its degradation byproducts, polylactic acid and polyglycolic acid, could be metabolized and eliminated from body as carbon dioxide and water. Similar to PGA, PLGA was also developed into surgical suture in 1974, known under the tradename Vicryl. In recent years, PLGA has been studied extensively for drug delivery purpose [44]. They are made into micro- or nano-particles and fibers, or coated outside of another device, for the controlled release of vaccines, antibiotics, proteins, RNAs, DNAs, etc. Some groups have also made PLGA into stents to scaffold the soft tissue [45], as well as composited PLGA with other materials, such as ceramics and metals, for the fabrication of orthopedic devices to be used in bones and cartilage [46-49].

As the most abundant protein in the human body, collagen is a natural degradable polymer that has long been studied as a drug carrier [50, 51], as well as used in vascular tissue engineering since it is a major ECM component in the blood vessel [44, 52-54]. Collagen can be readily modified into various shapes and sizes, such as tubes, sheets, sponges, and more, according to the needs. The density and porosity of collagen scaffold can also be easily tuned by adjusting its

concentration [55, 56]. After *in vivo* implantation, collagen is absorbed in 6-8 weeks by enzymatic degradation in the body [50, 57].

Many other degradable polymers, including polycaprolactone (PCL), polyanhydrides, polycarbonates [44, 57], have been fabricated into implants. However, comparing to degradable metals, polymers have lower strength to sustain the load bearing applications, which can lead to loading failure. Higher recoil rate often occurs when used the polymers in stent application comparing to metallic implants [58, 59]. Overall, metallic biomaterials surpass polymers in biomechanical stability [60].

1.2 Biodegradable Magnesium Based Metals

1.2.1 Basic Degradation Mechanism of Magnesium Metals

Basic degradation mechanism of Mg metals can be summarized by the three equations below.

$$Mg + H_2O -> Mg(OH)_2 + H_2 \quad [1]$$

$$Mg -> Mg^{2+} + 2e^- \quad [2]$$

$$2H_2O + 2e^- -> H_2 + 2OH^- \quad [3]$$

According to equation 1, the overall degradation chemical reactions produces magnesium hydroxide and hydrogen gas after magnesium reacts with water. This overall reaction can be further broken down into anodic and cathodic reactions. As shown in equation 2, the anodic dissolution increases the Mg ions and electrons in the solution. The cathodic reaction (equation 3) reduces the water to give out hydrogen gas and hydroxyl ions, which causes the increase in pH

locally on the metal surface and creates corrosion pits [61, 62]. Such localized alkalization attracts calcium and phosphate that are saturated in the biological solution to deposit onto the undissolved magnesium hydroxide layer [25, 63]. The formation of gas cavities after Mg implantation has been widely reported in literatures [63-65]. Many have assumed that those are the degradation product, hydrogen gas, accumulating around the Mg implant, thus creating concerns that it may cause disintegration between implant and tissues. However, new study by Kuhlmann and colleagues has demonstrated that these gas pockets contained only low concentrations of hydrogen gas, concluding that hydrogen gas is rapidly exchanged though skin and/or accumulates in fatty tissues *in vivo* [66, 67].

1.2.2 Advantages of Magnesium-based Alloys as Biomaterials

Mg has been identified as the fourth most abundant cation and the second most abundant intracellular divalent cation in the human body. Mg is so ubiquitous and essential that it involves in almost all metabolic pathways and acts as enzyme cofactors in more than 300 biochemical reactions in the body [68, 69]. It participates in generating the energy-rich ATP and stabilizes DNA and RNA structures [70]. Over the last two decades, Mg and its alloys have been studied as a biomaterial for the fabrication of biomedical implants, such as bone fixation devices (screws and plates) and cardiovascular stents [6, 31, 34, 35, 60, 71-73]. Numerous studies have also confirmed that Mg is biocompatible and non-toxic to the physiological environment [15, 32, 74-76]. The case of hypermagnesemia is very rare under normal physiological condition unless the patients undergoes renal failure, since extra Mg is usually efficiently excreted through the urine [77].

According to the degradation mechanism mentioned previously, Mg starts to degrade once in contact with water, which means that its absorption by the host begins once being implanted

and touching the body fluid. At the end of the metal degradation process, the treated tissues are healed, and the implant is gone. Such biodegradability of this new generation of biomaterial has been the major applauding advantage over traditional permanent materials, which, in the case of cardiovascular stents, caused in-stent restenosis, late stent thrombosis, and chronic inflammation thus the need for prolonged anti-platelet therapy [32, 33]. Implantation for pediatric population would demand an implant removal surgery so the implant would not interfere with the child's development. Ideally, the implant would maintain its mechanical integrity during which the injured tissues are supported, then disappear without a trace after tissues heal. This requires careful tailoring and modifying the material so that its corrosion rate can be controlled accordingly. The most common methods of adjustment include alloying Mg with other elements and surface modification such as coating [58].

Mg can be alloyed with different percentages of other elements to form Mg alloys. For example, Mg alloying with aluminum and zinc forms the alloy AZ31 (containing 3% aluminum, 1% zinc, and 96% Mg in this case). By modifying the alloying elements, properties of the Mg metals can be controlled and adjusted. Impurities such as nickel, iron, and copper within Mg accelerate the metal corrosion rate [60]. Casting 4 wt% zinc with Mg greatly increases the mechanical properties of the metal, such as the tensile strength and elongation, while reduces hydrogen evolution during degradation [78, 79]. Adding calcium and strontium refines the microstructure of the alloy and improves the metal strength [80, 81]. Alloying aluminum in Mg increases the metal corrosion resistance and strength [82, 83]. Many material scientists are developing new alloys to meet the requirements for the intended devices [84].

The density of Mg is 1.74 g/cm^3. As shown in table 1, its density nearly overlaps with the density of natural bone, which ranges between 1.8 – 2.1 g/cm^3 [6]. Compared to other commonly

used metallic materials, the differences of elastic modulus, compressive yield strength, and fracture toughness between Mg and natural bone are the smallest. Mg implant could also reduce stress shielding when used as bone implant [60]. When the stiffness, or the elastic modulus, of an implant is too high compared to the natural bone, a condition called stress shielding will likely occur. This is because that materials with higher stiffness "shield" the physiological loading that was supposed to be loaded onto the bone, leading to reduced bone density, or osteopenia, resulting in a weaker bone condition [85]. Although the mechanical properties of hydroxyapatite are also close to the natural bone, its low fracture toughness may introduce another risk of fracture to the patients.

Table 1. Comparison on physical and mechanical properties between implant materials and natural bone [6].

Properties	Natural bone	Magnesium	Ti alloy	Co–Cr alloy	Stainless steel	Synthetic hydroxyapatite
Density (g/cm^3)	1.8–2.1	1.74–2.0	4.4–4.5	8.3–9.2	7.9–8.1	3.1
Elastic modulus (Gpa)	3–20	41–45	110–117	230	189–205	73–117
Compressive yield strength (Mpa)	130–180	65–100	758–1117	450–1000	170–310	600
Fracture toughness ($MPam^{1/2}$)	3–6	15–40	55–115	N/A	50–200	0.7

Moreover, Mg was found to have antibacterial properties, which makes it an even more suitable implant material. Magnesium oxide powder has been reported to have antibacterial characteristics, although such effect was not found when dissolving in similar concentration of magnesium chloride in the solution [86]. An *in vitro* culture containing Mg metals of different weights also revealed the suppressed colony formation of three common aerobic bacterial organisms, as Mg ion concentrations and pH increased in the medium [87]. *In vivo* implantation of pure Mg and titanium nails in rat femur cavities by Li and colleagues concluded that Mg was effective in protecting bone and the surrounding tissues from infection [88].

In addition, many studies have linked Mg with osteogenesis, which has become a popular topic in recent years. Research groups worldwide have reported different findings to prove the effect of Mg ions on osteogenesis. More details can be found in the next section.

1.2.3 Osteogenesis of Magnesium Ions

When Li and colleagues were confirming the antibacterial properties of Mg metal in rat femur, they have also noticed the new bone formation from the groups implanted with Mg nails [88]. They were not alone.

99% of total body Mg are stored in bone, muscle, and non-muscular soft tissues. Within which, 50 – 60% are stored in bone [89]. Low dietary Mg intake has been associated with osteoporosis in rats [90]. When mice were fed with Mg deficient diet, femur length, strength, and volume were significantly reduced [90-93]. It is reasonable to say that Mg has an inseparable relationship with bone.

Mg ions added in culture medium have shown to stimulate the proliferation of human mesenchymal stem cells [94]. When human bone marrow stromal cells were cultured in medium containing different concentrations of Mg ions, extracellular matrix mineralization and collagen type X mRNA expression were enhanced when 10 mM of $MgSO_4$ was added. COL10A1 and VEGF gene expressions were also found to be up-regulated [95]. Moreover, Wu and colleagues have found that the activities of osteoblasts and osteoclasts are Mg concentration- dependent. 15 mM of $MgCl_2$ enhanced osteoclasts proliferation and differentiation. However, Mg extract from Mg metal with lower ion concentrations reduced cell metabolism [96, 97].

New bone formation has been observed around Mg devices implanted in different animal models. When Mg rod was implanted in rabbit femur condyle, increased bone volume in the vicinity was observed [98]. When Mg screws and plate was implanted in a rabbit ulna fracture model, not only fracture healing was observed by 8 weeks, stunning new bone regeneration was detected surrounding the degrading Mg implants by 16 weeks [30]. Witte et al have compared the bone response between Mg alloys and polymeric implant materials in the femora of guinea pigs.

Calcein green staining of the cross section of Mg rod showed large accumulation of calcium phosphate deposit on the corrosion layer and the contacting bone, and the bone mass was increased significantly compared to the control polymer implant [64]. In a recent study by Zhang and colleagues, an ultrapure Mg pin was implanted in rat distal femur. They reported not only new bone formation, but have also found that an overexpression of Calcrl and Ramp1 genes could substantially enhance Mg-induced osteogenesis [29]. They demonstrated that Mg device could induce the neuronal production of calcitonin gene-related peptide-α (CGRP) locally, which then further contributed to the bone fracture healing. Hence, the effect of Mg on osteogenesis was indirect through the stimulation of CGRP. However, our group believes that Mg could also directly induce osteogenic differentiation of periosteal cells, which further contribute to new bone growth next to Mg implant. Our results are included in the later chapter.

Many studies have also tried to understand the fundamental mechanisms relating Mg to osteogenesis, explaining from the perspective of signaling pathways, such as the Wnt and Notch. One study used different concentrations (up to 1.8 mM) of $MgCl_2$ to treat rat mesenchymal stem cells. This study found that the osteogenic differentiation of the rat MSCs was induced through activation of Notch1 signaling by Mg [99]. On the other hand, several studies using various concentrations of Mg ions supplemented in culture have observed conflicting results. Leidi and colleagues found that the mineral matrix deposition and ALP activities from normal human osteoblasts and SaOS-2 cells were inhibited by 5 mM of $MgCl_2$ in culture [100]. Lu and colleagues extracted normal human osteoblasts from bone chips of human wisdom teeth, and treated the cells with different $MgCl_2$ concentrations ranging from 1 to 16 mM. While 1 mM and 2 mM Mg supplemented in culture were able to up-regulate the gene and protein expressions, down-regulation of the same genes and proteins was observed when 8 mM and 16 mM Mg were added

in osteogenic medium. The mineral matrix formation was also inhibited [101]. Li and colleagues showed, with more comprehensive analyses including EDX, TEM, and qPCR analysis of osteogenic gene expressions, that 1 mM Mg ions ($MgCl_2$) in culture was sufficient to inhibit the mineralization of human bone marrow-derived mesenchymal stem cells [102]. By measuring mitochondrial Ca^{2+} levels, they concluded that as a Ca^{2+} antagonist, increasing Mg ions decreased Ca^{2+} accumulation in the mitochondria, hence reducing the formation of mineral vesicles and inhibiting the mineralization process. Moreover, Wnt/β-catenin pathway is usually associated with promoting bone formation. One interesting finding from Montes de Oca showed that Mg inhibits Wnt/β-catenin signaling pathway, which further reversed osteogenic transformation of vascular smooth muscle cells [103].

In general, most studies agreed that Mg promotes cellular osteogenic differentiation in a concentration-dependent manner, through in vitro cell culture and observations from in vivo implantation of Mg devices. Additional studies on basic understanding of Mg to influence osteogenesis from the molecular level should still be continuously conducted. With more solid knowledge, we could then confidently use Mg in the clinics to benefit the patients with bone-related injuries.

1.2.4 Biomedical Implants Made of Magnesium Alloys

The history of using Mg on patients can be dated back to 1878, shortly after the element was discovered in 1808. Physician Edward Huse used Mg wires as ligatures to stop vessel bleeding in patients [14]. Soon after that, due to its uncontrolled corrosion rate, Mg was no longer studied for the clinical use, but investigated primarily in the automobile industry because of its light weight and strength-to-weight ratio [83], until recently when the techniques of alloying and surface

modification have advanced to better control its corrosion rate. Mg and its alloys have been mainly researched in two areas: orthopedic and cardiovascular.

1.2.4.1 Orthopedic Devices

In the previous section, we have discussed the effect of Mg on osteogenic differentiation of different cells. Along with its mechanical properties, the osteogenic effect of Mg on the surrounding cells designated Mg a suitable biomaterial for orthopedic applications. In 1906, Lambotte stabilized a leg fracture of a 17-year-old child with Fe plate and Mg screws, and was astonished in the discovery of electrochemical reaction between the two metals [15]. More animal studies and clinical implantation in children led to the conclusion that Mg implant absorbed completely within 1 year after surgery, after the bone fracture was healed. Lambotte then proposed the use of Mg as biomaterials in almost all body areas of bone fracture, based on these successful studies [15].

Recently, our group has fabricated Mg alloys into screws and plates, and tested the implants in rabbit ulna fracture model [30, 31]. After 16 weeks, microtomography images and analyses identified a layer of new bone growth in the vicinity of Mg implant. Hu and colleagues implanted high-purity Mg screws in rabbit tibiae model for a long-term local and systemic evaluation [104]. They monitored the serum and urine Mg levels and reported no abnormal elevation. Rabbit liver and kidney functions were normal as well. After 52 weeks, they also observed new bone formation at the tissue-implant interface. A Mg ring device for injured anterior cruciate ligament (ACL) was developed by Woo and colleagues, and tested on goat. Results demonstrated that Mg ring was able to stabilize the joint and load ACL immediately after surgery [105]. Koo and colleagues tested Mg pins made of different Mg alloys in mouse subcutaneous and dog tibia models [106]. While the corrosion rate was similar in both animal models, they found that cancellous bone healed well at

the implantation site. But interestingly, cortical bone was degraded with gas pocket formation from alloy degradation. These studies confirmed the biosafety and osteoinductive potential of Mg. But in order to fabricate Mg alloys into orthopedic devices, more research needs to be conducted to tailor the Mg corrosion rate with the bone healing rate to avoid the possible early mechanical failure or adverse effect on bone regeneration.

1.2.4.2 Cardiovascular Devices

The most common cardiovascular device made of Mg alloys is the cardiovascular stent, which is a tubular mesh that expands inside an occluded vessel segment to keep the vessel open and restore blood flow. After vessel remodels and heals completely, stent is no longer needed. Permanent stents left in the body for long term was found to cause problems, such as late stent thrombosis, chronic inflammation, in-stent restenosis, and stent strut fracture [27]. Studies have shown that a stent is only necessary to provide mechanical supports for 3-6 months [107]. Therefore, a degradable stent that could satisfy the mechanical integrity and safely consumed by the host was developed.

As early as 2005, a biodegradable Mg stent was successfully implanted in the left pulmonary artery of a preterm baby [72]. Many more clinical trials have been conducted ever since [73, 108-112]. After years of study, Biotronik launched a resorbable stent made of Mg alloy backbone in 2016. It is the first clinically proven Mg stent worldwide to receive the CE mark [36, 59].

1.3 Calcium Phosphate Deposition

Many phases of calcium phosphate (CaP) exist, classified by the ratio between Ca and P (table 2). Different factors, such as temperature, pH, and environment element composition, can affect the phases of the formed CaP. Belong to the orthophosphate group, naturally occurring CaP can be found in our bone and teeth.

Table 2. List of various calcium phosphate phases [113]

Name	Formula	Ca/P ratio
Calcium phosphate dihydrate (brushite)	$CaHPO_4 \cdot 2H_2O$	1.0
Anhydrous calcium phosphate (monetite)	$CaHPO_4$	1.0
Octacalcium phosphate	$Ca_8H_2(PO_4)_6 \cdot 5H_2O$	1.33
Tricalcium phosphate (whitlockite)	$Ca_3(PO_4)_2$	1.5
Fluorapatite	$Ca_{10}(PO_4)_6F_2$	1.67
Hydroxyapatite	$Ca_{10}(PO_4)_6(OH)_2$	1.67

CaP is sometimes used as a coating on Mg alloys, to improve corrosion resistance, increase biocompatibility, and reduce wear particles from the metal [114]. Compared to other biomedical coatings like the polymers, CaP coating on Mg sparks the most interest for researchers specialized in orthopedic implant.

When Mg metal starts to degrade, in addition to an unstable thin film of magnesium hydroxide and mixed carbonate, a layer of amorphous CaP also progressively precipitates onto the metal surface, and gradually replaces the original metal implant. This phenomenon has been observed by many research groups across the globe [35, 104, 106, 115-118]. Some groups have intentionally adjusted the mineral layer for coating using the bio-mimetic process, by immersing Mg alloy in simulated body fluid at 37°C with a pH of 7.4 [119].

1.3.1 Use of Calcium Phosphate in Bone Research

According to Table 2 shown above, many forms of CaP exist. Hydroxyapatite (HA), with a chemical formula $Ca_{10}(PO_4)_6(OH)_2$, is the most studied biomaterial that can be found naturally in bone [120]. The osteoconductivity and biocompatibility of HA have made it a popular research object. Researchers have developed synthetic HA as bone substitute that aims to match the properties of natural bone and aides in fracture healing [121].

CaP can be utilized on different applications. It can guide new bone growth or implant directly in bone defect to support the fracture site. The similarity in density between the natural bone and synthetic HA can greatly reduce the stress shielding effect introduced by other commonly used implant biomaterials, such as titanium and stainless steel. Other studies have used HA as a drug delivery scaffold. Porous HA has been designed and developed to load drugs. Such construct was shown to better interact with bone tissue as well as increase drug efficiency, controlled release, and site-specific delivery [122]. As more processing techniques were developed, more forms of HA were developed as well, including the nano- and micro-crystals of the HA, making this synthetic material even closer to its natural form [123]. In another study, researchers combined HA with collagen, a protein that composed of 95% of organic component in bone, providing bone with strength and flexibility [124]. Results have shown that this composite promoted bone formation and fulfilled the role of donor cell retention.

1.3.2 Adverse Effect of Calcium Phosphate in Soft Tissues

Calcium phosphate deposition in soft tissues have been classified into three categories: metastatic calcification, dystrophic calcification, and calcinosis [125]. Metastatic calcification

happens when calcium and phosphorous levels in the body are elevated even when tissues are still normal. What we concern the most here, vascular calcification belongs to the second category, the dystrophic calcification. It happens injured tissues even under normal body metabolism. Calcinosis are mostly seen in subcutaneous tissues, skin, and connective tissues [126]. Although calcification, normal or ectopic, can develop in every tissue in the body, it seems that cardiac muscle tissue is more prone to this process [125].

In vasculature, vascular calcification occurs in arteries, most likely in intima and media. Calcification in intima, the inner most layer of the arteries, is usually associated with atherosclerosis, while medial calcification usually concerns with chronic kidney disease [127]. Although the causes of disease are different, the outcome all leads to the calcium phosphate formation, mostly hydroxyapatite, in the vessels. When intima calcification happens, the vessels usually are occluded due to plaque buildup, leading to myocardial infraction and mortality. Medial calcification does not narrow the vessels, but stiffens them instead, and can result in heart failure. Many studies have shown that vascular calcification and its progression are related to cardiovascular events or death [128].

Another common soft tissue calcification happens in the heart valves. It can narrow and stiffen the heart valve, and eventually lead to mortality [129]. The passive calcium phosphate deposition is not the only cause for calcification in the heart valves; the major cause is an active process that involves the collaboration of native valve endothelial cells, circulating inflammatory cells, and bone marrow derived cells, transition into osteoblast-like cells and form matrix vesicles, which serve as the nidus for calcification. The only therapy currently available for valves calcification is the surgical or transcatheter valve replacement [129].

1.4 Calcification Inhibitors

The common knowledge of calcification is usually “the accumulation of calcium or calcium salts in a body tissue,” happens normally during bone formation. However, calcification can be ectopic, which is defined as “the inappropriate biomineralization occurring in soft tissue [125],” such as in the cartilage, arteries, and heart valves.

Calcification can be self-regulated and inhibited. With many calcification inhibitors exist, seventeen of them are vitamin K dependent and would need to undergo carboxylation to function properly [130], including the osteocalcin (bone gla protein), matrix gla protein (MGP), and Gla-rich protein. These are among the most common inhibitors. Other inhibitors, such as fetuin-A and pyrophosphate, will be introduced below.

1.4.1 Matrix GLA Protein

Matrix GLA protein (MGP) was discovered in 1983 while isolating bone morphogenic protein from demineralized bovine cortical bone [131]. It is associated with organic bone matrix and contains several negatively charged γ-carboxyglutamic acid (Gla) residues, hence the name [132, 133]. MGP is a 14 KDa extracellular secretory protein that is synthesized by vascular smooth muscle cells, endothelial cells, fibroblasts, and chondrocytes [134].

To become functional active, MGP must undergo post-translational modification with the help of vitamin K. Therefore, it belongs to the family of vitamin K dependent protein (VKDP). Five out of nine of its glutamic acid residues (Glu) in its amino acid sequence can be post-translated into Gla in the endoplasmic reticulum, during the vitamin K cycle, or gamma-glutamate carboxylation [135]. Such modification adds an extra carboxyl group on this particular amino acid,

introducing a binding affinity for calcium ions or calcium crystals, thus inducing conformational changes [136].

Many studies have concluded that MGP is an ectopic calcification inhibitor. In one MGP knockout mice study, Luo and colleagues showed that these mice were born normally but all died within 2 months due to aorta rupture. Histology identified calcification at multiple sites in each knockout mouse [137]. Another study by Murshed and colleagues demonstrated that by restoring MGP expression in knockout mice, arteries were saved from calcification and mice were growing normally [138]. In a study that determined the serum calcification factors in devitalized arteries, MGP was found to be an essential secreting factor in living vessels to prevent the calcifying process, whereas warfarin-treated uncarboxylated MGP caused the vessel calcification. The addition of 30 μg/mL to 100 μg/mL MGP effectively prevented the 3 mm to 4 mm of carotid artery from calcifying when cultured in medium [139]. Numerous studies have also confirmed that warfarin induces rapid calcification in arteries and heart valves, which could be prevented in the presence of 2% or normal MGP level [140, 141].

The precise mechanism of how MGP functions is still under investigation. Several hypotheses have been proposed. It was suggested that the circulating MGP either aggregates or binds to larger molecular weight proteins, through which transporting calcium phosphates to where they belong through the circulation [142]. Another mechanism was proposed by Schurger and colleagues that MGP inhibits calcification via binding to matrix vesicles derived from vascular smooth muscle cells, where the initial nucleation begins. When MGP is present, the vesicles do not calcify [134, 143, 144]. A third proposed mechanism involves the bone morphogenetic proteins (BMP2). MGP acts as a regulatory protein for BMP2. BMP2 binds to the Gla region of the MGP in the presence of calcium ions [145, 146]. Lastly, MGP is found at the site of calcification. It is

proposed that MGP prevents further growth of calcium crystals and hydroxyapatite, by bounding tightly with hydroxyapatite nuclei. This way, the continuous seeding of the daughter crystal is inhibited, and the further aggregation of the crystal is ceased [140, 143]. Regardless of the underlying mechanism, MGP has been confirmed by many studies to be the vascular calcification inhibitor.

1.4.2 Fetuin-A

Fetuin-A was discovered in 1944 from fetal bovine serum [147]. It is a 48 KDa alpha-2-HS-glycoprotein synthesized in the liver and secreted into the circulation [130]. Fetuin-A has many functions, including bone metabolism regulation, insulin resistance, protease activity control, etc [147]. Similar to the MGP, one of its important functions dedicates to be the inhibitor of soft tissue and vascular calcification. Jahnen-Dechent and colleagues created the Fetuin-A deficient mice by targeted deletion of the Fetuin gene [148]. Although no anatomical abnormalities were detected, alizarin red staining revealed that ectopic microcalcification was developed in soft tissues. Different from MGP, Fetuin-A circulates in serum, acts systemically instead of locally [149].

Fetuin-A has also been linked to clinical practice as a diagnostic biomarker [150]. Since 95% being secreted by the liver, Fetuin-A can be an indicator for the liver function in the clinics as suggested by some studies [150-152]. A decreased serum Fetuin-A level has been associated with sever liver damage, such as in the case of patients with chronic hepatitis and cancer [153]. Moreover, higher Fetuin-A level in serum has reported to signal a higher risk for cardiovascular diseases including myocardial infarction and ischemic stroke [154].

1.4.3 Pyrophosphate

Inorganic pyrophosphate (PP_i) is a small molecule and metabolic byproduct that is generated by the hydrolysis of the phosphodiester bond in nucleotide triphosphates, not produced directly by mammalian cells [155]. It is ubiquitously abundant in human body. In human liver alone, more than 30g of PP_i are synthesized daily as the byproduct of albumin synthesis [156].

Already proved in many studies, PPi is a well-known mineralization inhibitor. Fleisch and colleagues first discovered the inhibitory function of PPi in the 1960s [157]. Not only is pyrophosphate able to prevent the binding between calcium and phosphate to form hydroxyapatite, this molecule can prevent further crystallization by strongly binding to the surface of hydroxyapatite [158, 159]. A study in which uremic rats were administrated with pyrophosphate significantly reduces the progress of vascular calcification, without affecting the normal skeletal mineralization [160]. When pyrophosphate was degraded by enzyme alkaline phosphatase, its mineralization inhibitory function was vanished [161]. However, since pyrophosphate has a very short half-life, researchers are still questioning whether this could be an option of a suitable long-term treatment for patients with vascular calcification, while trying to optimize the methods for its administration [161].

2.0 Hypothesis and Specific Aims

As the title indicates, this dissertation will explore two parts, both revolving around Mg: 1) the mineralization on Mg metal surface, and 2) the effect of Mg^{2+} on periosteal cell differentiation.

The first part (specific aim 1, chapter 3) studies the metal corrosion and mineralization induced by the Mg degradation process. The second part (specific aim 2, chapter 4) explores the direct and indirect effect of Mg^{2+} on periosteal cells. Therefore, two hypotheses will be developed for each specific aim. We aim to reduce the mineralization on Mg metal surface for Mg-based devices, such as the endovascular stents, used in soft tissues, while trying to determine whether Mg^{2+} could drive the osteogenic differentiation of periosteal cells for bone regeneration. We expect that this work will help to understand the effect and underlying mechanism of Mg^{2+} released from Mg-based implants on periosteal cells for accelerated bone healing, and improve the function of these degradable biomedical devices in both soft and hard tissue implantations.

2.1 Hypotheses

2.1.1 Hypothesis for Specific Aim 1

The central hypothesis of specific aim 1 is that calcium phosphate deposition on Mg-based metal surface will be inhibited by MGP. To test the hypothesis of this specific aim, we propose three experimental sub aims.

In the first sub aim, we will test the mineral deposition on Mg and its alloy surface in the presence of MGP using an *in vitro* submersion test. Characterization techniques, including scanning electron microscopy (SEM), energy dispersive x-ray spectroscopy (EDS), and Fourier-transform infrared spectroscopy (FTIR) will be used to determine the Mg surface composition after the submersion test.

In the second sub aim, we will develop a scaffold that can deliver the protein to the Mg metal surrounding. Cell localization and protein secretion in the scaffold will be studied using histology and immunohistochemistry.

In the third sub aim, we will evaluate the effectiveness of the MGP to reduce the mineralization on Mg metal surface, by implanting the scaffold in mouse intramuscular model for four and six weeks. Surface mineralization and Mg corrosion rate will be determined using microCT analysis. Mineral distribution around Mg rod will be studied using histology and EDS.

2.1.2 Hypothesis for Specific Aim 2

The central hypothesis for specific aim 2 is that Mg^{2+} will directly enhance the osteogenic differentiation of periosteal derived cells and promote new bone formation. To test the hypothesis of specific aim 2, we propose three experimental sub aims.

In the first sub aim, the direct and indirect effect of Mg^{2+} on the osteogenic differentiation of mouse and human periosteal cells will be determined *in vitro*. qPCR and Western blotting will evaluate the osteogenic gene and protein expressions from the mouse and human periosteal cells after treatment with different concentrations of Mg^{2+} at different time points. Alkaline phosphatase (ALP) activities and mineralization of the extracellular matrix will also be determined.

In the second sub aim, Mg metal nanopowder will be electrospan into PLGA scaffold. We will study the distribution of the ions in the scaffold using SEM and EDS. The release profile of the Mg metal nanopowder from the scaffold will also be evaluated through inductively coupled plasma mass spectrometry (ICP-MS).

In the third sub aim, we will implant the scaffolds developed in the second sub aim into both female and male rat calvarial defect model for one month. New bone volume will be assessed using high resolution microCT and histology.

3.0 Controlling Magnesium Corrosion and Degradation-Induced Mineralization using Matrix GLA Protein

3.1 Acknowledgements

The work presented in this chapter was supported by the NSF ERC RMB (grant 0812348) and the University of Pittsburgh's Center for Craniofacial Regeneration. MicroCT file processing was done on a system supported by the NIH S10-OD021533 Shared Instrumentation Grant. All work was done in collaboration with Dr. Samer H. Zaky, Rong Chong, Lyudmila Lukashova, Dr. Elia Beniash, Dr. Konstantinos Verdelis, Dr. Frank Witte, and Dr. Charles Sfeir. We also would like to thank Dr. Michael Epperly (University of Pittsburgh) for device sterilization, Dr. Daeho Hong (University of Pittsburgh) for the help using the machine shop, Dr. Avinash Patil and Dr. Hajime Yamazaki (University of Pittsburgh) for assistance with the FTIR analyses, Dr. Xu Yang and Dr. Yurong Ouyang (University of Pittsburgh) for helping with tissue harvesting, and Dr. Denise Janicki (University of Pittsburgh) for editing the manuscript.

3.2 Detailed Abstract of Mineralization Inhibition

Biomedical devices made of magnesium (Mg) alloys, such as stents, are embraced for their biodegradability and biocompatibility. However, Mg degrades spontaneously in the biological environment in vivo and in vitro, triggering deposition of calcium phosphate on the metal. Upon complete metal absorption, minerals remain in the tissue, which could lead to pathogenic

calcification. Hence, our aims are to test the feasibility of matrix GLA protein (MGP) to locally inhibit Mg mineralization that is induced by metal alloy degradation. MGP is a small secretory protein that has been shown to inhibit soft tissue calcification. We exposed Mg to MGP, stably transfected into mammalian cells. Results showed that less calcium and phosphorous deposition on the Mg surface when MGP was present relative to when it was not. In the in vivo mouse intramuscular model conducted for 4 and 6 weeks, Mg rods were embedded in collagen scaffolds, seeded with cells overexpressing MGP. Microtomography, electron dispersive x-ray spectroscopy, and histology assessments revealed lower deposited mineral volume around Mg rods from the MGP group. Compared to other groups, higher volume loss after implantation was observed from the MGP group at both time points, indicating a higher corrosion rate without the protective mineral layer. This study is the first to our knowledge to demonstrate that local exposure to a biomolecule, such as MGP, can modulate the corrosion of Mg-based implants. These findings may have important implications for the future design of endovascular stents and orthopedic devices.

3.3 Introduction

Characteristic properties of magnesium (Mg) and its alloys, including biodegradability and biocompatibility, have brought the metal to the attention of researchers in the biomedical field. Mg alloys have been fabricated into implants including the endovascular stents. Traditional metallic stents are left permanently inside the vessel. However, the continuous metal-tissue interaction can lead to in-stent restenosis, long term endothelial dysfunction, and chronic inflammation [162, 163]. The ideal solution to the potential adverse outcomes of permanent implants in soft tissue environment such as the stents would be to develop a device that could both satisfy mechanical

requirements for the duration they are needed, and then gradually disappear so to reduce the extent of metal-tissue contact.

A biodegradable Mg stent was successfully implanted into the left pulmonary artery of a preterm baby [72], and findings from several subsequent clinical trials have further demonstrated the effectiveness of Mg stents for the treatment of vascular stenosis [108-112]. However, pre-clinical and clinical data have shown that when Mg-based alloys degrade, a layer of amorphous calcium phosphate progressively develops on the metal surface [35, 110, 115, 116]. This calcium phosphate deposition is due to the increase in the local alkalization of the metal, during metal corrosion and the saturation of calcium and phosphate ions in biological environment [25, 63]. Hydroxyl ions are generated as an end product of Mg reacting with water, thus accounting for the pH increase locally on the metal surface and corrosion pits. Once the nucleation begins, calcium crystals continue to grow and extract more calcium and phosphate ions in the body fluid onto the substrate [164]. Because this mineral layer is not homogenously intact, the exposed metal surface continues to interact with the surrounding aqueous environment and continues to corrode until the whole metal is replaced by the precipitated minerals [165].

Mineral deposition in the soft tissues is harmful, as it can contribute to the pathogenesis of ectopic calcification [125]. Pathological calcification is of particular concern with respect to cardiovascular tissues both because they are especially vulnerable to calcification [125, 166], and because calcification is reliably correlated with higher risk of myocardial infarction and other vascular diseases [138].

Ca^{2+} and PO_4^{3-} precipitate as calcium phosphate minerals under both physiological and pathological conditions. In a healthy subject, the presence of various calcification inhibiting macromolecules prevents precipitation of calcium phosphate [164]. Matrix GLA protein (MGP) is

one such inhibitor. MGP is a 14 kDa vitamin k-dependent secretory protein synthesized by vascular smooth muscle cells, endothelial cells, and chondrocytes [134, 167]. Several studies have shown that MGP acts primarily as an ectopic calcification inhibitor in vasculature and cartilage [137-139]. However, to become functionally active, MGP must undergo post-translational modification. Five out of nine glutamic acid residues (Glu) in its amino acid sequence can be post-translationally modified into γ-carboxyglutamic acid (Gla) in endoplasmic reticulum during gamma-glutamate carboxylation, a vitamin K-dependent process [135]. This modification both increases binding affinity for Ca^{2+} or calcium containing crystals, the only known property of the Gla residues [168], and induces conformational change [136].

In this study, we explored the ability of MGP to inhibit mineral deposition onto Mg metal surface. Our *in vitro* transwell tested the extent of mineral precipitation on Mg surface when MGP was expressed by the cells cultured in the same medium. To further test the ability of MGP secreting cells to reduce mineral precipitation *in vivo*, we developed a model consisting of a collagen scaffold seeded with MGP stably transfected cells surround a Mg metal rod. We anticipated that MGP in the collagen gel will inhibit mineral deposition on the Mg rod and affect the corrosion rate. In the present report, we demonstrate both *in vitro* and *in vivo* that release of MGP in the proximity of a degrading Mg device can effectively minimize mineralization of the metal implant and increase the alloy corrosion rate.

3.4 Materials and Methods

3.4.1 MGP Stable Transfection and Expression

Matrix GLA protein (MGP) cDNA plasmid fused with a green fluorescent protein (GFP) tag (OriGene, MD, USA) was transfected both into human embryonic kidney 293 cells (HEK293) via Lipofectamine 2000 (ThermoFisher Scientific, USA), and human umbilical vein endothelial cells (HUVECs) via electroporation (Amaxa Nucleofector II, Lonza, Switzerland). HEK293 cells were used because they are known for their high transfection efficiency and the ease of establishing stable transfection. HUVECs are endothelial primary cells, thus are harder to transfect and were transiently transfected with the MGP gene. To select for the stably transfected HEK293 cells, 48 hours after transfection, geneticin (G418 Sulfate, Gibco by Life Technologies) was added into the cell culture medium, which is eagle's minimal essential medium (DMEM) supplemented with 10% FBS and 1% L-glutamine. Medium containing increasing concentrations of G418 was changed every two days for at least one month. GFP expression was observed under an inverted microscope (Eclipse TE2000-E, Nikon Instruments, Japan). Cells were also lysed and underwent gel electrophoresis and immunoblotting with both MGP (Santa Cruz Biotechnology, USA) and GFP (OriGene, MD, USA) antibodies to confirm stable transfection. Cell culture medium was collected and Dynabeads protein G immunoprecipitation (ThermoFisher Scientific, USA) was used to confirm stable protein secretion and measure MGP concentration in the medium.

3.4.2 Magnesium Surface Preparation

Pure magnesium rods (99.9% purity, GoodFellow, PA) of 1.66 mm diameter were cut into 5 mm length pieces. Mg alloy WE43 was a generous gift of Dr. Frank Witte (Charité - Universitätsmedizin Berlin, Germany), and cut into 2 mm thick, 10x10 mm square plates using the Buehler IsoMet 1000 precision saw (Buehler, IL). Rods and plates were polished sequentially on 600/P1200, 800/P2500, and 1200/P4000 grit size silicon carbide metallurgical paper (Allied Hightech Products, CA). Samples were then washed for 30 sec in an ultrasonic bath containing 85% glycerol, 65% nitric acid, and 100% acetic acid, followed by repeated wash (twice) in 100% ethanol for 1 min each. Cleaned samples were dried overnight in a 50°C vacuum oven, and then packed and numbered in parafilm for microCT scanning. Before implantation, gamma radiation was used to sterilize all samples (2 $x10^6$ cGy, 23.5 Gy/min, cesium 137 source, Mark I 68, JL Shepherd and Associates, San Fernando, CA).

3.4.3 In vitro Transwell Test

An in vitro transwell experiment was conducted to test the effect of MGP on Mg surface. HEK293 cells and HUVECs with and without MGP transfection were plated in 6-well plates. 7 μg/mL of vitamin K1 was supplemented to the medium to stimulate γ-carboxylation [169]. After allowing 48 hours of protein secretion from the cells, pure Mg rod and Mg alloy WE43 plates were placed on a 24mm transwell insert of 3.0μm polyester membrane (Transwell permeable supports, Costar, USA), and suspended in the medium in 6-well plates for 5 days.

3.4.4 Surface Element Analysis

After the transwell test, Mg rods and WE43 alloy plates were collected and scanning electron microscopy was conducted using JSM 6610-LV SEM (JEOL, Japan) equipped with electron dispersive x-ray spectroscopy (EDS, Oxford Instruments, UK) at 200x magnification and 20kV accelerating voltage. Electron spectroscopy analysis was conducted on at least 4 areas per sample and the weight % data for Ca and P was collected.

3.4.5 Attenuated Total Reflectance Fourier Transform Infrared Spectroscopy

A Vertex- 70 ATR- FTIR (Bruker Optics, Bellerica, MA) equipped with a diamond Miracle ATR accessory (Pike Technology, WI, USA) was used to identify the surface products present on the Mg rods. The present study focused on calcium phosphate and compared observations between sample groups with and without MGP treatment. At least three separate areas were scanned per sample and the spectra were obtained at 4 cm^{-1} resolution averaging 120 scans in the 600- 1200 cm^{-1} frequency range. A polished and etched Mg rod was used to obtain a background spectrum. The spectra were analyzed using the PerkinElmer Spectrum software.

3.4.6 Collagen Scaffold Construct

The function of the collagen scaffold was to homogeneously encapsulate MGP producing in the proximity to the surface of Mg metal, which was placed in the center of the collagen scaffold after the gelation process. The transfected HEK293 cells were seeded into 4.0 mg/ml of type I rat tail collagen (Advanced BioMatrix, CA, USA) in a concentration of 10 million cells/ml of collagen

solution. 200 μl of the gel/cell mixture was then added into each well of the 96-well plate that served as a gelling mold. The plate containing the gel/cell mixture was incubated in a cell culture incubator for approximately 1 h for gel solidification. Upon gelling, cell culture medium was added into each well. To access whether the cell seeding was homogenously distributed along the entire volume of the scaffold, collagen gel was embedded using Tissue-Tek OCT embedding medium (VWR, Rednor, PA), flash frozen and sectioned into 5 μm thickness using Microm cryostat (HM505EP, Richard-Allan Scientific, CA). Sections from different depths of the gel were stained with hematoxylin and eosin (HE) staining. Immunohistochemistry using MGP antibody was performed to analyze MGP secretion after cell seeding. Gel/cells construct was also lysed using cell lysis buffer and underwent immunoblotting using GFP antibody.

3.4.7 Mouse Intramuscular Implantation of the Sample Construct

All protocols for the animal surgeries were approved by the University of Pittsburgh Institutional Animal Care and Use Committee. Twenty male, BALB/C nude mice (Charles River, USA), 8-10 weeks of age, were used in this study. Four mice were held in each cage in a controlled environment. Twenty animals were randomized into 4 testing groups and 2 time points (10 animals at each time point): pure Mg rod only (abbreviated as Mg only); pure Mg rod encapsulated in collagen gel (Gel); pure Mg rod encapsulated in collagen gel seeded with regular HEK293 cells (HEK293s); and pure Mg rod encapsulated in collagen gel seeded with cells stably secreting MGP (MGP). Two samples were implanted intramuscularly on the left and right dorsal side above the femur. A 2cm incision of the skin and the fascia underneath was created by blunt dissection. Samples were transplanted into individual pocket and incisions were closed with sutures. Four and

six weeks after implantation, mice were anaesthetized and euthanized. The implant and the surrounding soft tissue were excised and fixed in buffered 10% formalin.

3.4.8 High Resolution Micro-Computed Tomography Analysis

3.4.8.1 Alloy Corrosion Assessment

Before implantation and after harvesting, all Mg rod samples were scanned using the high resolution μCT SkyScan 1172 (Bruker-microCT, Kontich, Belgium) system with a voxel size of 5.93 μm (59kV beam energy, 167uA current intensity -0.5mm Al filter, 800ms exposure, 1.61 degree-rotation step, 8 frames per view, default by manufacturer median filtering). Samples were wrapped and stabilized using parafilm inside custom-made holders in the air. 3D volumes of the scanned samples were reconstructed from the 2D projections using NRcon software (Bruker-microCT, Kontich, Belgium), using a 20 value for ring artifact correction and no smoothing of images. For analysis, the reconstructed Mg rod volumes were first reoriented reoriented to a standard position using the SkyScan DataViewer, followed by evaluation of the change in Mg rod volume before and after implantation using the SkyScan CTAn software. A region of interest (ROI) was drawn around the rod on sequential slices of 5.93 μm and segmentation between the rod and the surrounding soft tissue was done using a global threshold of 55 greyscale units. The distinct difference in absorption coefficient between the Mg rods and the surrounding tissues resulted in a sharp boundary between them. Total volume of Mg rods before and after implantation were then calculated using the 3D morphometry function of the software.

3.4.8.2 Mineralization Assessment

The explanted Mg rods were embedded in Osteo-Bed Plus (Polysciences, PA, USA) following the manufacturer's instructions. For a more sensitive quantitative analysis of the deposited minerals, these samples were scanned again using high resolution μCT 50 compact cabinet microCT scanner (Scanco Medical, Brüttisellen, Switzerland) at 55 kVp voltage and 200 mA current. The scanning voxel size was 4.4 μm. 0.36 degrees rotation step (180 degrees angular range) and a 3000ms exposure per view were used for the scans which were performed in air. Scanco μCT software OpenVMS (HP, DECwindows Motif 1.6) was used to evaluate the total mineral deposition on Mg rod surface, 3D reconstruction, and viewing of images. The threshold was set at 325 (grey scale) for all samples. Differences between the metal core and mineral density allowed us to segment the ROI, or the mineral deposit around the rod circumference. The cross-sectional elemental mapping obtained above was also used as a reference to define the ROI.

3.4.9 Mg Rod Cross-Sectional Elemental Mapping

Blocks of PMMA- embedded Mg rods and the surrounding soft tissues were trimmed until the cross section of the Mg rod was exposed. Samples from all groups were sectioned into similar depth before being coated with palladium using Denton V TSC sputter coater (Denton Vacuum, NJ). EDS analysis was conducted using JSM 6610LV SEM (JEOL, Japan) equipped with an EDS detector (Oxford Instruments, UK). Samples were mounted onto an SEM stage. The samples were studied at the 10 mm working distance and the microscope was operated at 20 kV accelerating voltage. Each sample cross section was scanned at least 4 times and at a magnification of 60x to maximally display the entire rod cross section for EDS element analysis and elemental mapping.

Only Mg, calcium (Ca), and phosphorus (P) within the ROI were included. Weight percentage of each element was analyzed using Aztec software (Oxford Instruments, UK).

3.4.10 Histological Assessment

Mg rods and the surrounding tissues were fixed in 10% formalin after harvesting, and before being embedded and polymerized in Osteo-Bed Plus (Polysciences, PA, USA) following manufacturer's instructions. All blocks were cut into sections of 5 μm thickness using a RM2255 microtome (Leica, Benshiem, Germany) with tungsten carbide blade (ThermoFisher Scientific, USA) and placed on slides pre-coated with Haupt's adhesive (DHM, IL, USA). Sectioned slides were pressed and dried in a 37°C oven overnight. Before each staining, slides were deacrylated in xylene twice, and 2-methoxyethylacetate for 20 min, followed by a series of decreasing percentage of ethanol and finally water for rehydration.

3.4.10.1 Von Kossa Staining

Von Kossa staining was used to visualize the phosphate minerals deposited around the Mg implant. Staining was performed according to the manufacturer's instructions (American MasterTech, CA). Briefly, after washing the rehydrated samples in water, 5% silver nitrate was added, and the samples were then placed above an ultraviolet light for 20 min exposure. After washing slides in distilled water, 5% sodium thiosulfate was added for 3 min, and then rinsed in running tap water. Samples were counter-stained with nuclear fast red for 5 min before rinsing in tap water. Finally, samples were dehydrated in absolute alcohol, cleaned in xylene, and mounted with mounting medium (Thermo Fisher Scientific, USA).

3.4.10.2 Alizarin Red S Staining

Alizarin red s staining was used to determine Ca^{2+} distribution around the implanted Mg rod. Slides were stained in 2% alizarin red solution (Electron Microscopy Sciences, PA) at pH 4.2 for 5 min, and rinsed in distilled water. At least five slides from each group were randomly selected for staining.

3.4.11 Statistical Analysis

Five biological replicates per experimental group were analyzed at each time point. Statistical analysis was conducted using IBM SPSS Statistics 19 software (IBM, Armonk, NY) and Graph Pad Prism 6 software. Differences between groups were tested with two-way analysis of variance (ANOVA) at a 95% confidence interval, followed by Tukey multiple comparisons and post-hoc test. Statistical significance was set at $P<0.05$.

3.5 Results

3.5.1 MGP Expressed from HUVECs and HEK293 Cells

GFP expression was observed in HUVECs and HEK293 cells (Figure 1A and 1B) following gene transfection. The stably transfected HEK293 cells were harvested and the culture medium collected. MGP was detected in cell lysate of the transfected HUVECs and HEK293s by western blot (Figure 1C). The molecular weight of the band was 43KDa as expected, since the transfected MGP plasmid was fused with GFP. Immunoprecipitation (figure 1D) confirmed the

expression of MGP in HEK293 cell culture medium, compared with control medium (from non-transfected cells). The total MGP concentration in the medium was on average 339.3 µg/mL. Stable transfection in primary HUVECs was not successful; thus, all experiments were performed using transiently transfected HUVEC cells.

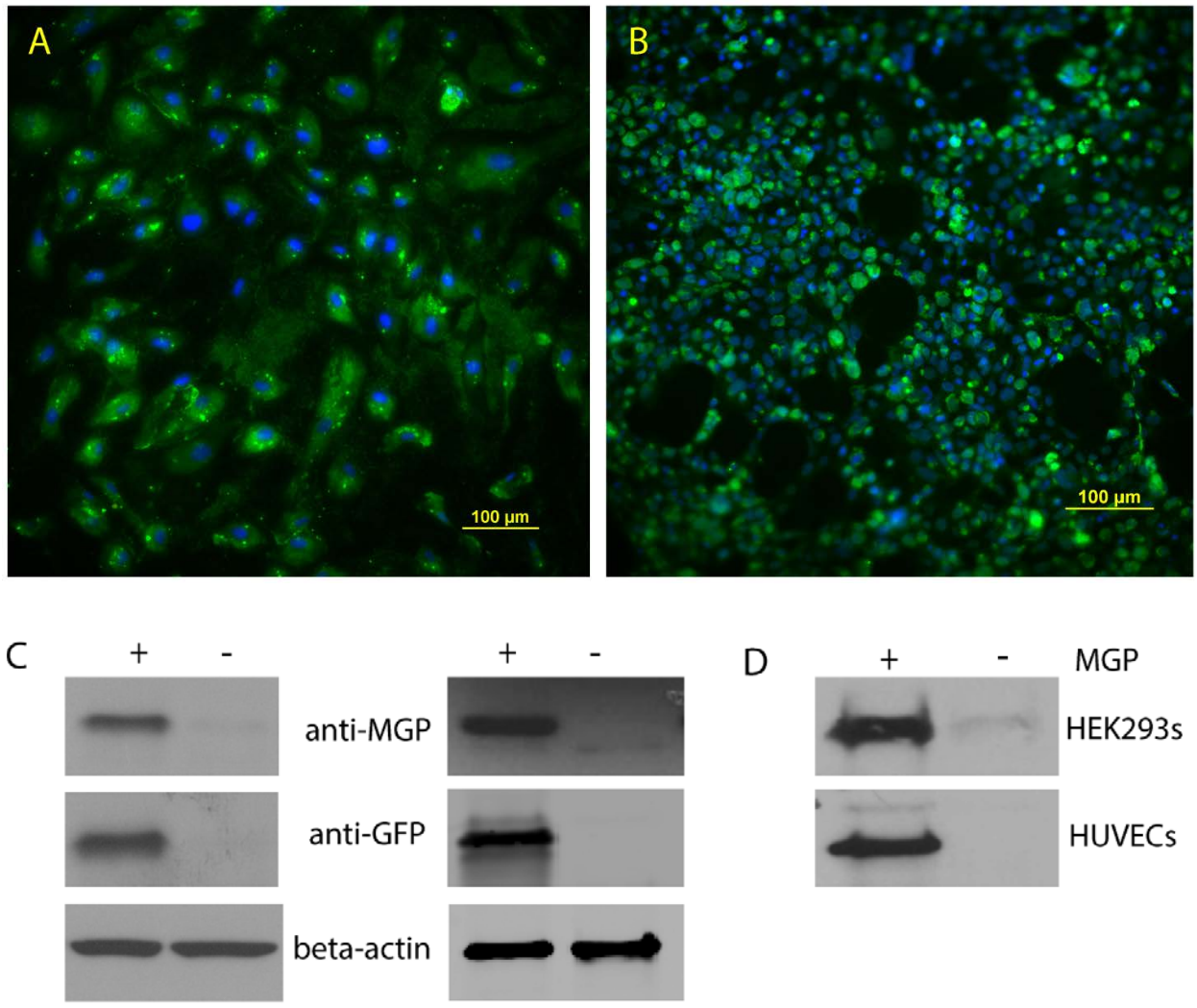

Figure 1. Immunocytochemistry and Western blotting confirming MGP transfection

Immunocytochemistry shows that GFP (green) expression was observed from HUVECs (A) and HEK293s (B) 5 days after MGP transfection. Magnification: 20x. C: Western blotting shows that cell lysates of HUVECs (left) 5 days after MGP transfection, and HEK293s (right) 1 month after transfection. D: MGP secretion in medium 1 month after transfection into HEK293s and 5 days into HUVECs, obtained using immunoprecipitation.

3.5.2 In Vitro Transwell Experiment

3.5.2.1 MGP Reduced Mineralization on Mg Metal Surface

EDS analysis showed that the weight percent of Ca and P on pure Mg surface was significantly less in medium containing MGP than in the medium without MGP (Figure 2A, 2C). Similarly, the weight percentage of deposition of both elements on WE43 was reduced in the presence of MGP (Figure 2B). Morphological differences between the Mg rods from each of the two treatments were negligible.

Figure 3 shows the ATR-FTIR spectra of Mg rod with and without the presence of secreted MGP in culture medium. As expected, polished and etched Mg rod (Mg control) did not have any major absorbance peaks. The spectra of Mg rod in the medium of HEK293 without MGP (Mg +HEK293s) presented a sharp peak around 1050-1100 cm^{-1} that corresponds to phosphate antisymmetric stretching as in amorphous calcium phosphate, whereas the spectra of the rod with MGP in the medium (Mg +MGP) had a nearly negligible smooth bump around the same wavenumber, indicating suppressed mineral formation on the Mg surface.

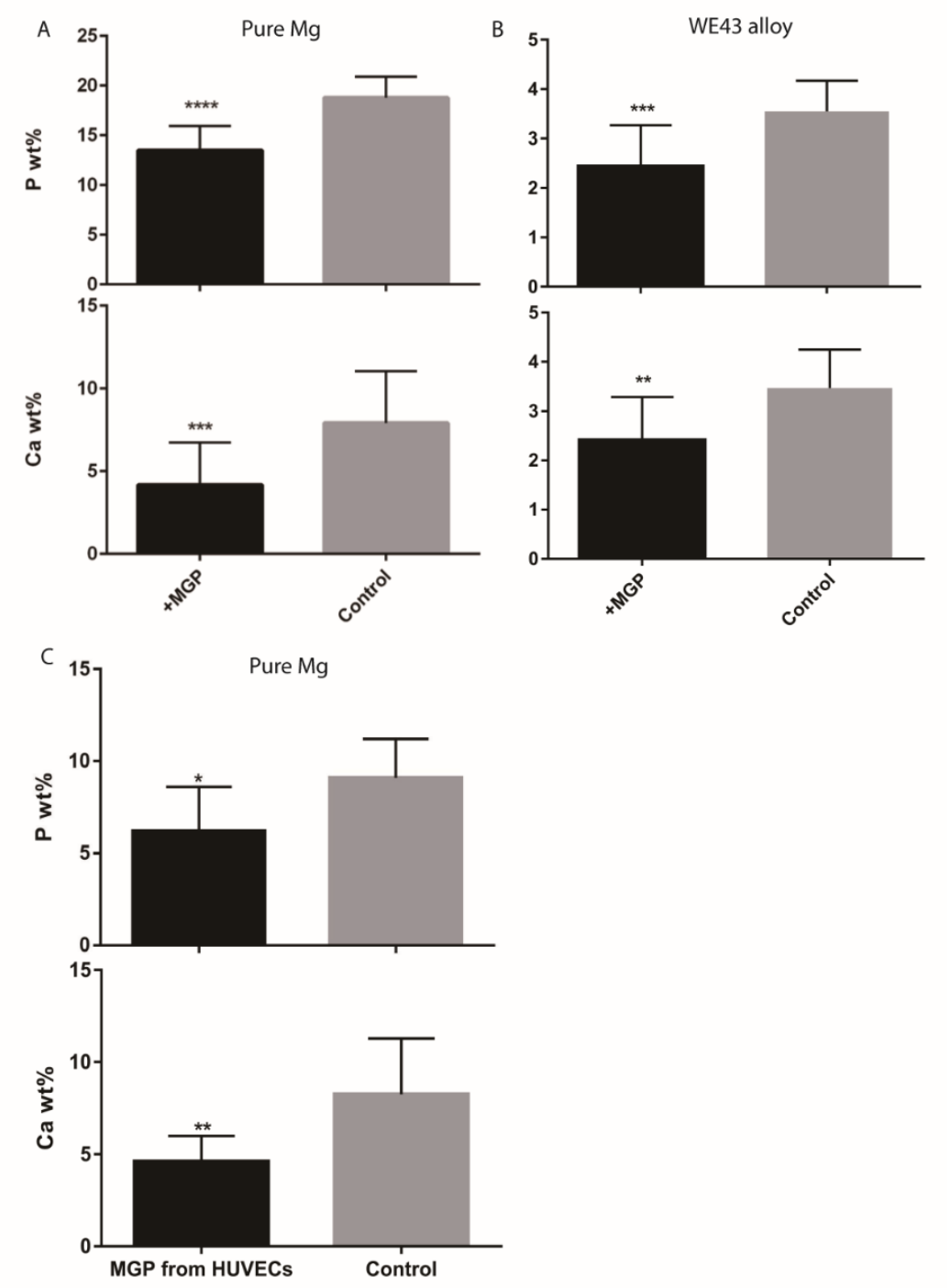

Figure 2. EDX analysis of Ca and P wt% on pure Mg and WE43 alloy surfaces

EDX detected higher Ca and P wt% on pure Mg (A) and WE43 (B) from culture medium with (+MGP) and without (Control) MGP secreted from HEK293s. MGP overexpressed from HUVECs also reduced Ca and P wt% from pure Mg rod (C).

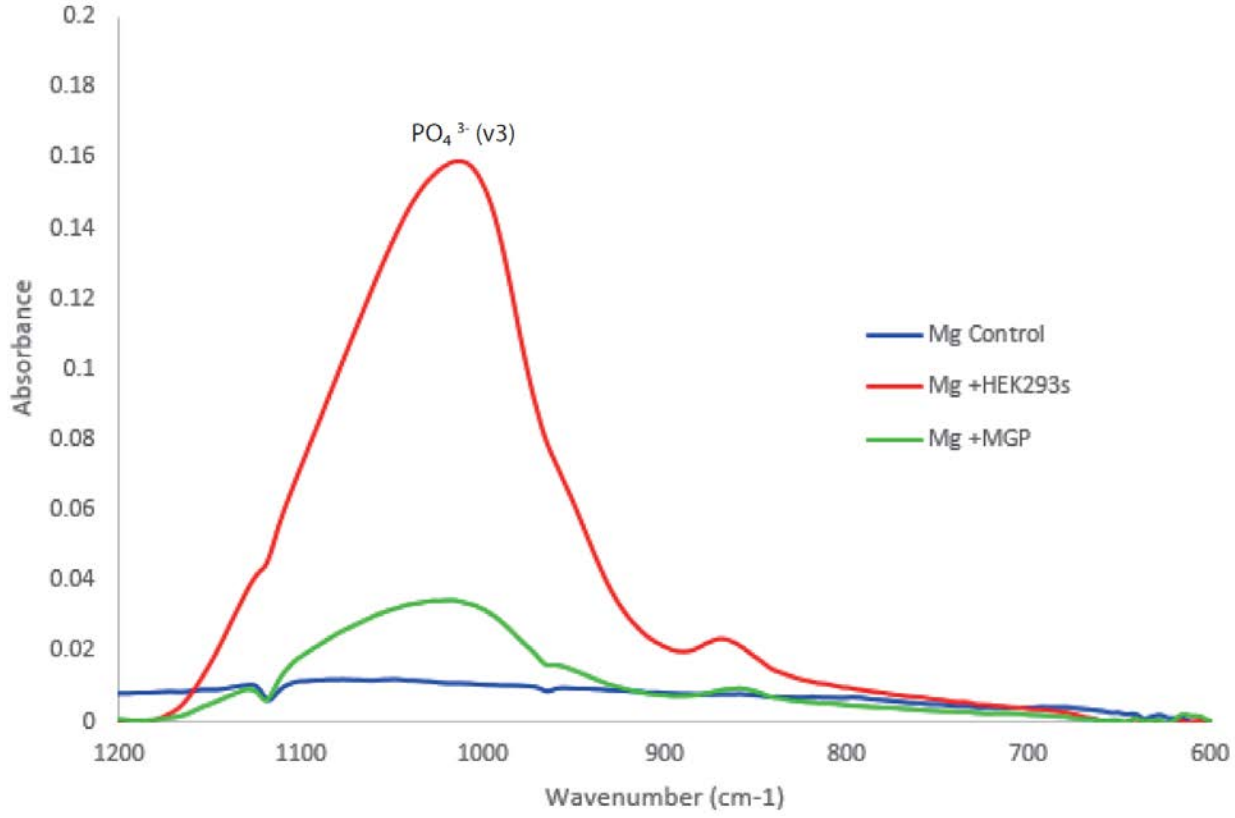

Figure 3. ATR-FTIR spectra captured on Mg rod surface

General ATR-FTIR spectra captured on Mg rod surface of different treatment after in vitro transwell test through 5 days.

3.5.3 Collagen Scaffold Construct

The collagen scaffold had a diameter of 6.35 mm and a height of 6.31 mm, and was able to maintain its shape after being removed from the mold (Figure 4A, 4B). The pure Mg rod with a diameter of 1.66mm and a height of 5mm was inserted by hand in the middle of the collagen scaffold (Figure 4C).

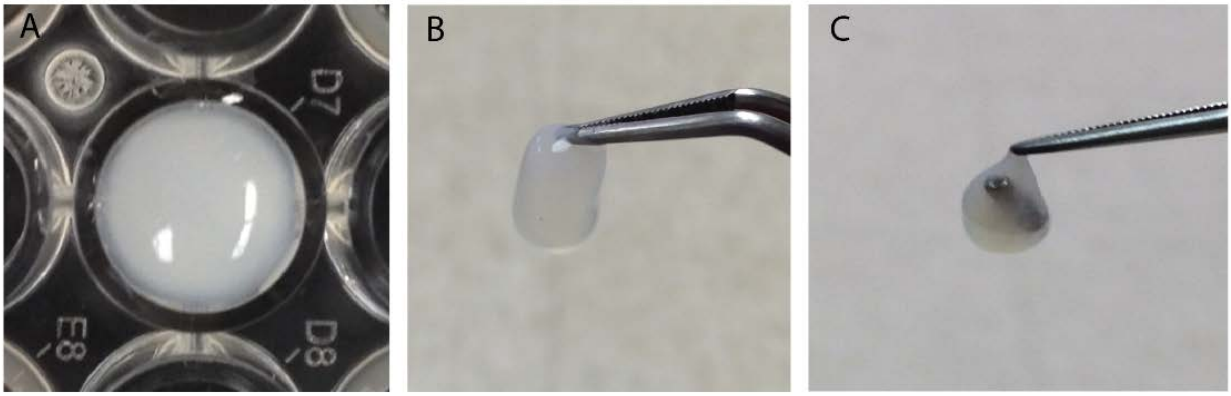

Figure 4. Formation of collagen scaffold

A: Cell seeded collagen scaffold was formed in 96-well plate used as a mold. B: Collagen scaffold was removed from the mold; C: A Mg rod was placed by hand in the middle of the scaffold.

Hematoxylin and eosin (HE) staining on the sectioned construct (Figure 5A) confirmed that the cells were seeded homogenously along the collagen gel. Sections stained using MGP antibody (green: MGP; blue: DAPI) revealed that MGP was secreted after cell seeding and evenly expressed across the scaffold (Figure 5B).

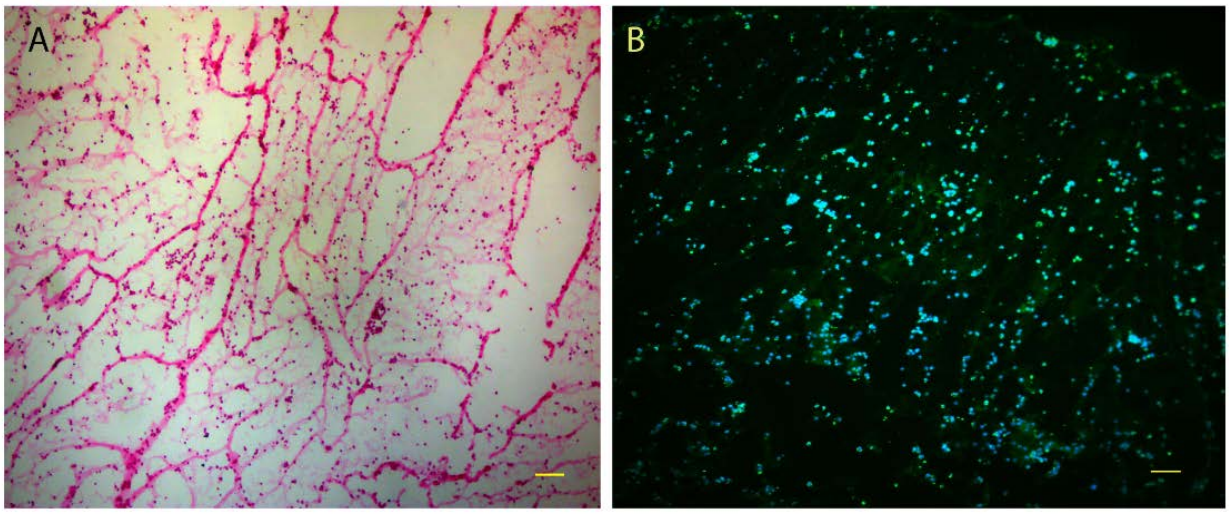

Figure 5. HE and immunohistochemistry staining showing cells seeded in collagen gel

Cell cultured in collagen gel was sectioned and stained with H&E staining (A) and MGP antibody (B). Scale bar = 100 µm.

3.5.4 In vivo Intramuscular Implantation

3.5.4.1 MGP Reduced Minerals on Mg Rod and Surrounding Tissues

Shown in Figure 6A, mineral deposition was segmented in the ROI and the total mineral was calculated from high resolution μCT scans. However, as shown in figure 6B, mineral deposition is almost unnoticeable when displayed in 3D images, with observation of degradation being limited to that of a relatively large scale, as in the MGP group. Quantitative analysis (figure 6C) revealed that continued local MGP secretion resulted in a significant nearly 5-fold reduction in deposited mineral volume on Mg rod surface compared to the bare Mg rods without MGP (Figure 6C). The group with collagen gel scaffold enclosing the Mg rod also had decreased mineral deposition on the metal surface, but the detected mineral volume was not statistically different from the Mg only group. Similar mineral volume on the implant surface was detected in collagen gel seeded with untransfected HEK293 cells group. As expected, surface mineral volume was higher at the 6-week time point compared to that at 4-week.

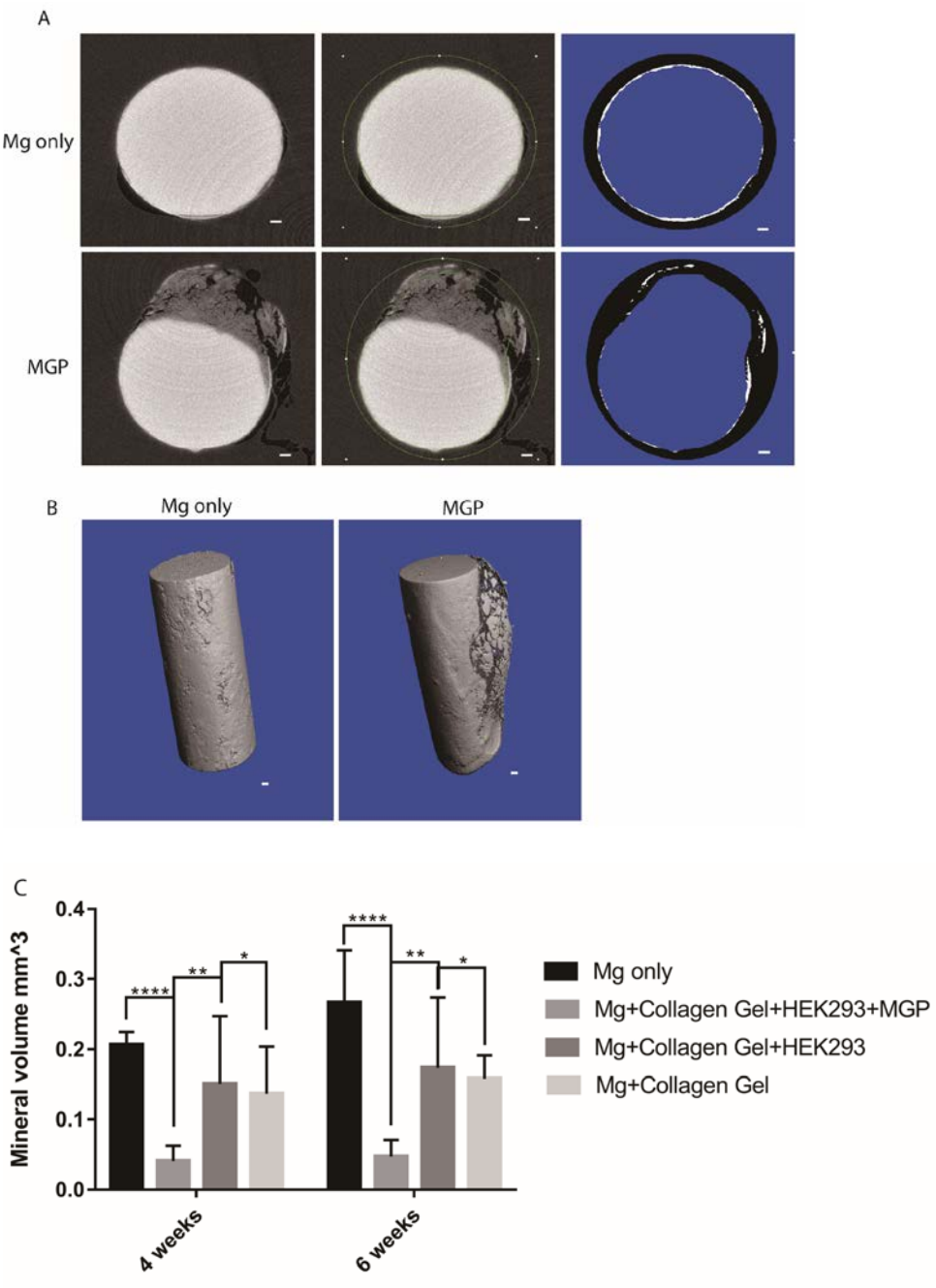

Figure 6. High resolution microCT analysis showing mineralization on Mg rod surface

A: Mineral deposition was segmented according to density difference from the metal core (middle). Threshold was defined to calculate the total deposited mineral volume (right). B: Representative 3D images of Mg rods. C: Mineral volume in mm3 measured from Mg rod surface using microCT. Scale bar = 100 µm for figure 6A and 6B.

Elemental mapping on the cross-sectional area of each Mg rod revealed the distribution of the mineral layer deposited on the metal periphery, showing variations in thickness and intensity of the elements from each group. The samples were scanned at X60 magnification, which allowed to include the full metal cross-sectional area in the field of view. As shown in representative images (figure 7A), we observed a thinner and less dense ring of Ca and P signal in the MGP group, confirming the lower mineral deposition at the Mg surface when it is exposed to MGP.

The corresponding area of each Mg rod was also scanned to compare the weight percentage of Ca and P between groups for quantitative analysis (figure 7B). At both time points after implantation we detected significantly less Ca and P signals around the Mg rods in MGP group compared to the rods from the other three groups.

Samples were stained with Alizarin red (Figure 8A) and von Kossa (Figure 8B) to visualize Ca and P deposition around Mg rods. Both staining methods showed that MGP group at both time points displayed the least mineral deposition outside of the Mg surface, compared to other groups without MGP. Mg only and non-transfected HEK293s groups had the most mineral deposition at 4 weeks after implantation. Mineral deposit from the collagen gel group was greatly increased at week 6.

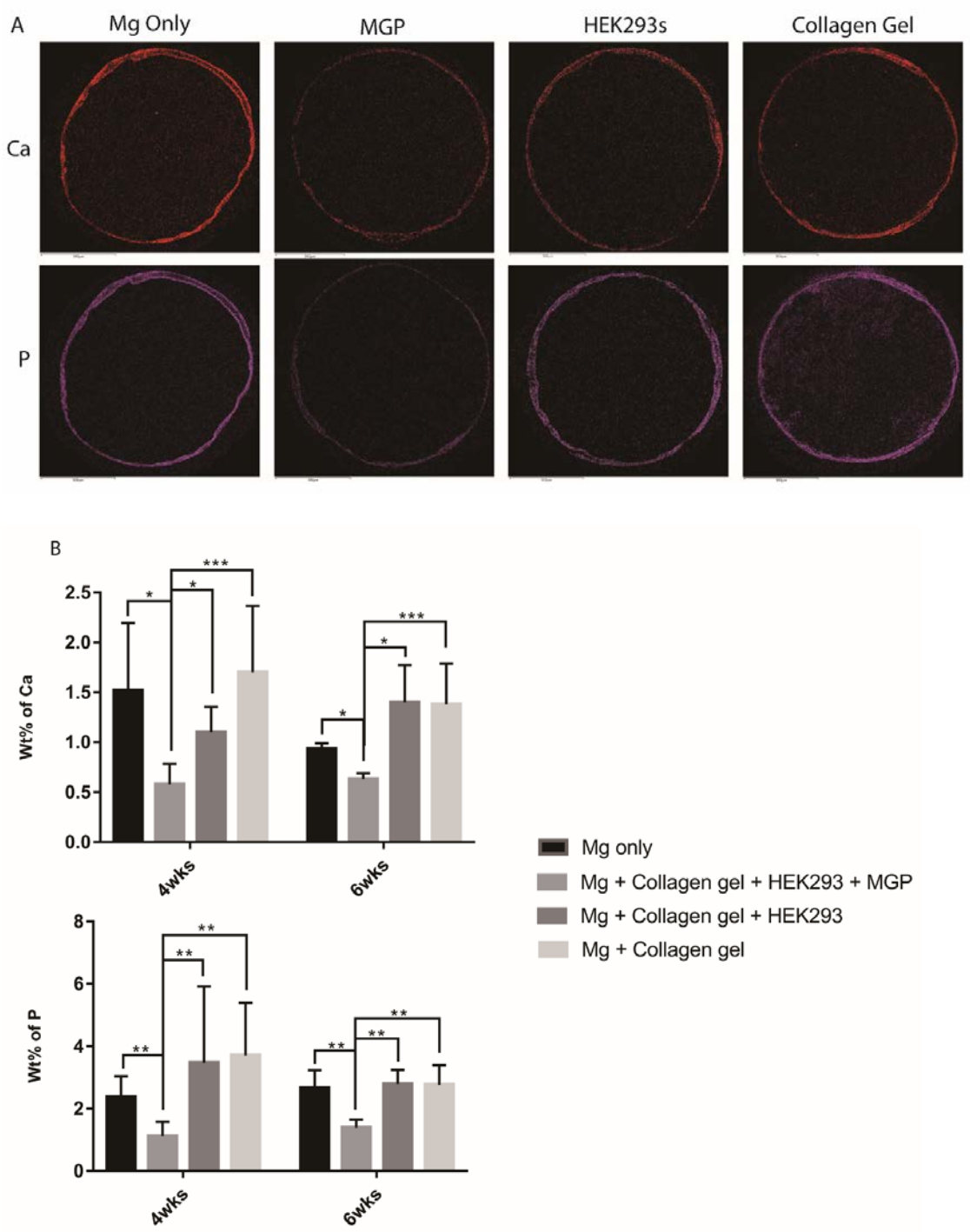

Figure 7. EDS showing minerals around Mg rod cross sections

A: Representative images of sample cross sections from each group, obtained using EDS with 60x magnification. Calcium (red, top row) and phosphorous (purple, bottom row) maps are displayed. B: Quantitative measurement of the weight percent of calcium (top) and phosphorous (bottom).

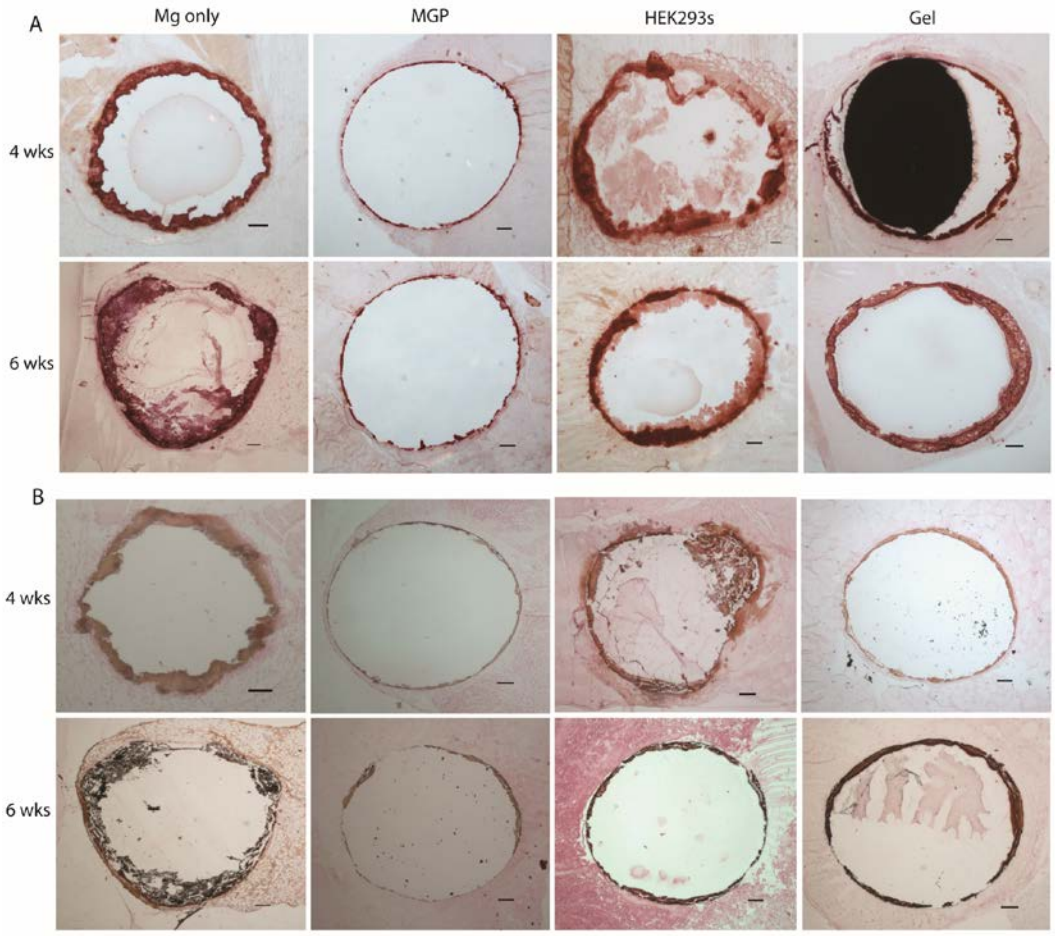

Figure 8. Alizarin red s and von Kossa staining showing mineral deposit around Mg cross sections

Representative images of Alizarin red (A) and von Kossa (B) staining on samples from all groups at 4 and 6 weeks. Magnification: 4x (scale bar = 100 µm).

3.5.4.2 Mineral Precipitation on Mg Surface vs. Mg Corrosion Rate

Figure 9 illustrates the calculated percentage difference of each rod volume before and after implantation. We observed the highest volume difference at both time points from the MGP group and the lowest from the Mg only and collagen gel groups. Interestingly, volume difference of the HEK293 group was 2 magnitudes higher at week 6 relative to week 4. We conclude that MGP reduced the mineral layer that deposited on the metal surface, leading to decreased Mg corrosion protection, and thus caused a greater loss in rod volume after *in vivo* implantation.

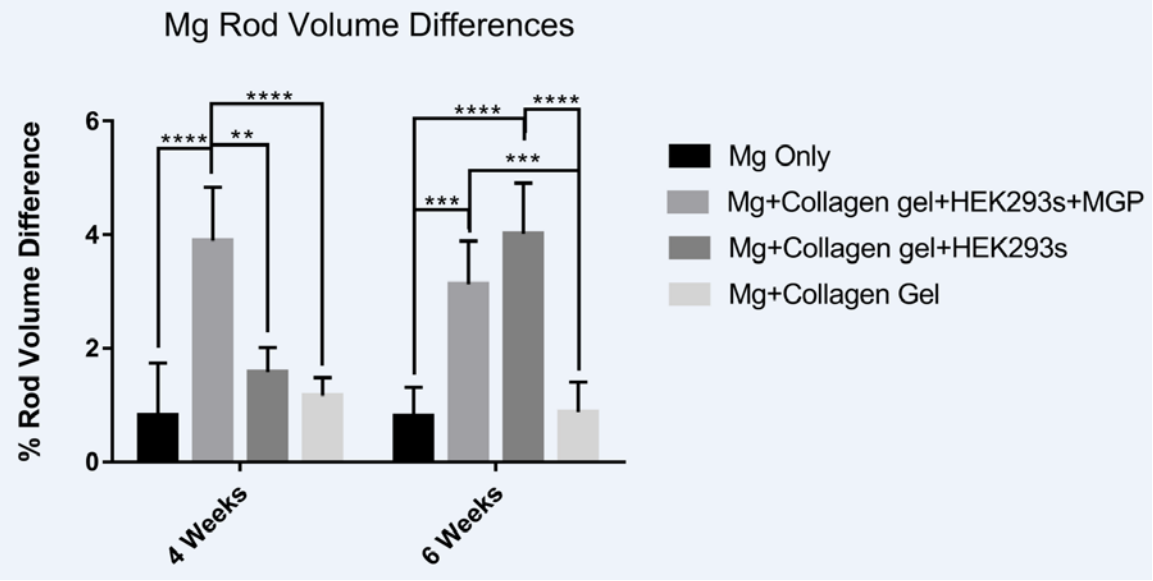

Figure 9. MicroCT analysis showing Mg rod volume difference

Mg rod volume percentage difference was calculated using microCT analysis.

3.6 Discussion

In this study, we showed in both *in vitro* and *in vivo* models that calcium phosphate deposition on Mg-based metals can be reduced significantly by exogenous MGP secreted locally by nearby cells. Researchers have shown that MGP is involved in the inhibition of spontaneous apatite crystal formation, which contributes to pathological calcification [131]. MGP contains 5 γ-carboxyglutamic acid (Gla) residues in its protein sequence; and Gla has been linked to the binding of Ca ions. Luo et al. [137] showed that MGP knockout mice born without MGP die within two weeks due to arterial calcification and rupture. However, MGP knockout mice with genetic rescue of arterial MGP expression remained healthy. Price et al. [139] reported that cultured elastic lamellae from rat aortas in high-phosphate medium for 9 days with or without warfarin, an

antagonist of vitamin K and thus an inhibitor of MGP secretion. Results showed increased calcification when warfarin was added into the culture medium. However, addition of 100 µg/mL of MGP to the culture medium, completely prevented warfarin-induced calcification in a 4 mm living artery. It has been proposed that MGP forms a complex with ambient calcium, prevents calcium supersaturation, and binds with hydroxyapatite to prevent crystal growth [134]. Our study is the first to test the function of MGP on controlling mineral deposition on a metal implant. Overexpression of MGP from transfected cells, regardless of their origin of the cells serving as the protein delivery vehicle, showed reduced mineral deposition and apatite growth on the metal surface and surrounding tissues both *in vivo* and *in vitro*, and thus confirmed our hypothesis that MGP is capable of reducing mineralization on Mg surface.

The ability to control mineral deposition on Mg allowed us to explore the effect of the calcium phosphate mineral layer on metal corrosion. Several studies have deliberately coated calcium phosphate onto Mg and other degradable metals to control the metal corrosion rate for the use of materials in orthopedic applications [63, 113, 170, 171]. The extent of Mg corrosion was determined by the volumetric microCT analysis of Mg rods before and after *in vivo* implantation (Figure 9). A higher percentage of rod volume change indicated an increased metal corrosion. We observed a higher volume change at both time points in the MGP group when compared to other groups. At the same time less mineral deposited on the implants in the MGP group in the biological environment. These observations imply that Mg degradation products, as well as the calcium phosphate deposits, provide a passivating layer for the metal core, which slows down Mg corrosion. Without this protective layer, Mg corrodes much faster, as demonstrated by the differences in rod volume reduction between MGP and Mg only groups. An *in vitro* study conducted by Wagener and Virtanen has tested Mg in different culture conditions and suggested

that the Mg corrosion resistance depends on the morphology, not the thickness, of the formed layer under different conditions [172]. It is well known that Mg degradation rate differs across *in vitro* and *in vivo* environments. The abundance of different ions, proteins, cells in the biological environment, as well as the anatomical location of the implant may induce changes in mineral deposition when compared to *in vitro* testing. Our *in vivo* experiments shown an inverse correlation between the Mg implant corrosion and the volume of the mineral precipitate. This difference was especially noticeable between MGP and Mg only groups. The collagen gel group showed a small and similar rod volume difference compared to the Mg only group, presumably due to breakdown of the collagen gel. Interestingly, the HEK293 group displayed a small volume change at week 4 that increased significantly by week 6. We presume that the cause of the large volume increase in the HEK293 group at week 6 is different than that in MGP group. Other studies have demonstrated that proteins have an impact on Mg-based biodegradable metal corrosion rates [173]. In the present study, several proteins may have been secreted from HEK293 cells and absorbed onto the implant surface, hence accelerating the metal corrosion and contributing to the large volume difference detected at the later time point.

Bowen and colleagues have proposed a long-term corrosion mechanism for bioabsorable materials including Mg alloys [115]. From mass transport and ion exchange aspects, they have suggested that a quasi-steady state happens at 3 weeks, during which metal corrosion decreases due to the developed apatite layer that protects the metal core. At the terminal stage, the Mg/O corrosion layer becomes unstable, but the precipitated hydroxyapatite remains and is more crystallized. Also reported by Patil et al., initial corrosion burst usually occurs over the first 24 hrs, then slows down and remains stable *in vivo* for weeks thereafter [174, 175]. Therefore, if we significantly reduce at an early stage the initial mineral deposit that would later become

hydroxyapatite, we could greatly reduce the terminal stage mineral crystallization when the metal core finally breaks down. A similar theory was proposed by Lee and colleagues [116]. Amorphous calcium phosphate appears first on the Mg metal surface before transforming to a thermodynamically more stable crystalline hydroxyapatite.

We used a collagen scaffold to incapsulate the cells that secrete MGP near the Mg metal in the *in vivo* study. Collagen is a natural polymer that has long been studied as a drug carrier [50, 51], and used in vascular tissue engineering since it is a major component of the vascular extracellular matrix (ECM) [52, 53, 55]. After *in vivo* implantation, collagen is enzymatically degraded in the body within 6-8 weeks [50, 57]. Its biodegradability, biocompatibility, and 3D structure are ideal for cell growth and differentiation for our study. In this study, 4 mg/mL collagen gel was used, since higher concentrations has been shown to yield heterogeneous hydrogel due to high viscosity [176]. The collagen gel can significantly impede diffusion of the ions and molecules [177]. In our study, collagen scaffold surrounding the Mg rod hindered the mineral deposition (Figure 6C), but not corrosion, as the rod volume difference in the Gel group were similar to the Mg only group at both time points (Figure 9). This suggests that the gel slowed down the diffusion of mineral ions but not water to the surface of the implant.

Our results demonstrate the feasibility of using MGP for reducing mineral deposition on Mg implantable devices. Our future experiments will focus on the translational aspect of MGP drug delivery system for Mg metal implants. One approach would be to incorporate MGP peptides containing Gla residues, instead of the full protein, in a polymer coating on the metal device that will be released in a sustained fashion. These MGP peptide containing sites of γ-carboxyglutamate (GLA) were shown by O'Young et al., to reduce mineral deposition [144].

The results of this study suggest that the corrosion resistance of the metal can be compromised significantly when the mineral layer is reduced. Metals without deposited minerals will degrade much faster than those covered by minerals. Thus, metal degradation rate should be taken into consideration during the device design process, because reducing the mineral layer could cause faster break down of the metal core.

3.7 Conclusion

Our study demonstrates that mineal precipitation on the Mg implant surface can be significantly reduced by local delivery of MGP. Moreover, the higher Mg metal volume loss in the MGP group suggests that the mineral layer may serve as a protective shield that slows down metal corrosion. This study has potential to inform the design of biodegradable Mg medical implants for soft tissues. Additionally, our results further expand our insight into the relation between mineral deposition and Mg metal degradation, thus increasing the understanding of the mechanism of Mg degradation to enhance cardiovascular and orthopedic applications.

4.0 Local Release of Magnesium and CGRP Enhances Osteogenic Differentiation of Periosteum

4.1 Acknowledgements

The work presented in this chapter was supported by the University of Pittsburgh's Center for Craniofacial Regeneration. MicroCT file processing was done on a system supported by NIH S10-OD021533 Shared Instrumentation Grant. All work was done in collaboration with Dr. Samer H. Zaky, Dr. Jin Gao, Rong Chong, Lyudmila Lukashova, Chu-Chih (George) Hung, Dr. Liu Kai, Dr. Giuseppe Intini, and Dr. Charles Sfeir. The authors are greatly indebted to the support and excellent assistance of Dr. Daniel Bain, Department of Geology and Environmental Science at the University of Pittsburgh, for the use of ICP machine, Dr. Hajime Yamazaki, Department of Oral Biology at the University of Pittsburgh, for tissue harvesting. Dr. Yingfei Xue, Department of Pharmaceutical Sciences at the University of Pittsburgh, for assistance with electrospinning. Dr. Denise J. Deverts, School of Dental Medicine, University of Pittsburgh, for editing this manuscript.

4.2 Detailed Abstract of Periosteal Differentiation

Magnesium (Mg) has been reported to induce osteogenic differentiation of various cell types. In previous *in vivo* studies, we observed bone regeneration around Mg-based implants below the periosteum. To understand the effect of Mg on periosteal cells, we harvested and cultured

mouse and human periosteal cells, and exposed them to increased Mg^{2+} concentration. Mg^{2+} has been shown to facilitate the process of fracture healing by stimulating local production of calcitonin gene-related peptide (CGRP). Thus, we explored the direct effect of Mg^{2+} on osteogenic induction of periosteal cells, compared to CGRP. We found that expression of osteogenic genes and proteins was both cell- and concentration-dependent. Alkaline phosphatase activity and Alizarin Red staining were both regulated by CGRP and $MgSO_4$. We then electrospan Mg metal nanopowder and CGRP into PLGA nanofibers, and implanted in male and female rat calvaria defect model with or without periosteum for one month. Harvested samples were analyzed using microCT and histology. CGRP+ and Mg+ periosteum groups generated a greater volume of new bone compared to control groups (empty defect and PLGA scaffold only). In conclusion, this is the first study to compare the effect of Mg and CGRP on mouse and human periosteal cells. Our *in vivo* results also indicated that the direct release of Mg and CGRP are able to induce the differentiation of rat periosteal cells to form new bone. Furthermore, we have developed novel electrospun PLGA scaffolds that release Mg metal powder and CGRP that facilitate cranial repair in rat calvarial defect.

4.3 Introduction

More than 6.3 million Americans each year experience one or more bone fracture [178], and this number is expected to rise as the average age of the population continues to increase. In many cases, internal fixation devices are required to stabilize the fracture. Current devices, including bone screws and plates, are fabricated primarily using permanent and inert metals, such as titanium and surgical stainless steel [179, 180]. While these materials satisfy the mechanical

load-bearing requirement, they also put patients at risk for post-surgical complications such as stress shielding, inflammation and infection, and the need to undergo a second surgery to remove the implant [8, 11, 60]. Given the continually increasing incidence of bone fracture in the population, it is imperative to identify alternative implant materials that can reduce or even eliminate the risk for these complications and thus improve patient outcomes.

Degradable biomaterials, such as magnesium (Mg) and its alloys, represent promising, lower-risk alternatives to titanium and steel, and already are being used in the fabrication of orthopedic and cardiovascular devices [2, 7-9]. Mg is an essential trace element in the human body that has been found to play a critical role in multiple physiologic processes including those related to osteogenesis. For example, an *in vitro* study found that adding Mg^{2+} to cultured human bone marrow stromal cells stimulated the intracellular signaling pathway, leading to enhanced extracellular matrix (ECM) mineralization and bone regeneration [95]. Similarly, cell proliferation has been found to increase when human mesenchymal stem cells are cultured in medium containing Mg powder [94].

In a previous study, our group demonstrated that the observed facilitative effect of Mg on osteogenic activity *in vitro* can be extended to physiologic repair of fractured bone *in vivo* [30, 31]. Briefly, we used Mg alloy to fabricate bone screws and plates, which were then used to repair experimental fracture sites on rabbit ulnae. After 8 and 16 weeks of *in vivo* implantation, x-ray microtomography analysis revealed a layer of newly regenerated subperiostial bone in proximity to the Mg device [30, 31].

Formation of new bone around the implanted Mg screws and plates raises the possibility that Mg^{2+} can stimulate osteogenesis of the periosteum and thus induce cell differentiation and local bone regeneration. Support for this hypothesis is provided by a recent study in which Mg

pins were implanted in the intramedullary space of rat femora [29]. Zhang and colleagues reported that Mg^{2+} released from the device could induce the production of calcitonin gene-related peptide-α (CGRP) on periosteum, which further contributed to bone fracture healing [29].

Based on the collective findings of the aforementioned research, we hypothesized that the Mg facilitates osteogenesis *in vivo* both indirectly through induction of CGRP as well as directly via stimulation of osteogenic differentiation of mesenchymal progenitor cells or periosteal derived cells (PDCs). PDCs, which can be found in large numbers within the inner cambium layer of the periosteum, are critical to the process of bone repair and remodeling [181]. Periosteum envelops the majority of bone surfaces; and when bone is fractured, the periosteum is injured as well. It is the response of periosteum to injury that initiates the bone-repair process [182].

For the present report, we tested our hypothesis using both *in vitro* and *in vivo* methods. For the in vitro experiment, we harvested and characterized mouse and human periosteum, and then cultured these PDCs with varying concentrations of Mg^{2+} and CGRP. To test our hypothesis, in vivo, we developed a 3D poly (lactic-co-glycolic acid) (PLGA) scaffold for the slow release of Mg^{2+} and CGRP into the periosteum. PLGA is a widely used degradable polymer that has been approved by the U.S. Food and Drug Administration (FDA) for clinical use, applied mainly for drug delivery and implantable devices [43, 183]. Its degradation rate can be tailored specifically for the intended applications, by adjusting the ratio between lactic and glycolic acid and its molecular weight: PLGA degrades slower with higher lactic acid content and molecular weight [184]. We used electrospinning, an electrostatic fiber fabrication technique, to shape PLGA supplemented with Mg metal nanopowder and CGRP into uniform 3D nanofibers. The utility of electrospun PLGA for the fabrication of biodegradable scaffolds is well-supported. The overlaying structure of the PLGA fibers closely mimics the extracellular matrix, providing tunable porosity,

high surface area to volume ratio, better support to the cells, and stronger cell adhesion [185-187]. After determining the release profile of Mg^{2+} and CGRP from the PLGA nanofibers, we implanted the scaffolds in rat calvaria defect model to observe bone regeneration. Here we report the osteogenic effect of Mg^{2+} on periosteum and PDCs, thus shedding light on the processes underlying the formation of new bone adjacent to Mg bone implants.

4.4 Materials and Methods

4.4.1 Isolation and Culture of Mice and Human PDCs

Femora of C57BL/6 male mice were dissected. Periosteum from mid-shaft to distal femur was collected and put into digestion medium, which is the Gibco MEM alpha minimum essential medium (α-MEM) supplemented with type I collagenase (1 mg/mL), 1% pen strep, and 1% GlutaMax (ThermoFisher Scientific, MA, USA). The periosteum was digested in a 37°C incubator for 1 hr. Supernatant was collected and filtered through a 70 μm cell strainer. Filtered medium containing cells was centrifuged (1,000 g for 5 min) before plating at a cell density of 1,000 cells/cm^2. Cells were cultured using maintenance medium, which is α-MEM supplemented with 10% FBS, 1% pen strep, and 1% GlutaMax, in a humidified condition at 37°C and 5% CO_2.

Human periosteum was obtained from the dental clinic of the University of Pittsburgh, during periodontal connective tissue graft surgical procedure. Samples were harvested from 2 healthy donors, following informed consent. Periosteum (approximately 3x1 mm) was scraped directly off the palatal bone of the patient and transferred immediately into Falcon tubes containing

alpha Modified Eagle Medium (α-MEM) supplemented with 1% pen strep and 1% GlutaMax. After rinsing twice in PBS with 1% pen strep, periosteum was digested as described above and the human PDCs were collected. Human PDCs were cultured in maintenance medium, which was α-MEM supplemented with 10% FBS, 1% pen strep, and 1% GlutaMax, in a humidified condition at 37°C and 5% CO_2.

The use of these human periosteal tissues for this study received a non-human subject determination from the University of Pittsburgh Institutional Review Board.

4.4.2 Cell Characterization

All antibodies and isotype controls for flow cytometry were purchased from BioLegend (San Diego, CA) unless otherwise specified.

A portion of the cultured cells were trypsinized and resuspended in cold PBS at a concentration of 1x 10^6 cells/mL. After rinsing, antibodies (listed in Table 3) were diluted in FACS staining buffer, which contains 1% BSA and 0.1% sodium azide diluted in PBS, and added into the cells for 20 min incubation. Stained cells were fixed in the mixture of formalin and PBS for 30 min. Cells were washed twice before resuspended in 300 μL FACS buffer for flow analysis.

Table 3. Antibodies and the corresponding fluorochromes used in flow cytometry to characterize the cells

Instrument: IMM Fortessa		
Antibody/Probe	Fluorochrome	Vendor/Cat. No./Clone
Anti-mouse CD90	PE/Cy7	BioLegend/#105325/30-H12
Anti-mouse CD34	APC	BioLegend/#128611/HM34
Anti-mouse CD45	Pacific Blue	BioLegend/#103125/30-F11
Anti-human CD90	Alexa Fluor 700	BioLegend/#328119/5E10
Anti-human CD34	PE	BD Pharmingen/#55822/581
Anti-human CD45	PE-Cyanine5	eBioscience/#15-0459/HI30

The strategy to isolate periosteal cells was based on previous research showing that mesenchymal stem cells are positive for CD90 and CD105 and negative for CD34 and CD45 [188-191]. The same markers have also been suggested to identify PDCs [29, 190]. Periostin has also been shown to be highly expressed in skeletal stem cells from periosteum [192].

Immunocytochemistry was also used to characterize the cells. Cells were plated in a 24-well plate with a density of 0.5 x 10^5 cells/well. 48 hr after plating, cells were fixed in 4% paraformaldehyde for 20 min at room temperature. After rinsing in PBS, cells were blocked in 3% donkey serum for 1 hr. Cells were then incubated in primary antibody against CD105 (Abcam, ab107595) diluted in blocking buffer overnight at 4°C, followed by Alexa Fluor 488 donkey anti-rabbit IgG (Life technologies, A21206) secondary antibody incubation, with a dilution of 1:2000 in blocking buffer. After washing the cells with PBS, a drop of DAPI fluoromount medium (Southern Biotech, AL, USA) was added onto the cells to mount the cover glass. Cell characterization was also performed by Western blotting using CD105 and periostin (NBP1-30042, Novus Biologicals, Colorado) antibodies.

4.4.3 Experimental Treatments of PDCs

Varying concentrations of $MgSO_4$ (1.2 mM, 5 mM, 10 mM, and 15 mM) were added in osteogenic induction medium, which is Eagle's minimal essential medium (DMEM) supplemented with 10% FBS, 1 nM dexamethasone, 50 μM ascorbic acid, and 20 mM β-glycerol phosphate.

4.4.4 Western Blot Analysis

Mouse and human PDCs were plated in 6-well plates at a density of $3.5x10^5$ cells/well. After 24 hr, cells were treated with various concentrations of $MgSO_4$ for 3 days. At the end of the treatment, cells were harvested for Western blotting analysis. Antibodies against human SP7/Osterix (R&D Systems, MAB7547) and Runx2 (Santa Cruz, sc-390351) were diluted in 1:500 in blocking buffer for incubation of the membranes overnight at 4°C, followed by 1hr incubation of HRP-conjugated secondary antibody (dilution of 1:2,000 in blocking buffer). After washing the membranes with TBST, HRP signals were detected using an enhanced chemiluminescent substrate (Thermo Fisher Scientific, IL, USA).

4.4.5 Alkaline Phosphatase (ALP) Assay

Alkaline phosphatase (ALP) is a marker of osteogenic activity. Its expression has been associated with osteoblast differentiation [193]. We quantitatively measure the concentration of ALP expression using the SensoLyte ρNPP ALP assay kit (AnaSpec, California, USA). In brief, PDCs were plated in 12-well plates in a density of $1x10^5$ cells/well. After 1 and 2 weeks of treatment in 12-well plates with biological triplicates, PDCs were first washed twice with dilution buffer before lysed. Cell suspension was incubated at 4°C for 10 min under agitation, and centrifuged at 2500 g for 10 min. 25 µL of standards and samples were first pipetted into a 96-well plate. Immediately after, 25 µL of ρNPP substrate was added into each well containing standards and samples. Mixture was incubated in a dark room for 30 min before reading the absorbance with a plate reader at a wavelength of 405 nm. Total concentrations of protein from the cell lysate were

also determined using the bicinchoninic acid (BCA) assay (Pierce BCA protein assay kit, ThermoFisher Scientific, MA) to normalize the ALP readings.

4.4.6 Quantitative Polymerase Chain Reaction (qPCR) Assay

Mouse and human PDCs were plated in 6-well plates at a density of $1x10^6$ cells/well and treated with osteogenic induction medium, 1.2mM, and 10mM Mg^{2+} supplemented in osteogenic induction medium. Total RNA extraction and purification were performed using RNeasy Mini Kit (Qiagen, Valenia, CA) following manufacturer's instructions. The quantity and quality of the extracted RNAs were measured using NanoPhotometer (Implen, p330). Samples were used only if the quality of absorbance readings 260/280 were higher than 1.5, and 260/230 were between 1.8 and 2.0. The extracted RNAs were reverse transcribed to cDNA and amplified using TaqMan RNA-to-CT 1-Step Kit (Applied Biosystems, 4392938). qPCR was performed using StepOnePlus Real-Time PCR Systems (Applied Biosystems) under repeated thermal cycling conditions consisting of 95°C denaturing for 15 sec and 60°C annealing for 60 sec. FAM-MGB TaqMan probes (Thermo Fisher Scientific, IL, USA) of each gene are listed in Table 4. Eukaryotic 18S (Applied Biosystems, 4352930E) was selected to be the endogenous control. Samples from each group were triplicated. Following the RNA extraction, a technical triplicate was performed for the qPCR analysis. A total of 9 samples were used for each gene and treatment. Relative quantification results were obtained by calculating the ΔΔCT and plotted in fold changes.

Table 4. FAM-MGB TaqMan probes used in qPCR

Species	Gene	Protein	Assay ID
Mouse	BGLAP	Osteocalcin	Mm03413826_mH
Mouse	COL1A1	Collagen 1	Mm00801666_g1
Mouse	IBSP	Bone Sialoprotein	Mm00492555_m1
Human	BGLAP	Osteocalcin	Hs01587814_g1
Human	COL1A1	Collagen 1	Hs00164004_m1
Human	IBSP	Bone Sialoprotein	Hs00173720_m1

4.4.7 Alizarin Red S Staining

Mouse and human PDCs were plated in a 6-well plate at a density of 3.5 x 10^5 cells/well in growth medium. 24 hr after plating, the medium was switched to osteogenic induction medium with the addition of various $MgSO_4$ concentrations and 10^{-10} M CGRP, with three biological replicates per group. After 21 days of treatment, cells were fixed in 10% formalin for 1 hr and washed with deionized and distilled water. A solution of 2% Alizarin Red S (Electron Microscopy Sciences, PA, USA) dissolved in 2% ethanol was adjusted to pH of 4.2 and used to detect the extracellular calcium deposits produced by the PDCs. Cells were stained with 2% Alizarin Red S solution for 20 min. The stain was removed and washed with distilled water repeatedly after incubation.

4.4.8 Electrospinning

High molecular weight (54,000- 69,000) poly (lactic-co-glycolic acid) (PLGA, Sigma-Aldrich, MO) was dissolved in hexafluoroisopropanol (HFIP) to make 16% PLGA solution. After rotating on a rotator at room temperature overnight, 100 mg of Mg metal nanopowder (800 nm, 99% metal basis, US Research Nanomaterials, Inc. TX, USA) was added into 1 mL of PLGA solution. The mixture was sonicated for 30 min before rotating for another 4 hr before electrospinning. Similarly, 10^{-8} M CGRP mixed in water was added to 1 mL of PLGA solution, rotated in 4°C overnight, and sonicated for 15 min before spinning. The apparatus for electrospinning consists of a syringe pump with the clamp and the ground collector for the deposited fibers. A high voltage source connects the needle tip and the collector (Figure 10). 1 mL of Mg nanopowder/PLGA solution was dispensed into a syringe of 12.45 mm diameter and clamped onto the pump, which was set with 18 kV voltage and 1 mL/hr pumping rate. The distance between the tip of the needle and the ground collector was adjusted to 15 cm. PLGA scaffolds were stored in vacuum overnight to allow evaporation of HFIP before further processing.

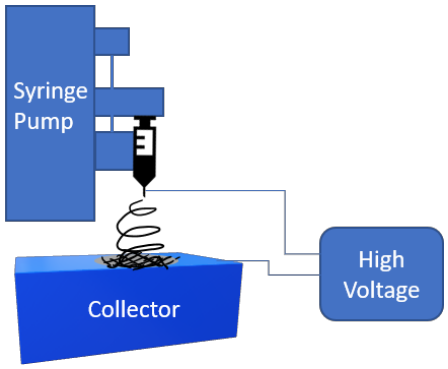

Figure 10. Schematic of electrospinning setup

4.4.9 In Vitro Release Study of the Electrospun Scaffold

Electrospun PLGA fiber sheets were punched into 5 mm diameter circular scaffolds using a multi-size hole punch (McMaster-Carr, Elmhurst, IL). The scaffolds including either Mg metal nanopowder or CGRP solution were placed in 1 mL PBS solution in a 1.5 mL microcentrifuge tube and rotated on a rotator in 37°C incubator. Samples were collected after first hour and once daily until complete degradation of the scaffold. At each time point, 500 μL of the PBS solution was collected from each tube and replaced with 500 μL fresh PBS. For scaffolds containing Mg metal nanopowder, 100 μL of samples were 50x diluted in 2% filtered nitric acid and measured for Mg ion concentration using an inductively coupled plasma mass spectrometry (ICP-MS) machine (NexION 300X, PerkinElmer, MA). For scaffolds containing CGRP solution, protein concentration was analyzed using enzyme-linked immunosorbent assay (CGRP EIA kit, Cayman Chemical, MI). Sample size was three for each group.

4.4.10 Rat Calvaria Defects Implantation

All protocols for the animal surgeries were approved by the University of Pittsburgh Institutional Animal Care and Use Committee. All samples were sterilized by UV irradiation prior to implantation. 16 male and 14 female, Sprague-Dawley rats (Charles River, USA) with 7-9 weeks of age were used in this study. Two rats were housed in each cage in a controlled environment. Rats were randomly assigned into 8 testing groups: empty defect controls +/- periosteum (abbreviated as Empty -, Empty +), PLGA scaffolds +/- periosteum (PLGA -, PLGA +), PLGA scaffolds electrospun with Mg metal nanopowder +/- periosteum (Mg -, Mg +), PLGA scaffolds electrospun with CGRP solution +/- periosteum (CGRP -, CGRP +). Two samples were

implanted in each rat. Each control group has seven samples (three in female and four in male rats), and each experimental group has eight samples (four in female and four in male rats). Rats were anesthetized with isoflurane through a nosecone. A 2 cm incision on the skin and the fascia underneath was created by blunt dissection. Periosteum above the bone was carefully retracted. Two circular defects, each 5 mm in diameter, were cut by a trephine in parallel on either side of the sagittal suture in the bone of the cranium. The scored calvaria was removed by lifting from the edge by an elevator. Sample was filled into each empty defect. Periosteum was sutured on top of the implant in groups containing the membrane, and removed in groups without periosteum. The fascia and incision was closed with sutures. After 1 month, rats were anaesthetized and euthanized. Calvaria and the soft tissue around the defects was explanted and fixed in buffered 10% formalin.

4.4.11 High Resolution Micro-Computed Tomography (µCT) Analysis

Explants were immersed in 70% ethanol before placing in a 34 mm diameter tube and scanned in high resolution µCT 50 compact cabinet microCT scanner (Scanco Medical, Brüttisellen, Switzerland) with voltage set at 55 kVp and current at 145 mA. 17.2 µm voxel size, 0.36 degrees rotation step (180 degrees angular range) and an 800 ms exposure per view were used for the scans which were performed in 70% ethanol. New bone volume in the rat calvaria defect was evaluated using the CTAn software. A 5 mm diameter circular region of interest (ROI) was drawn in the defect area on sequential slices. Volumes were segmented using a global threshold of 0.5 g HA/cc. Scanco µCT software OpenVMS (HP, DECwindows Motif 1.6) was used for 3D reconstruction, viewing of images, and creating 3D renderings.

4.4.12 Histology Assessment

Mg rods and the surrounding tissues were fixed in 10% formalin after harvesting, and before being embedded and polymerized in Osteo-Bed Plus (Polysciences, PA, USA) following manufacturer's instructions. All blocks were cut into sections of 5 μm thickness, which was attached on Tesa tapes (Beiersdorf, Germany), using a RM2255 microtome (Leica, Benshiem, Germany) with a tungsten carbide blade (ThermoFisher Scientific, USA) and placed in a tissue embedding cassette. Tissue sections on tapes were stained directly. Before each staining, sections were deacrylated in xylene twice, and 2-methoxyethylacetate for 20 min, followed by a series of decreasing percentages of ethanol and finally water for rehydration.

4.4.12.1 Goldner's Trichrome Staining

Goldner's trichrome staining was used to visualize new bone formation in the calvaria defect. All reagents for Goldner's trichrome staining were purchased from Electron Microscopy Sciences (Hatfield, PA). In brief, rehydrated samples were placed in hematoxylin for 20 min, rinsed in distilled water before being immersed in Ponceau-acid fusion for 5 min, followed by 1% acetic acid. Samples were transferred into orange G-phospho solution for 2 min before being rinsed with 1% acetic acid. Samples were then stained in light green solution for 20min for mineralized bone, and then rinsed in 1% acetic acid. Finally, samples were dehydrated in absolute alcohol, cleaned in xylene, and mounted with mounting medium.

4.4.12.2 Immunohistochemistry

Immunostaining with CGRP antibody (Abcam, Cambridge, UK) was used to detect the presence of CGRP around the rat calvaria defect on each tissue section. Briefly, each tissue section

was incubated in 2% donkey serum for 1 hr at room temperature before incubating in CGRP antibody overnight at 4°C. After washing in PBS for 5 min, each section was incubated with donkey anti-goat secondary antibody (Alexa Fluor 594, Abcam) for 1 hr. The section was then mounted with mounting medium containing DAPI (Vector Laboratories Inc, Burlingame, CA), and dried in 4°C overnight before imaging. CGRP expression from each tissue section was observed under an inverted microscope (Eclipse TE2000-E, Nikon Instruments, Japan).

4.4.13 Statistical Analysis

A mean value and standard deviation were calculated from three female and four male rats in control groups (empty and PLGA only), and four female and four male rats in experimental groups (Mg and CGRP). Statistical analysis was conducted using Graph Pad Prism 6 software. Differences between groups were tested with two-tailed t-test and one-way analysis of variance (ANOVA) at a 95% confidence interval, followed by Tukey multiple comparisons and post-hoc test. Statistical significance was set at $P<0.05$.

4.5 Results

4.5.1 Periosteal Cells Characterization

Our FACS (Figure 11A) analysis, based on the strategy described in Materials and Methods section, showed that CD34-APC stained mouse PDCs plotted against CD45-pacific blue to be 98.9% negative and CD90-PE-Cy7 stained mouse PDCs plotted against CD45-pacific blue to be

99.6% positive. Human PDCs were also analyzed using FACS (figure 11B): CD34-PE and CD45-PE-Cyanine5 were stained 97.7% negative, and 99.1% CD90-Alexa Fluor 700 positive for human PDCs. As expected, CD105 and periostin were detected around 70 KDa and 100 KDa, respectively, from mouse and human PDCs lysates by Western blotting (Figure 11C). Immunostaining (Figure 11D) also showed CD105 expression from both mouse and human PDCs. These findings are consistent with previous research confirming that these cells are derived from the periosteum [29, 188-191].

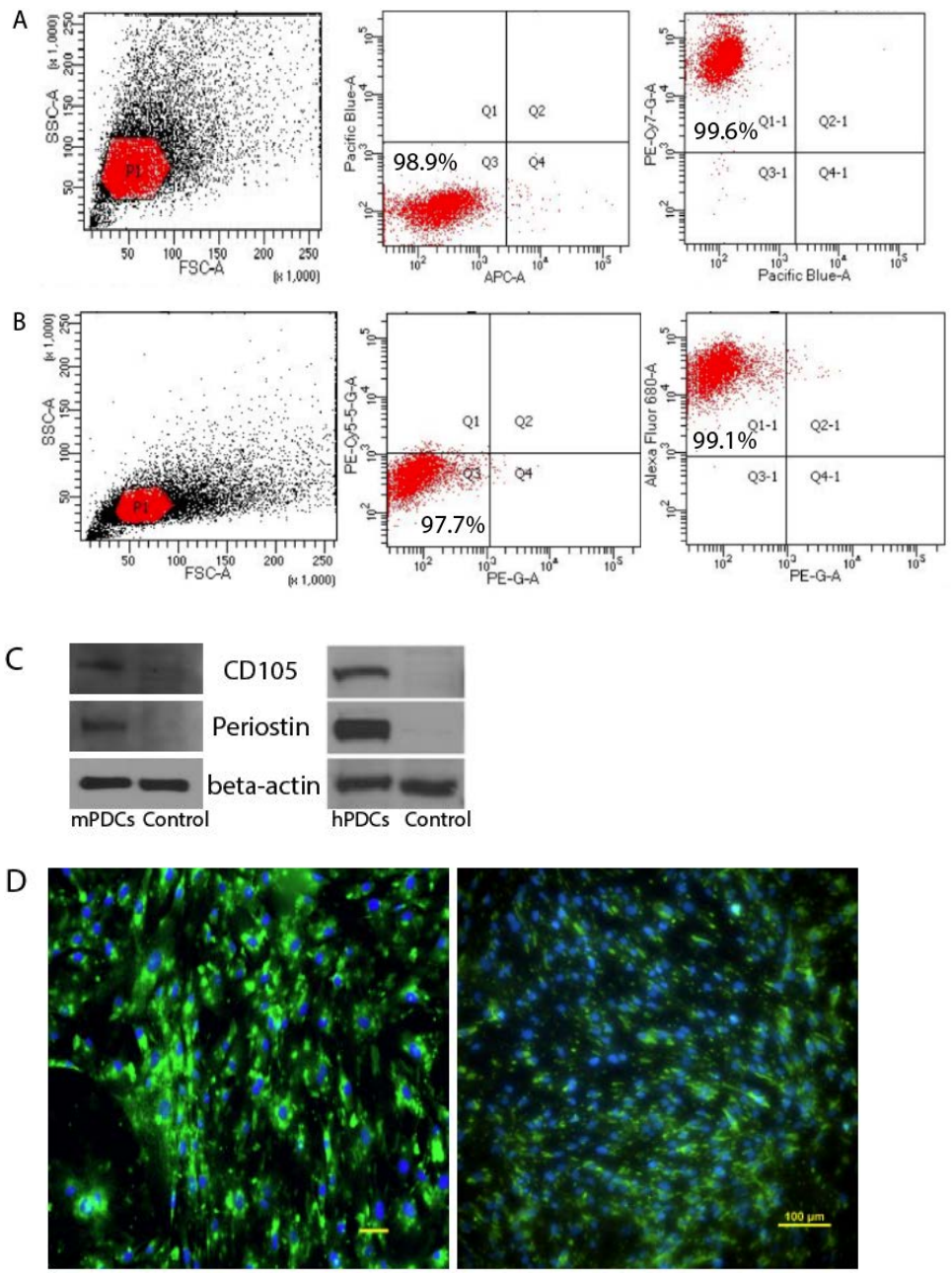

Figure 11. FACS, immunoblotting, and immunohistochemistry characterizing mouse and human PDCs

FACS using cell surface markers CD34, CD45, and CD90 were used to identify mouse (A) and human (B) PDCs. CD105, another common positive marker for PDCs, was also detected in mouse and human PDCs by Western blotting (C) and immunohistochemistry (D, mouse left, human right).

4.5.2 ALP Activities Elevated by Different Concentrations of Mg^{2+} and CGRP

ALP acts as an early indicator of the osteoblast differentiation [194]. As shown in Figure 12A, ALP activities measured from mouse PDCs increased after treated with 10^{-10} M and 10^{-8} mM of CGRP for 1 week, but decreased by the end of 2 weeks. Similarly, ALP activities measured from human PDCs (Figure 12B) increased significantly after treated with 10^{-12} M and 10^{-10} M of CGRP for 1 week, but continued to increase even after 2 weeks of treatment.

Effect of Mg^{2+} concentrations on ALP levels of mouse PDCs are shown in Figure 12C (left: 1 week; right: 2 weeks). Compared to osteogenic control, at 1 week, 15mM Mg^{2+} increased the ALP levels significantly in mouse PDCs. At 2 weeks, increasing Mg^{2+} in osteogenic medium induced continued increase of ALP in mouse PDCs, compared to osteogenic control.

The effect of Mg^{2+} concentrations on ALP levels of human PDCs are shown in Figure 12D. Evaluated on the same scale (left: 1 week; right: 2 weeks), ALP levels increased after both time points compared to osteogenic control. However, the increase became smaller after 2 weeks, except from 15mM Mg^{2+} treatment. We have also measured the quantitative ALP levels from mouse and human PDCs cultured in maintenance medium supplemented with increasing concentrations of Mg^{2+} (Supplemental Figure 3). Results showed that Mg^{2+} was able to induce osteogenic differentiation of mouse and human PDCs without the osteogenic induction.

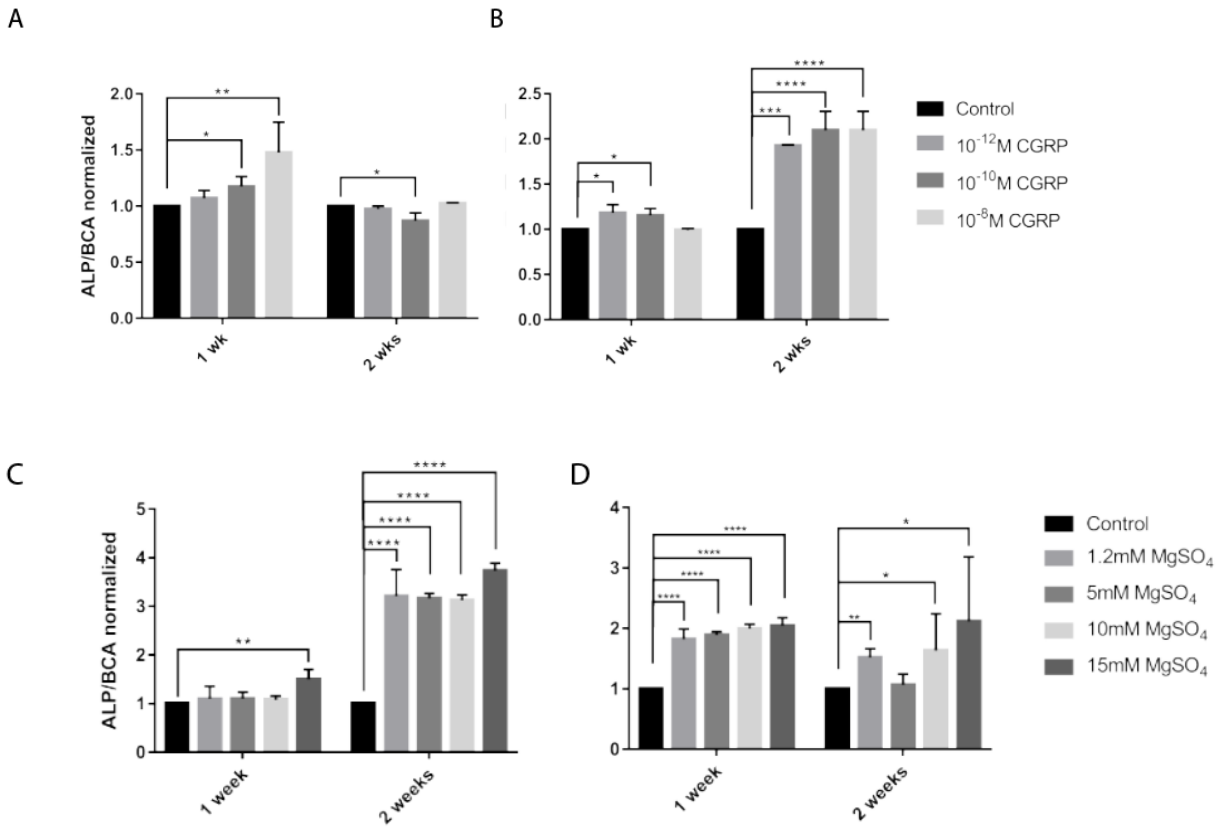

Figure 12. ALP activities of mouse and human PDCs after 1 and 2 weeks of CGRP and Mg^{2+} treatment

ALP levels were measured from mouse (A) and human (B) PDCs after CGRP treatment for 1 and 2 weeks. ALP levels were also measured from mouse (C) and human (D) PDCs after treated with Mg^{2+} for 1 and 2 weeks.

4.5.3 Protein Expressions Enhanced by Mg^{2+} and CGRP in Medium

Runt related transcription factor 2 (Runx2) and Osterix (also known as SP7) are two transcription factors that play a crucial role in the early stage of osteoblast differentiation [195-197]. Western blot results revealed that after 3 days, Runx2 and Osterix expressions were increased by Mg^{2+} in a concentration-dependent manner. As shown in Figure 13A, levels of expression from mouse PDCs (left) increased gradually and reached the maximum at 5mM $MgSO_4$, then decreased as Mg^{2+} increased. However, Runx2 and Osterix expressions from human PDCs (right) continued

to increase as Mg^{2+} concentrations increased, reaching the maximum at 15mM. Sulfate controls did not elicit remarkable change from both protein expressions. Human PDCs were also treated with higher Mg^{2+} concentrations (up to 50mM) in maintenance medium (Supplemental Figure 2). Results are in accordance with those presented here: higher level of osteogenic protein expression were obtained at higher concentrations (15mM and 25mM), but dropped at 50mM. Moreover, Figure 13B shows that human PDCs (right) expressed higher levels of both osteogenic proteins at higher CGRP concentration, while mouse PDCs (left) did not show noticeable change in response to all CGRP concentrations.

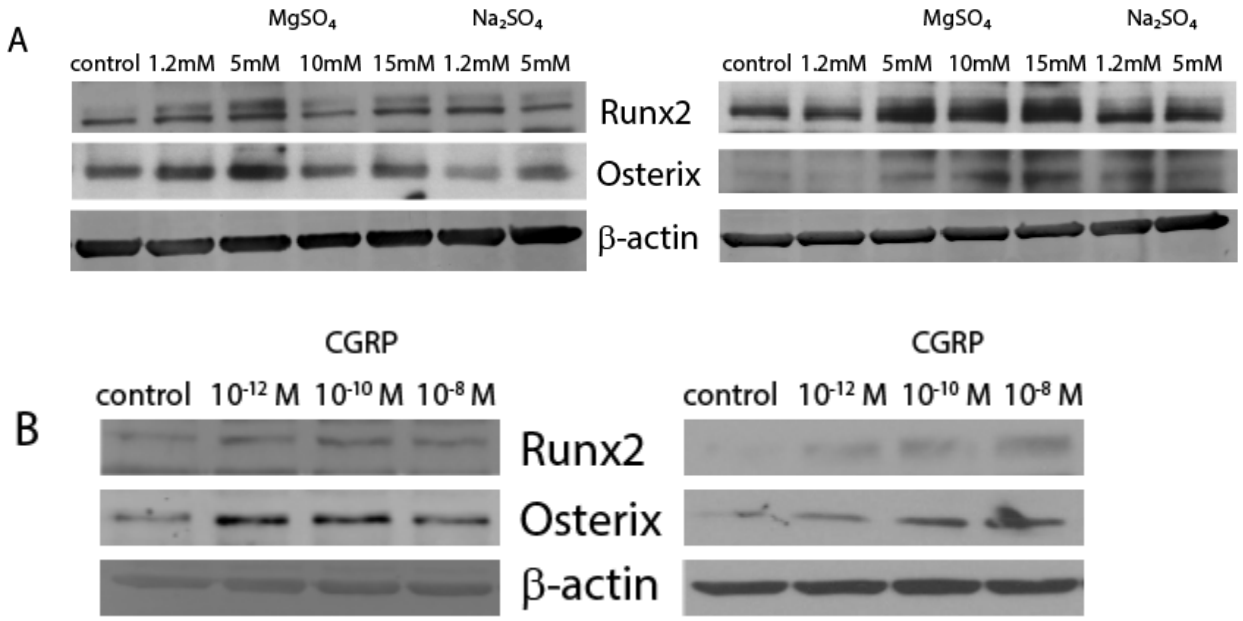

Figure 13. Western blot showing osteogenic protein expressions from mouse and human PDCs

A: Runx2 and Osterix expressions from mouse (left) and human (right) PDCs treated with different Mg^{2+} concentrations were detected using Western blot. B: Runx2 and osterix expressions from mouse (left) and human (right) PDCs treated with different CGRP concentrations.

4.5.4 Effect of Mg^{2+} on Osteogenic Gene Expressions of PDCs

The expression of osteogenic genes, including osteocalcin (BGLAP), collagen I (COL1A1), and BSP (IBSP), were determined using qPCR and shown in Figure 14. One week after the treatment, osteocalcin gene expression measured from mouse PDCs (Figure 14A) was upregulated significantly by 15 mM $MgSO_4$, compared to the cells cultured in osteogenic induction medium as osteogenic control, but decreased significantly for human PDCs (Figure 14C). Interestingly, collagen I and BSP genes were down-regulated after a week from both mouse and human PDCs when treated with 15 mM $MgSO_4$ compared to osteogenic controls. However, two weeks after treated in 1.2 mM and 10 mM MgSO4, gene expressions of osteocalcin and BSP in mouse PDCs were significantly upregulated (Figure 14B), and collagen I was increased as well. However, osteocalcin expression in human PDCs was further downregulated, while collagen level increased. BSP gene could not be determined at both time points (Figure 14D).

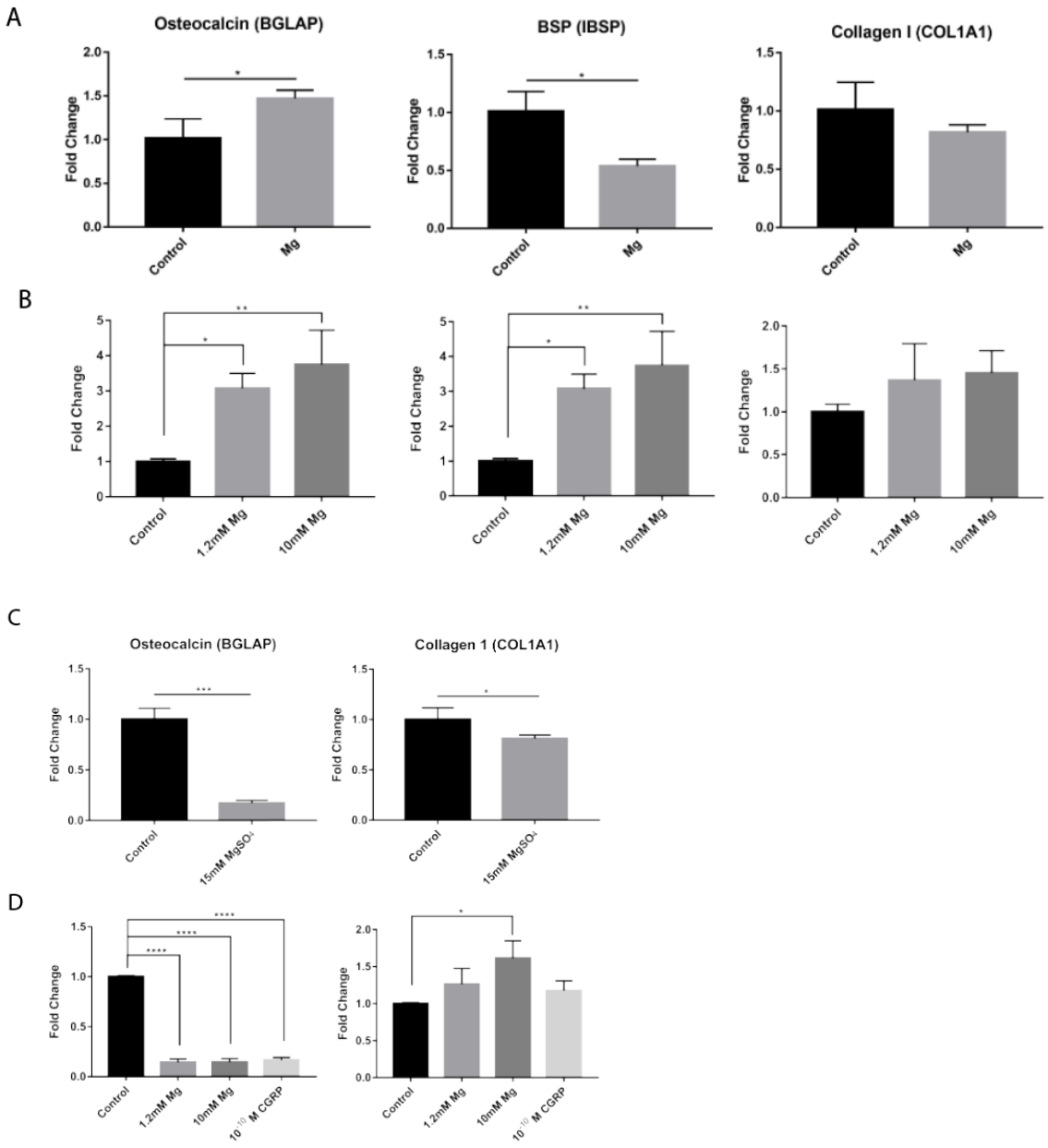

Figure 14. qPCR showing osteogenic gene expressions

Osteogenic gene expressions from mouse (A, B) and human (C, D) PDCs after 1 week (A, C) and 2 weeks (B, D) of Mg treatment.

4.5.5 Influence of Mg^{2+} on Extracellular Mineralization

After 3 weeks of treatment in different concentrations of $MgSO_4$ and CGRP, Alizarin Red S staining detected extracellular mineralization from both mouse and human PDCs cultured in osteogenic induction medium (Figure 15), as well as from the cells cultured in 10^{-10} M CGRP in osteogenic induction medium. However, fewer mineral nodules were detected when concentrations of $MgSO_4$ were increased in the medium. $MgSO_4$ concentrations at and above 5 mM completely inhibited the mineralization at 3 weeks. Interestingly, the same concentrations of sulfate controls also prevented the extracellular mineralization.

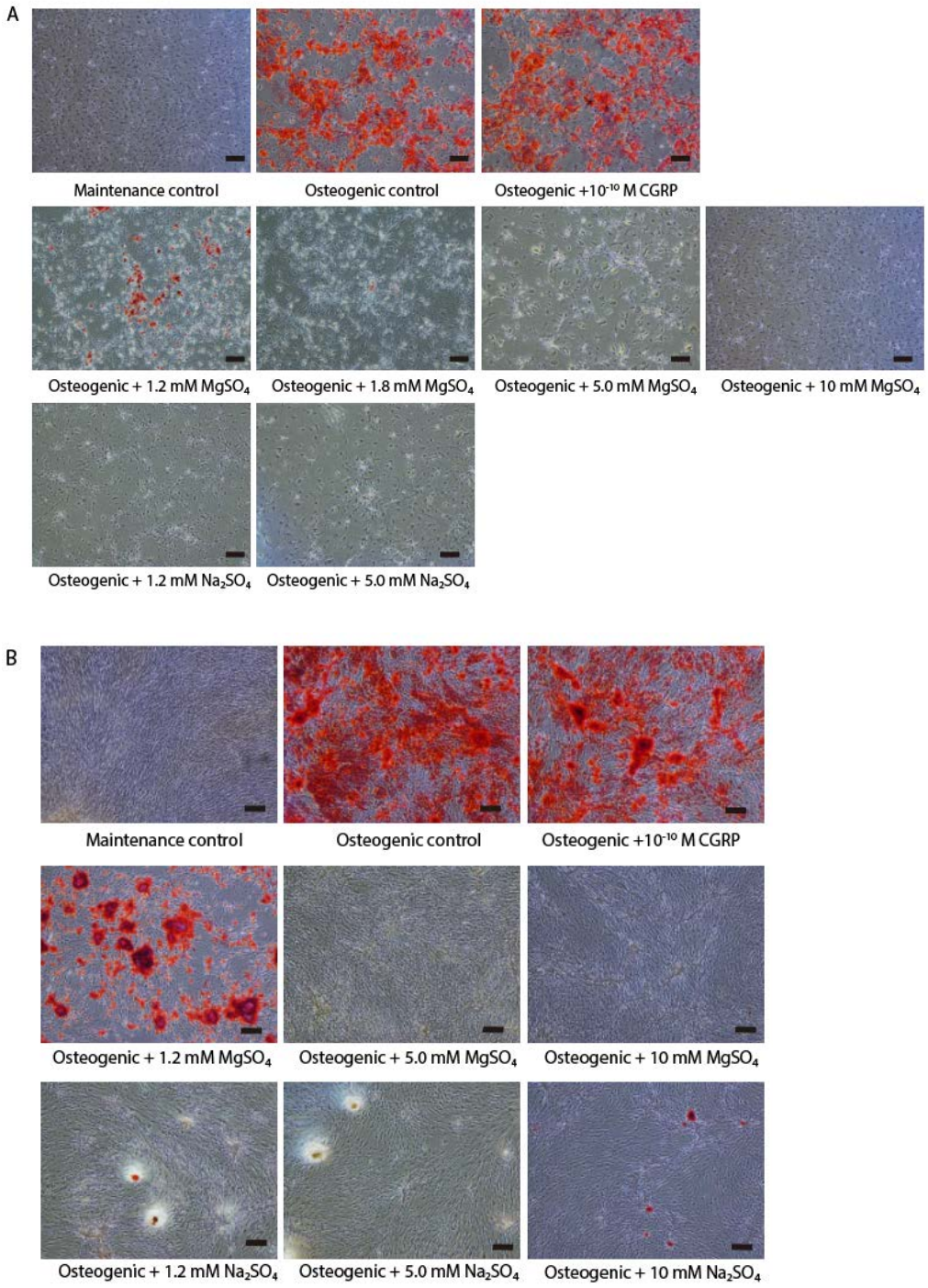

Figure 15. Alizarin red s staining on mouse and human PDCs after 3 weeks culture

Mouse (A) and human (B) PDCs were cultured in different concentrations of Mg^{2+} and 10^{-10} M CGRP for 3 weeks. Magnification: 4x. Scale bar = 100 µm.

4.5.6 Release of Mg and CGRP from PLGA Scaffold

Figure 16A shows the final product of the PLGA scaffolds containing Mg metal nanopowder (left) and CGRP (right), each to be 5 mm in diameter. Figure 16B shows the SEM image of Mg metal nanopowder, appeared as dark spots under the SEM, in the PLGA scaffold. As shown in figure 16D, Mg powder (green, right) are homogenously dispersed in the electrospun PLGA fibers (yellow, left), overlapped into multiple layers. Mg^{2+} accumulative release profile obtained by ICP-MS (figure 16C) shows that the Mg^{2+} could be detected at 1 hr after placed in the solution. Mg^{2+} in the solution continued to increase quickly until day 7. At day 12, almost all Mg nanopowder had been released into the solution, reaching a plateau of approximately 120 mg/L. Similarly, CGRP was also electrospun into PLGA scaffold, as shown in SEM image (Figure 16E). The accumulative CGRP release profile shows that about 2 pg/mL of CGRP was detected by ELISA in the solution starting at day 2 (Figure 16F). At week 7, total released CGRP was measured to be a total of 8.5 pg/mL.

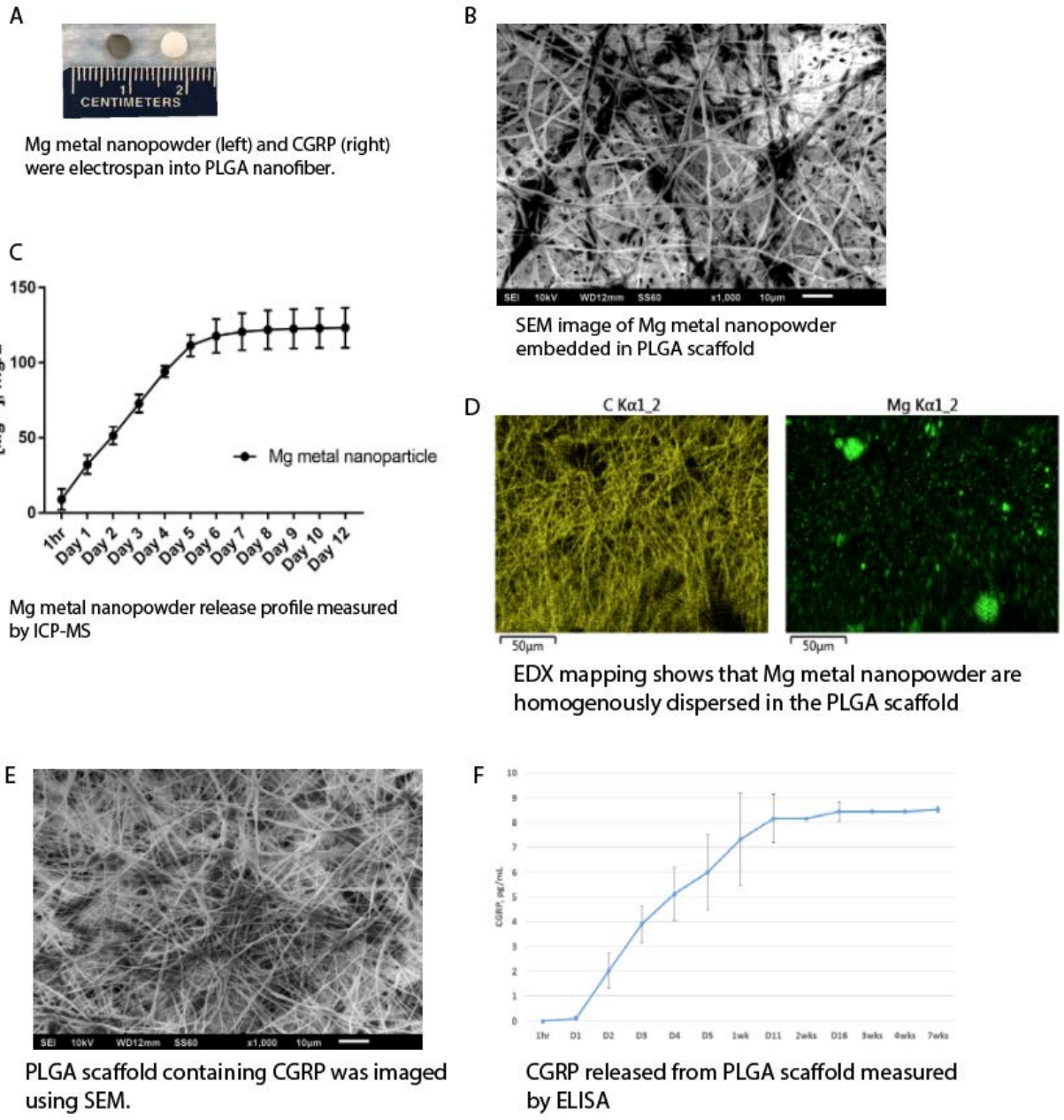

Figure 16. Chacterization of PLGA scaffolds containing Mg metal nanopowder or CGRP

4.5.7 Mg and CGRP Stimulated New Bone Growth from Rat Calvarial Defect

Figure 17A shows the 3D rendering of the representative images of new bone formation from rat calvarial defect after 1 month of implantation. In general, more new bone was generated when periosteum still covered the defect, compared to the groups without periosteum. This difference is especially striking in Mg and CGRP groups.

New bone volume from female and male rats were analyzed separately using high resolution μCT (Figure 17B). Except for the PLGA (both female and male) and empty (male) groups, periosteum had a significant impact on bone regeneration: new bone volume in groups containing periosteum was significantly higher than those without periosteum. Analysis from female rat calvaria measured the highest new bone volume to be from the CGRP+ periosteum group, followed by the Mg+ periosteum group. However, Mg induced higher new bone volume from periosteum than did CGRP groups in male rat calvaria. In general, female rats had more new bone growth compared to male rats.

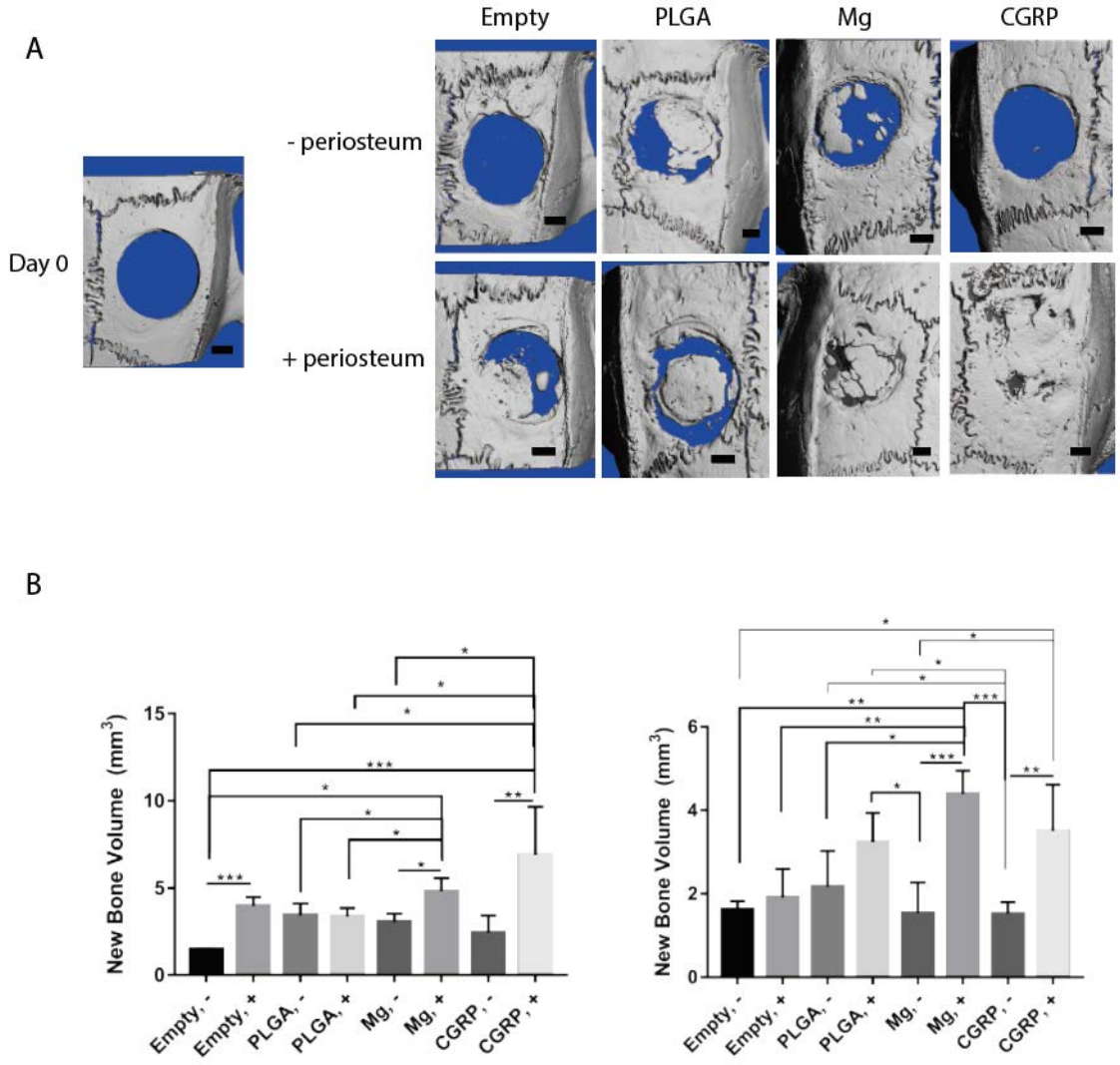

Figure 17. High resolution microCT analysis on rat calvarial defect

A: Representative images showing new bone formation in rat calvarial defect from all groups. B: High resolution microCT analysis on new bone volume from female (left) and male (right) rats.

Goldner's trichrome staining on calvarial samples (Figure 18A) was also used to visualize new bone, which almost completely bridging the calvaria after 1 month implanted with scaffold containing Mg or CGRP covered by the periosteum. Immunostaining using CGRP antibody (Figure 18B) detected CGRP expression (red) near the defect in Mg+ periosteum group, as well as in the CGRP+ periosteum groups.

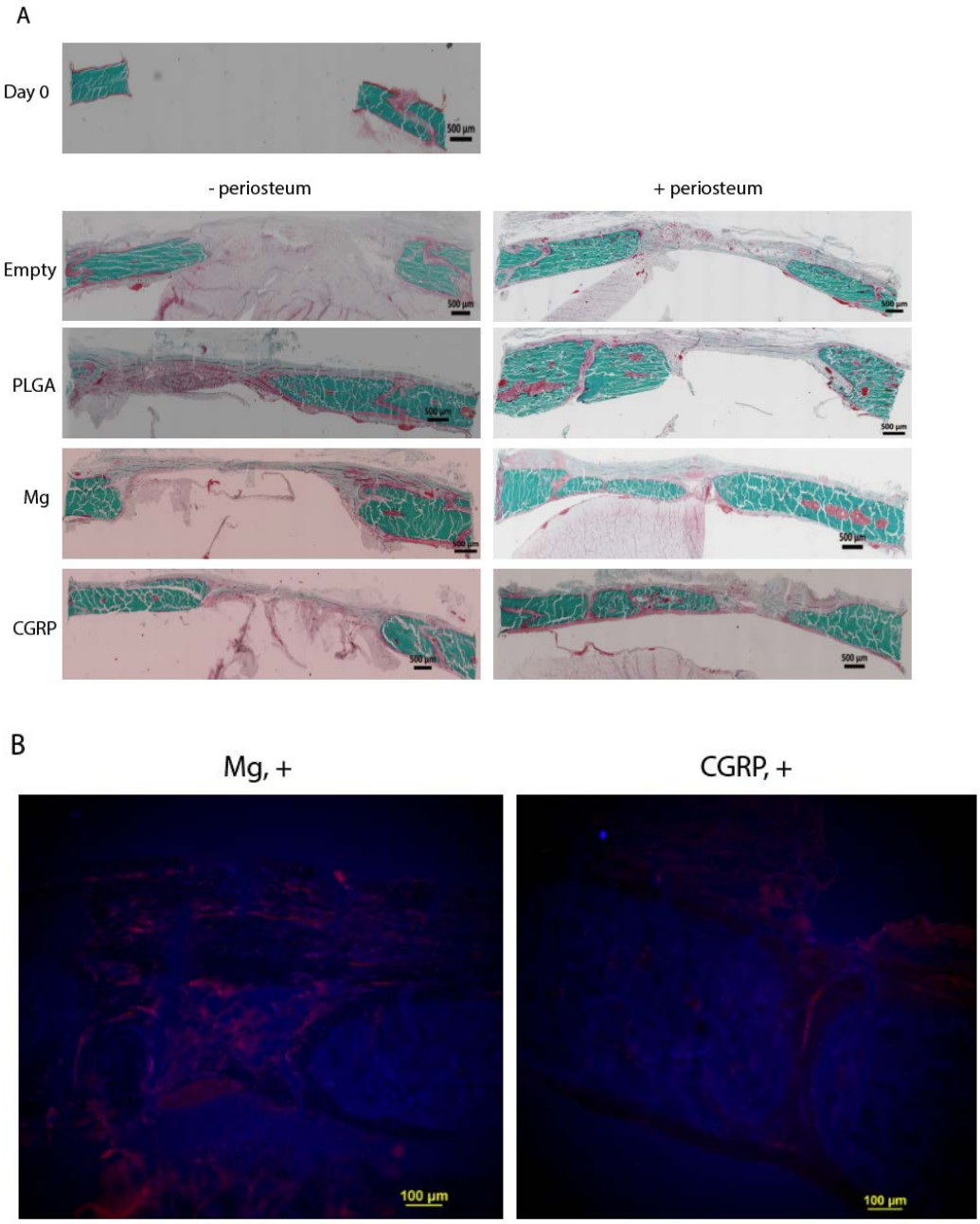

Figure 18. Goldner's trichrome staining and immunostaining on rat calvarial defect

A: Representative images of Goldner's trichrome staining on samples from all groups.

B: Immunostaining using CGRP antibody detected CGRP expression in calvarial defect from Mg+ and CGRP+ groups.

4.6 Discussion

In our previous work, we observed substantial new bone formation over Mg-based implants used to stabilize rabbit ulna fracture [30]. Mg has been shown to influence the osteogenic activity of many types of cells, including bone marrow stromal cells, osteoblast, osteoclast, and even vascular smooth muscle cells [18, 94, 95, 98, 99, 101, 103]. In the present study, we explored the direct effect of Mg on the periosteum by exposing various mouse and human PDCs to varying concentrations of $MgSO_4$ and CGRP.

Our initial finding was that exposure of mouse and human PDCs to CGRP and Mg^{2+}, respectively, had differing effects on ALP activity. When mouse PDCs were exposed to CGRP, ALP expression increased at week 1, but decreased by the end of week 2 (Figure 12A) when mineral nodules could be visually detected in culture (data not shown). This finding is consisted with that reported by Malaval and colleagues who observed reductions in ALP activity in association with the appearance of mineralized nodules [198]. By comparison, addition of CGRP to human PDCs resulted in ALP expression continuing to increase through week 2. This difference in response between mouse and human cells suggests that under the same CGRP treatment, mouse PDCs undergo an earlier switch to differentiation than human PDCs.

The addition of Mg^{2+} to mouse and human PDCs resulted in ALP expression continuing to increase beyond 2 weeks. This extended duration of ALP expression subsequent to Mg^{2+} exposure, in contrast to CGRP exposure suggests that CGRP accelerates the osteogenic differentiation of mouse PDCs compared to Mg^{2+}. Many studies have found that CGRP can stimulate osteogenic differentiation [199, 200]. Bone mesenchymal stem cells transfected with CGRP showed enhanced osteogenic differentiation capacity when compared to control cells [200]. Our cross-species finding that PDCs exposed to Mg^{2+} demonstrated increased expression of ALP relative to cells

exposed to CGRP suggests that Mg^{2+} has an additional and direct osteogenic effect on PDCs that is independent of the CGRP effect.

Our 3-day in vitro treatment of mouse and human PDCs with Mg^{2+} allowed us to examine osteogenic differentiation at early stage. Runx2 is the earliest marker of the osteoblast lineage, expressed as early as the differentiation of mesenchymal cells into preosteoblasts [201, 202]. Similarly, Osterix is downstream of Runx2 and expressed early when cells become committed to osteoblast lineage [196, 197, 203]. Results from our Western blots (Figure 13) indicated that higher concentrations of Mg^{2+} (up to 15 mM) caused human PDCs to commit early to osteoblast lineage, whereas lower concentrations of Mg^{2+} (1.2 mM and 5 mM) led to early response of mouse PDCs. Compared to osteogenic control, higher Runx2 and Osterix expressions were observed from both mouse and human PDCs treated with varying concentrations of CGRP. This finding not only confirms the results from ALP that CGRP can stimulate osteogenic differentiation, but also indicates that such stimulation can be observed very early.

In the next phase of the study, we used qPCR to examine late osteogenic markers of mature osteoblasts, including BGLAP (coded for osteocalcin) [201], BSP (bone sialoprotein) [204], and COL1A1 (collagen I), a main component of bone extracellular matrix [205]. Gene expressions of COL1A1 and BSP from both species were decreased after one week exposure to high Mg^{2+} concentration (15 mM). By comparison, osteocalcin decreased in human PDCs, but increased in mouse PDCs. This finding was unexpected because one week is a relatively early time point for osteoprogenitor cells to express late stage osteogenic markers. After two weeks, cells were treated with both low (1.2 mM) and high (10 mM) concentrations of Mg^{2+}. As expected, gene expression in mouse PDCs was upregulated, thus implying that the cells had progressed to immature osteoblast [195]. Surprisingly, osteocalcin expression in human PDCs was still decreased. Our

finding of species-specific effects of CGRP on ALP expression described above raises the possibility that mouse PDCs can undergo an earlier switch to osteogenic differentiation. Given these data and the qPCR findings just discussed, it seems reasonable to infer that two weeks maybe sufficient for mouse PDCs to differentiate, while still being too early for human PDCs to undergo the same activities.

Alizarin Red S staining provided further insight into extracellular mineralization in both mouse and human PDCs. After 3 weeks, exposure to 10^{-10} M CGRP in culture led to mineral formation in both mouse and human PDCs. However, exposure to Mg concentrations higher than 1.2 mM inhibited mineral matrix formation in PDCs from both species. We extended the treatment time point to 5 weeks, but obtained the same results (not shown). This finding is consistent with previous studies showing a similar inhibitory effect of Mg^{2+} on mineral matrix formation in other types of bone cells. For example, Leidi and colleagues found that addition of 5 mM $MgSO_4$ in osteogenic medium inhibited mineral matrix formation on both SaOS-2 cells and human osteoblasts [100]. Likewise, Lu and colleagues showed that both mineralization and ALP activity from human osteoblasts were increased when Mg concentrations were between 1-2 mM, but inhibited significantly when above 2 mM [101]. Li and colleagues further explored the inhibition of mineral formation at the molecular level. Compared to cells cultured in osteogenic induction medium, human bone marrow stromal cells cultured in 1 mM $MgCl_2$ for one week showed decreased expressions of Osteocalcin, Runx2, Osterix, and Collagen I [102]. Li also measured the mitochondrial Ca^{2+} concentrations in Mg-treated cells. His findings suggested that Mg^{2+}, as a Ca^{2+} antagonist, suppresses the Ca^{2+} concentration in mitochondria and reduces the nucleation activity of the matrix vesicles, thus resulting in the mineralization inhibition [102]. It appears that the effect

of Mg on matrix mineralization is dependent on the concentration used and the cell types (i.e. periosteal vs. human bone marrow stromal cells vs. SaOS-2 vs. human osteoblast).

Our microCT analysis on rat calvarial defect showed that periosteum plays a critical role in bone regeneration. Our data shows that higher new bone volume has been observed when periosteum was sutured above the defect in most groups, except in PLGA groups. Findings from existing research suggest that periosteum may provide source of cells that can induce osteogenesis [206, 207]. Zhang and colleagues [29] reported that Mg can stimulate the production of CGRP in the femoral cortex and dorsal root ganglia, hence indirectly induce the osteogenic differentiation of periosteum. Our microCT results showed that most bone growth was observed from Mg+ groups in male rat calvaria, but CGRP was able to induce higher bone volume in female rat calvaria. This difference might be dependent upon sex, as the influence of sex on bone healing has been reported by Mehta and colleagues [208]. Another reason to explain the difference from Zhang et al. could be the anatomical location of the periosteum. They tested in the long bone, while we used calvarial defect model. It has been shown that the osteogenic potential could be different between periosteum locations [209]. Periosteum at the calvaria, also named pericranium, has lower osteogenic potential compared to that from long bones. Moreover, the sensory nerve fibers at the periosteum of the calvarial bone may not produce as much CGRP as those from the long bones due to anatomy difference. Furthermore, the release of Mg^{2+} could have a more pronounced direct and indirect (via CGRP production) effect on periosteal cells in female rats vs male rats. We also performed preliminary immunostaining of CGRP. Visual observation suggest CGRP was also detected in the Mg^{2+}, suggesting that Mg stimulated CGRP secretion. More in vivo experiments are needed to elucidate the direct vs. indirect action of Mg^{2+}. Lastly, we observed no statistical difference in new bone volume between PLGA groups with and without periosteum from microCT

analysis. In PLGA groups, PLGA scaffolds that were placed in the defect could act as a temporary extracellular matrix. It is thus possible to mechanically support the growth of the bone marrow stromal cells, which could migrate from the nearby diploe of the cranium, and form the initial tissue structure. From our CGRP immunostaining, CGRP was also expressed around the defect in PLGA+ group, presumably from the nerve endings in periosteum, which could partially contribute to the new bone growth (Supplemental Figure 6). Taken together, these data from microCT reveal that our Mg or CGRP containing PLGA scaffolds are able to promote new bone formation in both female and male rat calvarial defect.

4.7 Conclusion

In the present study, we assessed the osteogenic effect of Mg and CGRP on mouse and human periosteal derived cells, and rat calvaria defect model. We demonstrated that the osteogenic differentiation of the periosteal cells depends on the Mg^{2+} concentration, and can be species-dependent. We also showed that periosteum is critical in new bone regeneration. Mg and CGRP released from electrospun PLGA scaffold effectively induced new bone formation from the periosteum in rat calvaria defect. Our results also suggest that new bone formation can be gender-dependent, as we observed higher new bone volume in general from female compared to male rats. Taken all the data together, we conclude that Mg has a direct effect on periosteum and periosteal derived cells. Furthermore, our novel, Mg- or CGRP-containing electrospun PLGA scaffold promote the osteogenic differentiation of the cells in rat calvarial periosteum, suggesting the therapeutic potential of this biomaterial to facilitate the repair of cranial injury.

5.0 Conclusions

In the present dissertation, we studied and reduced the mineralization on Mg metal surface that is triggered by Mg degradation process (aim 1). We also explored the effect of Mg on osteogenic differentiation of periosteal cells (aim 2). In aim 1, we hypothesized that calcium phosphate deposited on Mg surface can be inhibited by a vascular calcification inhibitor MGP. Reduction of the mineral layer on Mg metal surface can greatly improve the safety of Mg-based implants in soft tissue implantation. In aim 2, we hypothesized that Mg has a direct effect on the osteogenic differentiation of the periosteal derived cells, which can add to the benefit of using Mg as orthopedic implant materials.

For aim 1, we were able to transfect MGP plasmid into HUVECs and HEK293 cells (Figure 1), and study the mineral deposition on the surface of pure Mg rod and WE43 alloy plate in transwell experiment. Using EDS, we found that regardless of the origin of the cells that were used to secrete the protein, Ca and P wt% were significantly reduced from the surface of both pure Mg rod and WE43 plate when MGP was in the medium, compared to those from the surface of the metals immersed in medium without MGP (Figure 2). Similarly, spectra obtained from ATR-FTIR (Figure 3) showed a sharp ν3 phosphate peak as in amorphous calcium phosphate from Mg rods immersed in medium without MGP, but only a negligible smooth bump for Mg from medium containing MGP secreted from the cells. Next, these stably transfected cells were seeded homogenously in a collagen scaffold (Figure 5). Mg rod was placed in the center of this scaffold, and the whole construct was implanted intramuscularly in mice for 4 and 6 weeks. Compared to groups without MGP, microCT analysis (Figure 6), EDS cross-sectional mapping (Figure 7), and histology (Figure 8) all demonstrated the least minerals from the group containing MGP stably

transfected cells. Difference in wt% of the Mg rod before and after implantation obtained using microCT analysis (Figure 9) showed that the highest rod volume reduction was from the MGP group, suggesting that the calcium phosphate deposition can serve as a protective layer to slow down the metal corrosion rate.

For aim 2, we characterized the mouse and human periosteal derived cells harvested from mouse femur and human palate, respectively, using cell markers CD34, CD45, CD90, CD105, and periostin, a protein highly expressed at the cambium layer of the periosteum (Figure 11). Using these cells, we were able to determine the osteogenic effect from Mg^{2+} and CGRP, by quantitatively measuring the ALP levels (Figure 12), studying the early stage markers (Runx2 and Osterix, Figure 13) and the late markers (osteocalcin, BSP, and collagen I, Figure 14) of the osteogenic differentiation, on periosteal derived cells. Elevated Mg^{2+} and CGRP in medium promoted the osteogenic differentiation of the periosteal cells, which could be observed 3 days after the treatment. Mouse periosteal cells switched early to differentiation compared to human periosteal cells, under the influence of CGRP. Human periosteal cells were able to respond to higher concentrations of Mg^{2+} in medium than mouse periosteal cells, up to 25mM. Extracellular mineralization was examined using alizarin red s staining (Figure 15), but an inhibition was observed when Mg^{2+} in medium was above 1.2mM. We suspect such inhibition was caused by the significant increase in osmolality of the medium after adding $MgSO_4$ salt.

We electrospan Mg metal nanopowder and CGRP solution in PLGA nanofibers, and studied the release profile (Figure 16) before implanting them in female and male rat calvaria defect. Observed from analysis by high resolution microCT (Figure 17) and histology (Figure 18), Mg and CGRP generated significantly higher new bone volume from groups containing periosteum, compared to control, in which the periosteum was removed, and the groups implanted

with blank PLGA scaffold and left empty with and without periosteum. However, bone regeneration was not observed from Mg scaffold implanted in intact periosteum (Supplemental Figure 5). These results suggest that the periosteum is critical in bone regeneration. Injuring the periosteum stimulates this process. Furthermore, Mg and CGRP were able to accelerate the cellular differentiation and bone formation from the periosteal cells in the injured periosteum. Interestingly, a minor gender influence was observed from microCT analysis on bone volume. In general, female rats generated more bone volume in the defect and had better recovery compared to male rats. Female rats responded better to CGRP treatment, while male rats had more bone volume observed in Mg group. This result indicated that *in vivo* model should include both genders to be considered unbiased, since different genders may react differently to treatments and introduce variations in data analysis.

6.0 Future Directions

We have demonstrated in aim 1 the feasibility of MGP to significantly reduce the mineral deposition on Mg-based metals. Additional work should be done to further explore the translational aspect of MGP delivery system for Mg metal implants. One approach could be to incorporate the Gla residues of the MGP protein [144], instead of the full protein, in a polymer coating on Mg metal device for a sustained release. In addition, our *in vivo* model in this study was limited to mouse muscle implantation. Since our aim was to reduce the mineralization on Mg metals for soft tissue implantation, such as the stent application, future work can explore and validate these results in a more dynamic model, such as in the endothelial walls of the artery [115], where the implant and coating are in an environment more relevant to our current study, can interact with blood flow, and experience additional shear stress.

In aim 2, we showed the osteogenic effect of Mg and CGRP on periosteal cell differentiation in vitro and in vivo. Our *in vitro* results could be further strengthened by quantifying the protein expressions obtained from Western blots. In addition, extracellular mineralization should also identify the cellular differentiation. It would be ideal if we could regulate the osmolality of the medium after adding Mg salt, to minimize the difference in different treatment medium. Moreover, mouse and human periosteal cells used in this study were harvested from different anatomical locations. It was shown [209] that osteogenic potential could be different relative to locations. Our results also indicated that the rate of osteogenic differentiation could be different depending on species. Therefore, in the future, we can also harvest the periosteal cells from the same anatomical location, and compare the osteogenic effect from Mg^{2+} and CGRP between different species.

The same can also be applied to the *in vivo* model. Due to the anatomy of the cranial bone, which is a flat bone formed by two layers of compact bone (plates) separated by a thin layer of spongy diploe, results obtained from calvarial defect model could potentially be different from those implanted in long bone [29], on which the periosteum was reported to have more osteogenic potential [209]. However, more bone marrow is also present in the medullary cavity of the long bone, which could interfere with the osteogenesis of the periosteum. Future work may compare the osteogenic effect of Mg, released from electrospun PLGA scaffold developed for this study, on different anatomical locations of the animal model to study the new bone formation.

Appendix A Supplemental Figures

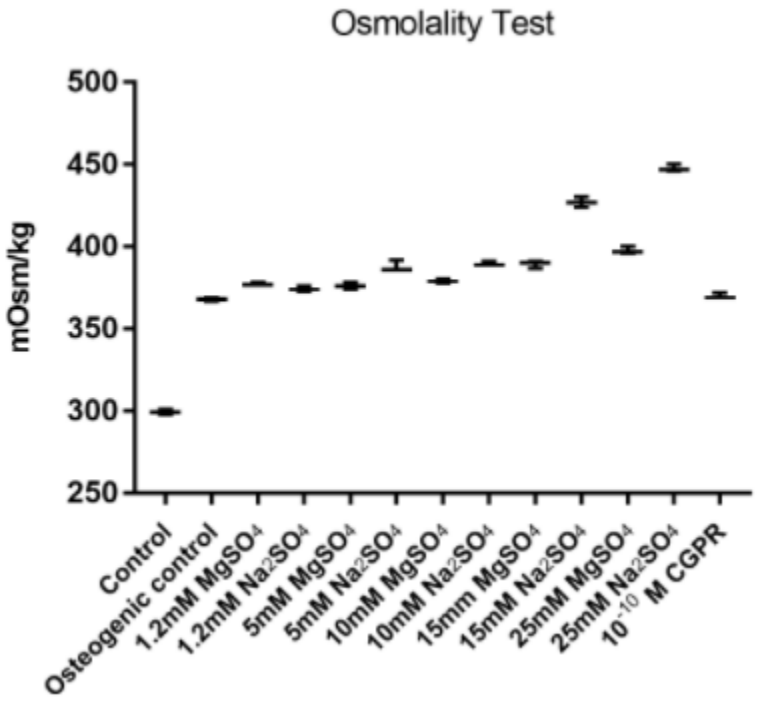

Supplemental Figure 1. Osmolality test on treatment medium

The osmolality of each treatment medium was tested using freezing point 3320 Single-Sample Micro Osmometer (Advanced Instruments, PA, USA). Biological triplicates were measured for each concentration. Control was maintenance medium. Osteogenic control was osteogenic induction medium. Each concentration of $MgSO_4$ and 10^{-10} M CGRP were added in osteogenic induction medium. Compared to control, the osmolality of the osteogenic induction medium was increased significantly. Compared to osteogenic induction medium, $MgSO_4$ and Na_2SO_4 supplements significantly increased the osmolality, especially the 15mM and 25mM Na_2SO_4, but not for the 10^{-10} M CGRP. No statistical difference was observed between different $MgSO_4$ and Na_2SO_4 concentrations up to 10mM and 5mM, respectively. Osmolality increase could

be one of the factors impact the ECM mineralization of both mouse and human periosteal cells, as observed in alizarin red staining in section 4.5.5.

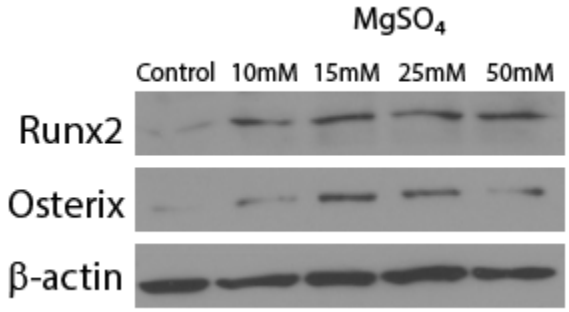

Supplemental Figure 2. Western blot showing osteogenic protein expressions from human PDCs treated with high Mg^{2+} concentration supplemented in maintenance medium

Human PDCs were cultured in maintenance medium, and Mg^{2+} were supplemented in maintenance medium for 3 days. Above Western blot shows that human PDCs were able to withstand higher concentrations of Mg^{2+} in the medium. No remarkable change of Runx2 was detected at different concentrations, but higher level of Osterix was detected at higher concentrations (15mM and 25mM Mg^{2+}), which reduced when the concentration reached 50mM. This is in accordance with results obtained from human PDCs treated in Mg^{2+} supplemented in osteogenic medium (Figure 13A).

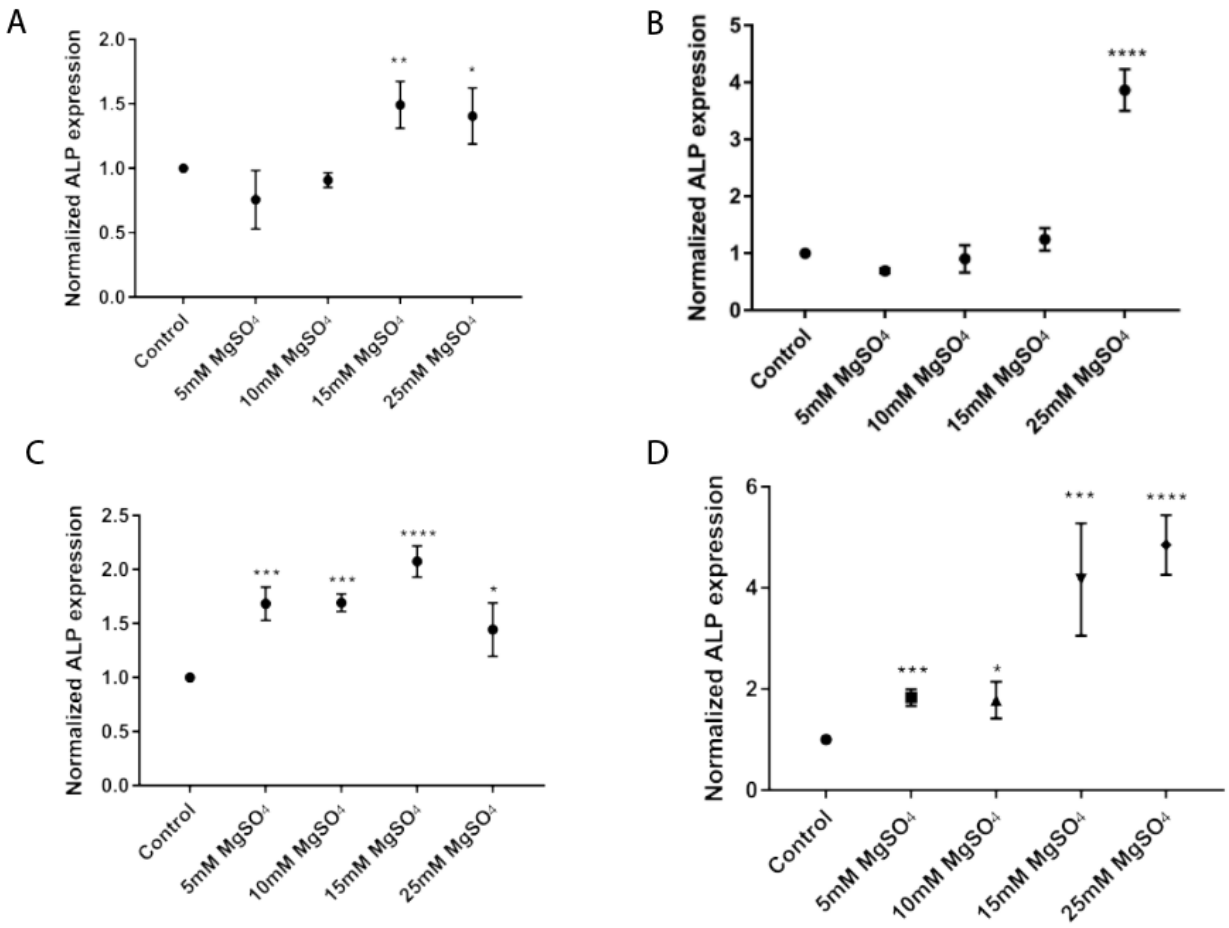

Supplemental Figure 3. Quantitative ALP from mouse and human PDCs cultured in maintenance medium

Mouse and human PDCs were cultured in maintenance medium for 1 (A, C) and 2 (B, D) weeks. ALP activities measured from mouse PDCs (A, B) showed higher expression at higher Mg^{2+} concentrations. Human PDCs (C, D) showed significantly higher ALP expression at all concentrations at both time points. This result suggests that Mg^{2+} is able to induce osteogenic differentiation of mouse and human PDCs without osteogenic induction.

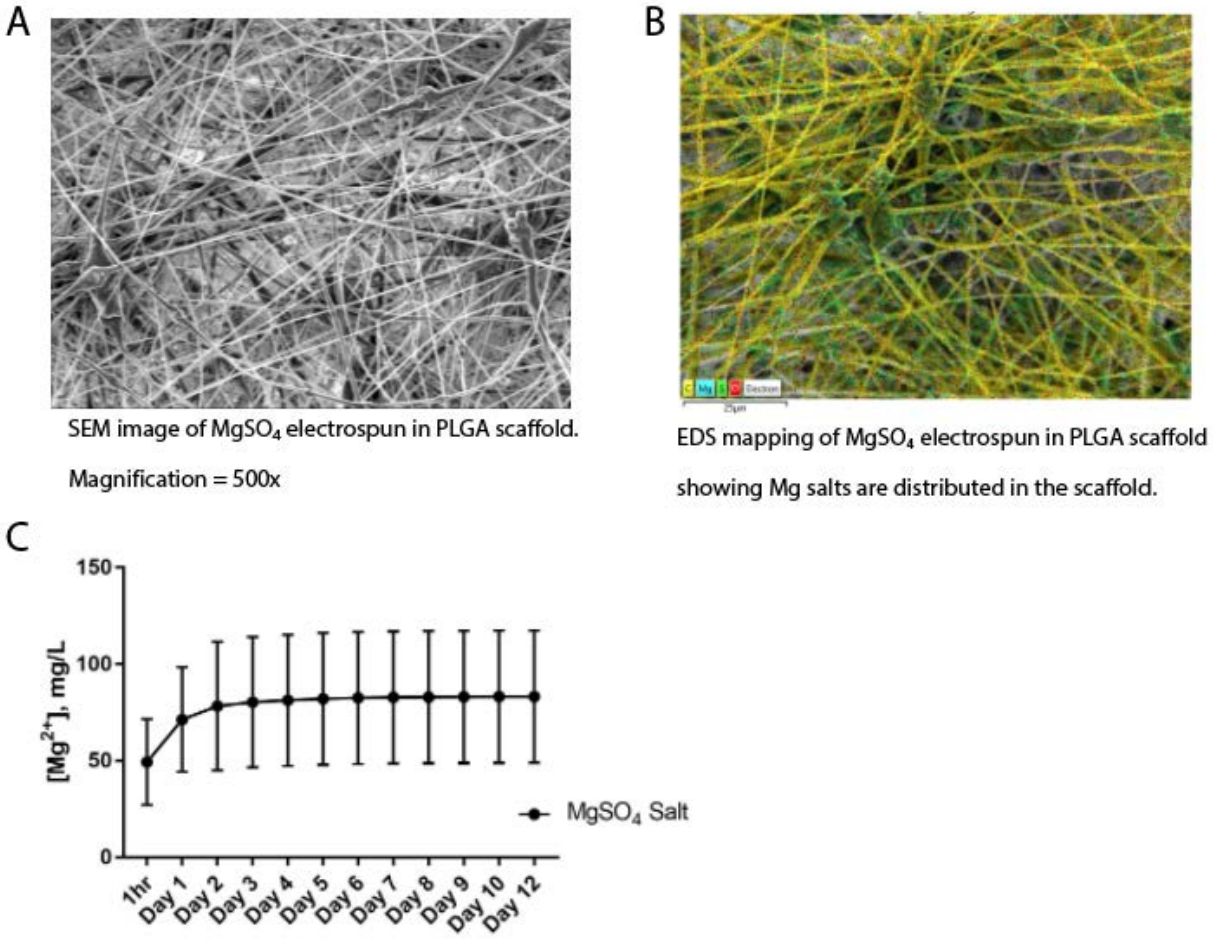

Supplemental Figure 4. SEM, EDS mapping, and release profile of $MgSO_4$ electrospun in PLGA scaffold

$MgSO_4$ salt was also electrospan in PLGA scaffold. The SEM image (A) shows the morphology of the salts in the woven PLGA nanofibers. EDS mapping (B) demonstrates the distribution of salts in PLGA nanofibers. Some areas show the aggregation of salts in the fiber. Figure C shows the release profile of the $MgSO_4$ salt in PBS, which indicates that almost all Mg^{2+} were released at day 2. Compared to the release profile of Mg metal nanopowder (Figure 16), standard deviations are relatively high, showing inconsistency of salt release from each scaffold.

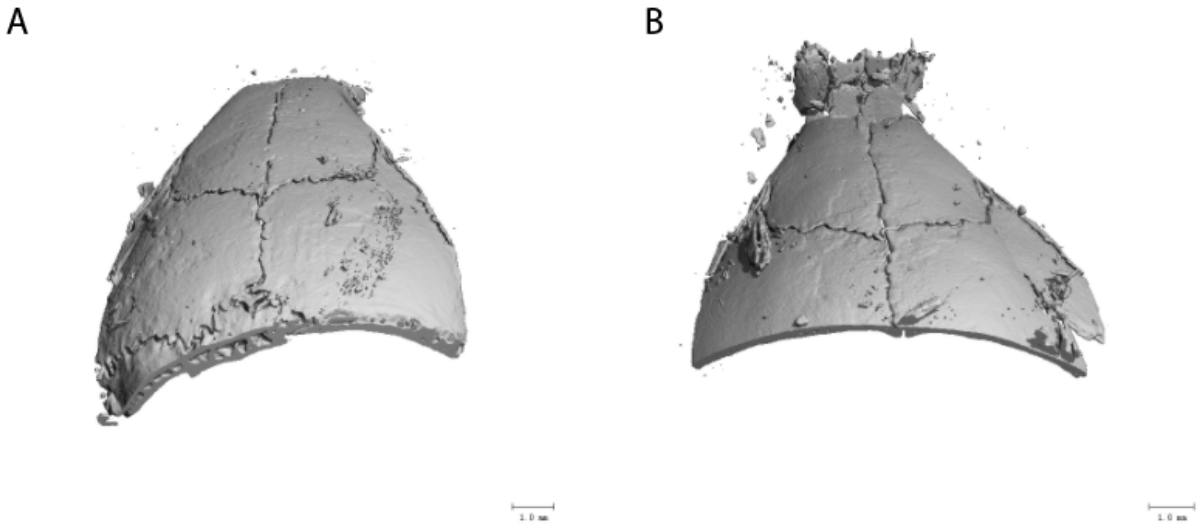

Supplemental Figure 5. MicroCT 3D rendering of mouse calvaria implanted with electrospun PLGA scaffold releasing Mg metal powder (A) and salt (B)

In a preliminary study, electrospun PLGA scaffolds releasing either MgSO4 salt (A) or Mg metal nanopowder (B) were implanted in four intact mouse calvaria for one month. A 2cm incision on the skin and the fascia underneath was created by blunt dissection. Scaffolds were placed directly under the soft tissue above the periosteum, without creating any defects on the calvaria. 3D rendering images from microCT reconstruction showed no difference on explanted mouse calvaria as a result of two implants. No new bone formation was observed from either treatment. We conclude from this preliminary study that without injuring the periosteum, which stimulated the bone repair process of the osteoprogenitor cells in periosteum [182], Mg will not have the osteogenic effect and new bone will not be regenerated from the periosteum.

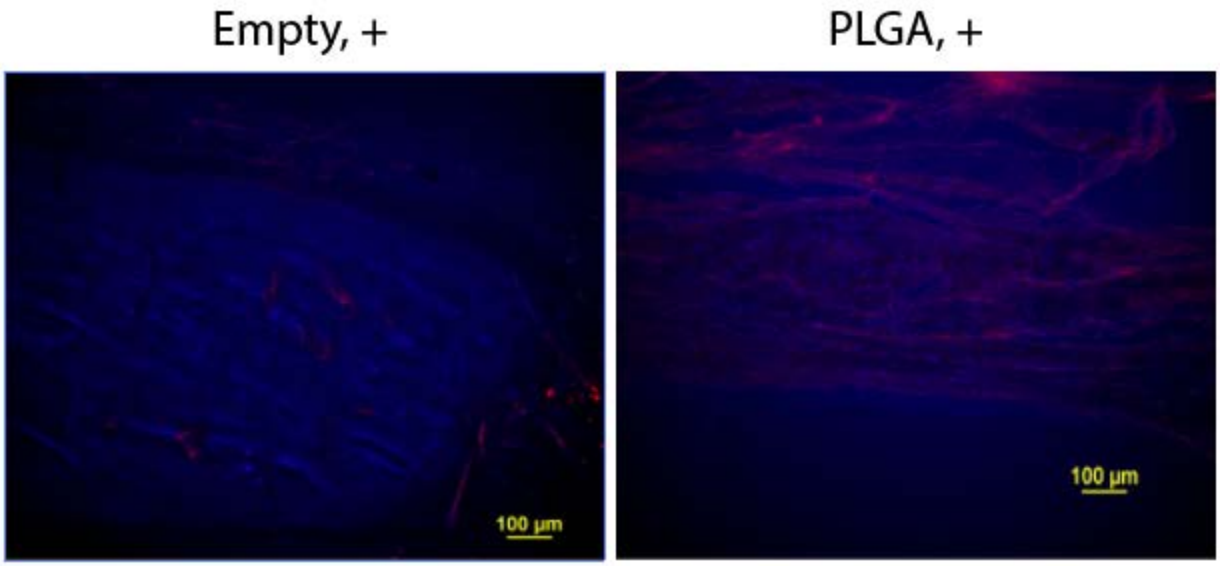

Supplemental Figure 6. Immunostaining using CGRP antibody detected CGRP expressions from empty and PLGA groups

Since the periosteum was remained in the defect, nerve endings in the membrane are still capable of generating CGRP at the site, which could partially contribute to the bone regeneration at these two groups.

Bibliography

[1] K. Frisken, G. Dandie, S. Lugowski, G. Jordan, A study of titanium release into body organs following the insertion of single threaded screw implants into the mandibles of sheep, Aust Dent J. 47(3) (2002) 214-217.

[2] T. Albrektsson, P.I. Branemark, H.A. Hansson, J. Lindstrom, Osseointegrated titanium implants. Requirements for ensuring a long-lasting, direct bone-to-implant anchorage in man, Acta Orthop Scand 52(2) (1981) 155-70.

[3] J.A. Disegi, L. Eschbach, Stainless steel in bone surgery, Injury 31 Suppl 4 (2000) 2-6.

[4] K. Walley, M. Bajraliu, T. Gonzalez, A. Nazarian, The Chronicle of a Stainless Steel Orthopaedic Implant, The Orthopaedic Journal at Harvard Medical School 17 (2016) 68-74.

[5] A. Mavrogenis, P. Papagelopoulos, G. Babis, Osseointegration of cobalt-chrome alloy implants, J Long Term Eff Med Implants 21(4) (2011) 349-358.

[6] M. Staiger, A. Pietaka, J. Huadmaia, G. Diasb, Magnesium and its alloys as orthopedic biomaterials: A review, Biomaterials 27 (2006) 1728-1734.

[7] D. Puleo, W. Huh, Acute toxicity of metal ions in cultures of osteogenic cells derived from bone marrow stromal cells, J Appl Biomater 6 (1995) 109-116.

[8] J. Jacobs, J. Gilbert, R. Urban, Corrosion of metal orthopaedic implants, J Bone Joint Surg Am 80(2) (1998) 268-282.

[9] C. Lhotka, T. Szekeres, I. Steffan, K. Zhuber, K. Zweymuller, Four-year study of cobalt and chromium blood levels in patients managed with two different metal-on-metal total hip replacements, J Orthop Res 21(2) (2003) 189-95.

[10] J.J. Jacobs, N.J. Hallab, A.K. Skipor, R.M. Urban, Metal degradation products: a cause for concern in metal-metal bearings?, Clin Orthop Relat Res (417) (2003) 139-47.

[11] J. Nagels, M. Stokdijk, P. Rozing, Stress shielding and bone resorption in shoulder arthroplasty, J Shoulder Elb. Surg 12(1) (2003) 35-39.

[12] P.K. Sullivan, J.F. Smith, A.A. Rozzelle, Cranio-orbital reconstruction: safety and image quality of metallic implants on CT and MRI scanning, Plast Reconstr Surg 94(5) (1994) 589-96.

[13] E. Marukawa, M. Tamai, Y. Takahashi, I. Hatakeyama, M. Sato, Y. Higuchi, H. Kakidachi, H. Taniguchi, T. Sakamoto, J. Honda, K. Omura, H. Harada, Comparison of magnesium alloys and poly-l-lactide screws as degradable implants in a canine fracture model, Journal of Biomedical Materials Research Part B Applied Biomateials 104B(7) (2016) 1282-1289.

[14] E. Huse, A new ligature?, Chicago Med J Exam 2 (1878) 172.

[15] F. Witte, Reprint of: The history of biodegradable magnesium implants: A review, Acta Biomater 23 Suppl (2015) S28-40.

[16] R.K. Kulkarni, K.C. Pani, C. Neuman, F. Leonard, Polylactic acid for surgical implants, Arch Surg 93(5) (1966) 839-43.

[17] Z. Saidak, P. Marie, Strontium signaling: molecular mechanisms and therapeutic implications in osteoporosis, Pharmacol Ther 136(2) (2012) 216-226.

[18] Y. Okuzu, S. Fujibayashi, S. Yamaguchi, K. Yamamoto, T. Shimizu, T. Sono, K. Goto, B. Otsuki, T. Matsushita, T. Kokubo, S. Matsuda, Strontium and magnesium ions released from bioactive titanium metal promote early bone bonding in a rabbit implant model, Acta Biomater 63 (2017) 383-392.

[19] Y. Li, Q. Li, S. Zhu, E. Luo, J. Li, G. Feng, Y. Liao, J. Hu, The effect of strontium-substituted hydroxyapatite coating on implant fixation in ovariectomized rats, Biomaterials 31(34) (2010) 9006-14.

[20] G. Boivin, A. Doublier, D. Farlay, Strontium ranelate--a promising therapeutic principle in osteoporosis, J Trace Elem Med Biol 26(2-3) (2012) 153-6.

[21] P. Naruphontjirakul, O. Tsigkou, S. Li, A.E. Porter, J.R. Jones, Human mesenchymal stem cells differentiate into an osteogenic lineage in presence of strontium containing bioactive glass nanoparticles, Acta Biomater (2019).

[22] H. Hermawan, A. Purnama, D. Dube, J. Couet, D. Mantovani, Fe-Mn alloys for metallic biodegradable stents: degradation and cell viability studies, Acta Biomater 6(5) (2010) 1852-60.

[23] S. Zhu, N. Huang, L. Xu, Y. Zhang, H. Liu, H. Sun, Y. Leng, Biocompatibility of pure iron: In vitro assessment of degradation kinetics and cytotoxicity on endothelial cells, Materials Science and Engineering: C 29(5) (2009) 1589-1592.

[24] B. Liu, Y.F. Zheng, Effects of alloying elements (Mn, Co, Al, W, Sn, B, C and S) on biodegradability and in vitro biocompatibility of pure iron, Acta Biomater 7(3) (2011) 1407-20.

[25] Y. Zheng, X. Gu, F. Witte, Biodegradable Metals, Materials Science and Engineering R 77 (2014) 1-34.

[26] M. Peuster, C. Hesse, T. Schloo, C. Fink, P. Beerbaum, C. von Schnakenburg, Long-term biocompatibility of a corrodible peripheral iron stent in the porcine descending aorta, Biomaterials 27(28) (2006) 4955-62.

[27] E. Mostaed, M. Sikora-Jasinska, J.W. Drelich, M. Vedani, Zinc-based alloys for degradable vascular stent applications, Acta Biomater 71 (2018) 1-23.

[28] H. Hermawan, D. Dube, D. Mantovani, Degradable metallic biomaterials: design and development of Fe-Mn alloys for stents, J Biomed Mater Res A 93(1) (2010) 1-11.

[29] X.J. Zhang Y, Ruan Y, Yu M, O'Laughlin M, Wise H, Chen D, Tian L, Shi D, Wang J, Chen S, Feng J, Chow D, Xie X, Zheng L, Huang L, Huang S, Leung K, Lu N, Zhao L, Li H, Zhao D, Guo X, Chan K, Witte F, Chan H, Zheng Y, Qin L, Implant-derived magnesium induces local neuronal production of CGRP to improve bone-fracture healing in rats, Nature Medicine 22(10) (2016) 1160-1173.

[30] A. Chaya, S. Yoshizawa, K. Verdelis, N. Myers, B. Costello, D. Chou, S. Pal, S. Maiti, P. Kumta, C. Sfeir, In vivo study of magnesium plate and screw degradation and bone fracture healing, Acta Biomaterialia 18 (2015) 262-269.

[31] A. Chaya, S. Yoshizawa, K. Verdelis, S. Noorani, B. Costello, C. Sfeir, Fracture healing using degradable magnesium fixation plates and screws, J. Oral Maxillofac. Surg. 73(2) (2015) 295-305.

[32] P. Erne, M. Schier, T.J. Resink, The road to bioabsorbable stents: reaching clinical reality?, Cardiovasc Intervent Radiol 29(1) (2006) 11-6.

[33] H. Hermawan, D. Dube, D. Mantovani, Developments in metallic biodegradable stents, Acta Biomater 6(5) (2010) 1693-7.

[34] C. Rapetto, M. Leoncini, Magmaris: a new generation metallic sirolimus-eluting fully bioresorbable scaffold: present status and future perspectives, J Thorac Dis 9(Suppl 9) (2017) S903-S913.

[35] E. Wittchow, N. Adden, J. Riedmuller, C. Savard, R. Waksman, M. Braune, Bioresorbable drug-eluting magnesium-alloy scaffold: design and feasibility in a porcine coronary model, EuroIntervention 8(12) (2013) 1441-50.

[36] C. Barber, BIOTRONIK Announces CE Mark for Magmaris, the First Clinically Proven Bioresorbable Magnesium Scaffold, 2016. (Accessed 03/29 2019).

[37] A. Amini, J. Wallace, S. Nukavarapu, Short-Term and Long-Term Effects of Orthopedic Biodegradable Implants, J Long Term Eff Med Implants 21(2) (2011) 93-122.

[38] D. Gilding, A. Reed, Biodegradable polymers for use in surgery- polyglycolic/poly(actic acid) homo- and copolymers: 1, Polymer 20(12) (1979) 1459-1464.

[39] K. Butterwick, N.J. Lowe, Injectable poly-L-lactic acid for cosmetic enhancement: learning from the European experience, J Am Acad Dermatol 61(2) (2009) 281-93.

[40] P. Simamora, W. Chern, Poly-L-lactic acid: an overview, J Drugs Dermatol 5(5) (2006) 436-40.

[41] Z.A. Ali, P.W. Serruys, T. Kimura, R. Gao, S.G. Ellis, D.J. Kereiakes, Y. Onuma, C. Simonton, Z. Zhang, G.W. Stone, 2-year outcomes with the Absorb bioresorbable scaffold for treatment of coronary artery disease: a systematic review and meta-analysis of seven randomised trials with an individual patient data substudy, Lancet 390(10096) (2017) 760-772.

[42] W.J. van der Giessen, A.M. Lincoff, R.S. Schwartz, H.M. van Beusekom, P.W. Serruys, D.R. Holmes, Jr., S.G. Ellis, E.J. Topol, Marked inflammatory sequelae to implantation of biodegradable and nonbiodegradable polymers in porcine coronary arteries, Circulation 94(7) (1996) 1690-7.

[43] H. Makadia, S. Siegel, Poly Lactic-co-Glycolic Acid (PLGA) as biodegradable controlled drug delivery carrier, Polymers (Basel). 3(3) (2011) 1377-1397.

[44] B. Ulery, L. Nair, C. Laurencin, Biomedical applications of biodegradable polymers, J Polym Sci B Polym Phys 49(12) (2011) 832-864.

[45] A. Kotsar, T. Isotalo, J. Mikkonen, H. Juuti, P. Martikainen, M. Talja, M. Kellomäki, P. Törmälä, T. Tammela, A new biodegradable braided self-expandable PLGA prostatic stent: an experimental study in the rabbit, J Endourol. 22(5) (2008) 1065-1069.

[46] R. Simpson, F. Wiria, A. Amis, C. Chua, K. Leong, U. Hansen, M. Chandrasekaran, M. Lee, Development of a 95/5 poly(L-lactide-co-glycolide)/hydroxylapatite and beta-tricalcium phosphate scaffold as bone replacement material via selective laser sintering, J Biomed Mater Res B Appl Biomater 84(1) (2008) 17-25.

[47] E. Jabbarzadeh, T. Starnes, Y.M. Khan, T. Jiang, A.J. Wirtel, M. Deng, Q. Lv, L.S. Nair, S.B. Doty, C.T. Laurencin, Induction of angiogenesis in tissue-engineered scaffolds designed for bone repair: a combined gene therapy-cell transplantation approach, Proc Natl Acad Sci U S A 105(32) (2008) 11099-104.

[48] Y. Tanaka, H. Yamaoka, S. Nishizawa, S. Nagata, T. Ogasawara, Y. Asawa, Y. Fujihara, T. Takato, K. Hoshi, The optimization of porous polymeric scaffolds for chondrocyte/atelocollagen based tissue-engineered cartilage, Biomaterials 31(16) (2010) 4506-16.

[49] K. Andreas, R. Zehbe, M. Kazubek, K. Grzeschik, N. Sternberg, H. Baumler, H. Schubert, M. Sittinger, J. Ringe, Biodegradable insulin-loaded PLGA microspheres fabricated by three different emulsification techniques: investigation for cartilage tissue engineering, Acta Biomater 7(4) (2011) 1485-95.

[50] H. Ho, L. Lin, M. Sheu, Characterization of collagen isolation and application of collagen gel as a drug carrier, Journal of Controlled Release 44(2-3) (1997) 103-112.

[51] S. Heinemann, T. Coradin, M. Desimone, Bio-inspired silica–collagen materials: applications and perspectives in the medical field, Biomaterials Science 1(7) (2013) 688.

[52] C.B. Weinberg, E. Bell, A blood vessel model constructed from collagen and cultured vascular cells, Science 231(4736) (1986) 397-400.

[53] S. Ravi, E.L. Chaikof, Biomaterials for vascular tissue engineering, Regen Med 5(1) (2010) 107-20.

[54] B. Albert, A. Johnson, J. Lewis, M. Raff, K. Roberts, P. Watson, Collagens are the major proteins of the extracellular matrix, Molecular Biology of the Cell, Garland Publishing, NY, 2002, pp. 1096-1098.

[55] B.A. Roeder, K. Kokini, J.E. Sturgis, J.P. Robinson, S.L. Voytik-Harbin, Tensile mechanical properties of three-dimensional type I collagen extracellular matrices with varied microstructure, J Biomech Eng 124(2) (2002) 214-22.

[56] M. Wozniak, P. Keely, Use of three-dimensional collagen gels to study mechanotransduction in T47D breast epithelial cells, Biol Proced Online 7 (2005) 144-161.

[57] L. Naira, C. Laurencin, Biodegradable polymers as biomaterials, Progress in Polymer Science 32(8-9) (2007) 762-798.

[58] D. Persaud-Sharma, A. McGoron, Biodegradable Magnesium alloys: A review of material development and application, J Biomim Biomater Tissue Eng 12 (2012) 25-39.

[59] P. Lyon, The Benefits of Magnesium Alloy for Medical Implants, 2017. (Accessed 03/29 2019).

[60] H. Waizy, J.-M. Seitz, J. Reifenrath, A. Weizbauer, F.-W. Bach, A. Meyer-Lindenberg, B. Denkena, H. Windhagen, Biodegradable magnesium implants for orthopedic applications, J. Mater. Sci. 48(1) (2013) 39-50.

[61] G. Song, A. Atrens, Recent Insights into the Mechanism of Magnesium Corrosion and Research Suggestions, Advanced Engineering Materials 9(3) (2007) 177-183.

[62] S. Virtanen, Biodegradable Mg and Mg alloys: Corrosion and biocompatibility, Materials Science and Engineering B 176 (2011) 1600-1608.

[63] J.E. Gray-Munro, M. Strong, The mechanism of deposition of calcium phosphate coatings from solution onto magnesium alloy AZ31, J Biomed Mater Res A 90(2) (2009) 339-50.

[64] F. Witte, V. Kaese, H. Haferkamp, E. Switzer, A. Meyer-Lindenberg, C.J. Wirth, H. Windhagen, In vivo corrosion of four magnesium alloys and the associated bone response, Biomaterials 26(17) (2005) 3557-63.

[65] Y.K. Kim, K.B. Lee, S.Y. Kim, K. Bode, Y.S. Jang, T.Y. Kwon, M.H. Jeon, M.H. Lee, Gas formation and biological effects of biodegradable magnesium in a preclinical and clinical observation, Sci Technol Adv Mater 19(1) (2018) 324-335.

[66] J. Kuhlmann, I. Bartsch, E. Willbold, S. Schuchardt, O. Holz, N. Hort, D. Hoche, W.R. Heineman, F. Witte, Fast escape of hydrogen from gas cavities around corroding magnesium implants, Acta Biomater 9(10) (2013) 8714-21.

[67] D. Zhao, A. Brown, T. Wang, S. Yoshizawa, C. Sfeir, W.R. Heineman, In vivo quantification of hydrogen gas concentration in bone marrow surrounding magnesium fracture fixation hardware using an electrochemical hydrogen gas sensor, Acta Biomater 73 (2018) 559-566.

[68] M.E. Maguire, J.A. Cowan, Magnesium chemistry and biochemistry, Biometals 15(3) (2002) 203-10.

[69] N.E. Saris, E. Mervaala, H. Karppanen, J.A. Khawaja, A. Lewenstam, Magnesium. An update on physiological, clinical and analytical aspects, Clin Chim Acta 294(1-2) (2000) 1-26.

[70] A. Hartwig, Role of magnesium in genomic stability, Mutat Res 475(1-2) (2001) 113-21.

[71] B. Heublein, R. Rohde, V. Kaese, M. Niemeyer, W. Hartung, A. Haverich, Biocorrosion of magnesium alloys: a new principle in cardiovascular implant technology?, Heart 89(6) (2003) 651-6.

[72] P. Zartner, R. Cesnjevar, H. Singer, M. Weyand, First successful implantation of a biodegradable metal stent into the left pulmonary artery of a preterm baby, Catheter Cardiovasc Interv 66(4) (2005) 590-4.

[73] R. Erbel, C. Di Mario, J. Bartunek, J. Bonnier, d.B. B, F. Eberli, P. Erne, M. Haude, B. Heublein, M. Horrigan, C. Ilsley, D. Böse, J. Koolen, T. Lüscher, N. Weissman, R. Waksman, Temporary scaffolding of coronary arteries with bioabsorbable magnesium stents: a prospective, non-randomised multicentre trial, Lancet 369(9576) (2007) 1869-1875.

[74] O. Charyeva, O. Dakischew, U. Sommer, C. Heiss, R. Schnettler, K.S. Lips, Biocompatibility of magnesium implants in primary human reaming debris-derived cells stem cells in vitro, J Orthop Traumatol 17(1) (2016) 63-73.

[75] F. Witte, N. Hort, C. Vogt, S. Cohen, K. Kainer, R. Willumeit, F. Feyerabend, Degradable biomaterials based on magnesium corrosion, Current Opinion in Solid State and Materials Science 12(5-6) (2008) 63-72.

[76] J. Walker, S. Shadanbaz, T. Woodfield, M. Staiger, G. Dias, The in vitro and in vivo evaluation of the biocompatibility of Mg alloys Biomedical Materials 2014 (2014) 015006.

[77] S. Mushlin, H. Greene, Hypermagnesemia, Decision Making in Medicine An Algorithmic Approach, Mosby2010, pp. 390-391.

[78] B.P. Zhang, Y. Wang, L. Geng, Research on Mg-Zn-Ca Alloy as Degradable Biomaterial in: R. Pignatello (Ed.), Biomaterials - Physics and Chemistry, InTech2011, pp. 183-204.

[79] R. Radha, D. Sreekanth, Insight of magnesium alloys and composites for orthopedic implant applications – a review, Journal of Magnesium and Alloys 5(3) (2017) 286-312.

[80] N.T. Kirkland, N. Birbilis, J. Walker, T. Woodfield, G.J. Dias, M.P. Staiger, In-vitro dissolution of magnesium-calcium binary alloys: clarifying the unique role of calcium additions in bioresorbable magnesium implant alloys, J Biomed Mater Res B Appl Biomater 95(1) (2010) 91-100.

[81] R. Guan, A. Cipriano, Z. Zhao, J. Lock, D. Tie, T. Zhao, T. Cui, H. Liu, Development and evaluation of a magnesium–zinc–strontium alloy for biomedical applications — Alloy processing, microstructure, mechanical properties, and biodegradation, Materials Science and Engineering: C 33(7) (2013) 3661-3669.

[82] M. Pogorielov, E. Husak, A. Solodivnik, S. Zhdanov, Magnesium-based biodegradable alloys: Degradation, application, and alloying elements, Interv Med Appl Sci 9(1) (2017) 27-38.

[83] G. Song, A. Atrens, Understanding Magnesium Corrosion—A Framework for Improved Alloy Performance, Advanced Engineering Materials 5(12) (2003) 837-858.

[84] O.I. Velikokhatnyi, P.N. Kumta, First-principles studies on alloying and simplified thermodynamic aqueous chemical stability of calcium-, zinc-, aluminum-, yttrium- and iron-doped magnesium alloys, Acta Biomater 6(5) (2010) 1698-704.

[85] D.R. Sumner, Long-term implant fixation and stress-shielding in total hip replacement, J Biomech 48(5) (2015) 797-800.

[86] J. Sawai, H. Kojima, H. Igarashi, A. Hashimoto, S. Shoji, T. Sawaki, A. Hakoda, E. Kawada, T. Kokugan, M. Shimizu, Antibacterial characteristics of magnesium oxide powder, World Journal of Microbiology and Biotechnology 16(2) (2000) 187-194.

[87] D.A. Robinson, R.W. Griffith, D. Shechtman, R.B. Evans, M.G. Conzemius, In vitro antibacterial properties of magnesium metal against Escherichia coli, Pseudomonas aeruginosa and Staphylococcus aureus, Acta Biomater 6(5) (2010) 1869-77.

[88] Y. Li, G. Liu, Z. Zhai, L. Liu, H. Li, K. Yang, L. Tan, P. Wan, X. Liu, Z. Ouyang, Z. Yu, T. Tang, Z. Zhu, X. Qu, K. Dai, Antibacterial properties of magnesium in vitro and in an in vivo model of implant-associated methicillin-resistant Staphylococcus aureus infection, Antimicrob Agents Chemother 58(12) (2014) 7586-91.

[89] W. Jahnen-Dechent, M. Ketteler, Magnesium basics Clin Kidney J 5(Suppl 1) (2012) i3-i14.

[90] R.K. Rude, M.E. Kirchen, H.E. Gruber, M.H. Meyer, J.S. Luck, D.L. Crawford, Magnesium deficiency-induced osteoporosis in the rat: uncoupling of bone formation and bone resorption, Magnes Res 12(4) (1999) 257-67.

[91] M.A. Kenney, H. McCoy, L. Williams, Effects of magnesium deficiency on strength, mass, and composition of rat femur, Calcif Tissue Int 54(1) (1994) 44-9.

[92] R.K. Rude, M.E. Kirchen, H.E. Gruber, A.A. Stasky, M.H. Meyer, Magnesium deficiency induces bone loss in the rat, Miner Electrolyte Metab 24(5) (1998) 314-20.

[93] R. Rude, H. Gruber, L. Wei, A. Frausto, B. Mills, Magnesium deficiency: effect on bone and mineral metabolism in the mouse, Calcif Tissue Int 72 (2003) 32-41.

[94] M. Siti Noor Fazliah, M. Yusuf, T. Abdullah, H. Zuhailawati, Human Mesenchymal Stem Cells Response to Magnesium-based Biomaterials, Procedia Chem. 19 (2016) 75-82.

[95] S. Yoshizawa, A. Brown, A. Barchowsky, C. Sfeir, Magnesium ion stimulation of bone marrow stromal cells enhances osteogenic activity, simulating the effect of magnesium alloy degradation, Acta Biomaterialia 10 (2014) 2834-2842.

[96] L. Wu, F. Feyerabend, A. Schilling, R. Willumeit-Römer, B. Luthringer, Effects of extracellular magnesium extract on the proliferation and differentiation of human osteoblasts and osteoclasts in coculture, Acta Biomaterialia 27 (2015) 294-304.

[97] L. Wu, B.J. Luthringer, F. Feyerabend, A.F. Schilling, R. Willumeit, Effects of extracellular magnesium on the differentiation and function of human osteoclasts, Acta Biomater 10(6) (2014) 2843-54.

[98] C. Janning, E. Willbold, C. Vogt, J. Nellesen, A. Meyer-Lindenberg, H. Windhagen, F. Thorey, F. Witte, Magnesium hydroxide temporarily enhancing osteoblast activity and decreasing the osteoclast number in peri-implant bone remodelling, Acta Biomater 6(5) (2010) 1861-8.

[99] J.M. Diaz-Tocados, C. Herencia, J.M. Martinez-Moreno, A. Montes de Oca, M.E. Rodriguez-Ortiz, N. Vergara, A. Blanco, S. Steppan, Y. Almaden, M. Rodriguez, J.R. Munoz-

Castaneda, Magnesium Chloride promotes Osteogenesis through Notch signaling activation and expansion of Mesenchymal Stem Cells, Sci Rep 7(1) (2017) 7839.

[100] M. Leidi, F. Dellera, M. Mariotti, J. Maier, High magnesium inhibits human osteoblast differentiation in vitro, Magnesium Research 24(1) (2011) 1-6.

[101] W. Lu, E. Pringa, L. Chou, Effect of magnesium on the osteogenesis of normal human osteoblasts, Magnesium Research 30(2) (2017) 42-52.

[102] Y. Li, J. Wang, J. Yue, Y. Wang, C. Yang, Q. Cui, High magnesium prevents matrix vesicle-mediated mineralization in human bone marrow-derived mesenchymal stem cells via mitochondrial pathway and autophagy, Cell Biol Int 42 (2018) 205-215.

[103] A. Montes de Oca, F. Guerrero, J. Martinez-Moreno, J. Madueno, C. Herencia, A. Peralta, Y. Almaden, I. Lopez, E. Aguilera-Tejero, K. Gundlach, J. Buchel, M. Peter, J. Passlick-Deetjen, M. Rodriguez, J. Munoz-Castaneda, Magnesium Inhibits Wnt/b-Catenin Activity and Reverses the Osteogenic Transformation of Vascular Smooth Muscle Cells, PLOS One 9(2) (2014) e89525.

[104] Y. Yu, H. Lu, J. Sun, Long-term in vivo evolution of high-purity Mg screw degradation - Local and systemic effects of Mg degradation products, Acta Biomater 71 (2018) 215-224.

[105] K.F. Farraro, N. Sasaki, S.L. Woo, K.E. Kim, M.M. Tei, A. Speziali, P.J. McMahon, Magnesium ring device to restore function of a transected anterior cruciate ligament in the goat stifle joint, J Orthop Res 34(11) (2016) 2001-2008.

[106] Y. Koo, H.B. Lee, Z. Dong, R. Kotoka, J. Sankar, N. Huang, Y. Yun, The Effects of Static and Dynamic Loading on Biodegradable Magnesium Pins In Vitro and In Vivo, Sci Rep 7(1) (2017) 14710.

[107] C.M. Campos, T. Muramatsu, J. Iqbal, Y.J. Zhang, Y. Onuma, H.M. Garcia-Garcia, M. Haude, P.A. Lemos, B. Warnack, P.W. Serruys, Bioresorbable drug-eluting magnesium-alloy scaffold for treatment of coronary artery disease, Int J Mol Sci 14(12) (2013) 24492-500.

[108] P. Peeters, M. Bosiers, J. Verbist, K. Deloose, B. Heublein, Preliminary results after application of absorbable metal stents in patients with critical limb ischemia, J Endovasc Ther 12(1) (2005) 1-5.

[109] M. Haude, H. Ince, R. Tolg, P.A. Lemos, C. von Birgelen, E.H. Christiansen, W. Wijns, F.J. Neumann, E. Eeckhout, H.M. Garcia-Garcia, R. Waksman, Sustained safety and performance of the second-generation drug-eluting absorbable metal scaffold (DREAMS 2G) in patients with de novo coronary lesions: 3-year clinical results and angiographic findings of the BIOSOLVE-II first-in-man trial, EuroIntervention (2019).

[110] M. Haude, H. Ince, A. Abizaid, R. Toelg, P.A. Lemos, C. von Birgelen, E.H. Christiansen, W. Wijns, F.J. Neumann, C. Kaiser, E. Eeckhout, S.T. Lim, J. Escaned, Y. Onuma, H.M. Garcia-Garcia, R. Waksman, Sustained safety and performance of the second-generation drug-eluting absorbable metal scaffold in patients with de novo coronary lesions: 12-month clinical results and angiographic findings of the BIOSOLVE-II first-in-man trial, Eur Heart J 37(35) (2016) 2701-9.

[111] M. Haude, R. Erbel, P. Erne, S. Verheye, H. Degen, P. Vermeersch, N. Weissman, F. Prati, N. Bruining, R. Waksman, J. Koolen, Safety and performance of the DRug-Eluting Absorbable Metal Scaffold (DREAMS) in patients with de novo coronary lesions: 3-year results of the prospective, multicentre, first-in-man BIOSOLVE-I trial, EuroIntervention 12(2) (2016) e160-6.

[112] M. Haude, R. Erbel, P. Erne, S. Verheye, H. Degen, D. Bose, P. Vermeersch, I. Wijnbergen, N. Weissman, F. Prati, R. Waksman, J. Koolen, Safety and performance of the drug-eluting absorbable metal scaffold (DREAMS) in patients with de-novo coronary lesions: 12 month results of the prospective, multicentre, first-in-man BIOSOLVE-I trial, Lancet 381(9869) (2013) 836-44.

[113] S. Shadanbaz, G.J. Dias, Calcium phosphate coatings on magnesium alloys for biomedical applications: a review, Acta Biomater 8(1) (2012) 20-30.

[114] H. Hornberger, S. Virtanen, A.R. Boccaccini, Biomedical coatings on magnesium alloys - a review, Acta Biomater 8(7) (2012) 2442-55.

[115] P.K. Bowen, J. Drelich, J. Goldman, Magnesium in the murine artery: probing the products of corrosion, Acta Biomater 10(3) (2014) 1475-83.

[116] J.W. Lee, H.S. Han, K.J. Han, J. Park, H. Jeon, M.R. Ok, H.K. Seok, J.P. Ahn, K.E. Lee, D.H. Lee, S.J. Yang, S.Y. Cho, P.R. Cha, H. Kwon, T.H. Nam, J.H. Han, H.J. Rho, K.S. Lee, Y.C. Kim, D. Mantovani, Long-term clinical study and multiscale analysis of in vivo biodegradation mechanism of Mg alloy, Proc Natl Acad Sci U S A 113(3) (2016) 716-21.

[117] M. Badar, H. Lunsdorf, F. Evertz, M.I. Rahim, B. Glasmacher, H. Hauser, P.P. Mueller, The formation of an organic coat and the release of corrosion microparticles from metallic magnesium implants, Acta Biomater 9(7) (2013) 7580-9.

[118] H. Kalb, A. Rzany, B. Hensel, Impact of microgalvanic corrosion on the degradation morphology of WE43 and pure magnesium under exposure to simulated body fluid, Corrosion Science 57 (2012) 122-130.

[119] M. Tomozawa, S. Hiromoto, Microstructure of hydroxyapatite- and octacalcium phosphate-coatings formed on magnesium by a hydrothermal treatment at various pH values, Acta Biomaterialia 59(1) (2011) 355-363.

[120] B. Ratner, A History of Biomaterials, in: B. Ratner, A. Hoffman, J. Lemons (Eds.), Biomaterials Science- An introduction to materials in medicine, Academic Press2013, pp. xli-liii.

[121] J. Shepherd, R. Friederichs, S. Best, Synthetic hydroxyapatite for tissue engineering applications, in: M. Mucalo (Ed.), Hydroxyapatite (HAp) for Biomedical Applications2015, pp. 235-267.

[122] D. Loca, J. Locs, A. Dubnika, V. Zalite, L. Berzina-Cimdina, Porous hydroxyapatite for drug delivery, in: M. Mucalo (Ed.), Hydroxyapatite (HAp) for Biomedical Applications, Woodhead Publishing2015, pp. 189-209.

[123] H. Zhou, J. Lee, Nanoscale hydroxyapatite particles for bone tissue engineering, Acta Biomater 7(7) (2011) 2769-81.

[124] M.M. Villa, L. Wang, J. Huang, D.W. Rowe, M. Wei, Bone tissue engineering with a collagen-hydroxyapatite scaffold and culture expanded bone marrow stromal cells, J Biomed Mater Res B Appl Biomater 103(2) (2015) 243-53.

[125] C. Giachelli, Ectopic Calcification Gathering Hard Facts about Soft Tissue Mineralization, American Journal of Pathology 154(3) (1999) 671-675.

[126] A.S. Black, I.O. Kanat, A review of soft tissue calcifications, J Foot Surg 24(4) (1985) 243-50.

[127] W.C. O'Neill, Treatment of vascular calcification, Kidney Int 74(11) (2008) 1376-8.

[128] W.C. O'Neill, K.A. Lomashvili, Recent progress in the treatment of vascular calcification, Kidney Int 78(12) (2010) 1232-9.

[129] J.A. Leopold, Cellular mechanisms of aortic valve calcification, Circ Cardiovasc Interv 5(4) (2012) 605-14.

[130] E. Theuwissen, E. Smit, C. Vermeer, The role of vitamin K in soft-tissue calcification, Adv Nutr 3(2) (2012) 166-73.

[131] P. Price, M. Urist, Y. Otawara, Matrix Gla Protein, a new gamma-carboxyglutamic acid-containing protein which is associated with the organic matrix of bone, Biochemical and Biophysical Research Communications 117(3) (1983) 765-771.

[132] P.A. Price, J.W. Lothringer, S.K. Nishimoto, Absence of the vitamin K-dependent bone protein in fetal rat mineral. Evidence for another gamma-carboxyglutamic acid-containing component in bone, J Biol Chem 255(7) (1980) 2938-42.

[133] M.L. Cancela, V. Laize, N. Conceicao, Matrix Gla protein and osteocalcin: from gene duplication to neofunctionalization, Arch Biochem Biophys 561 (2014) 56-63.

[134] L.J. Schurgers, J. Uitto, C.P. Reutelingsperger, Vitamin K-dependent carboxylation of matrix Gla-protein: a crucial switch to control ectopic mineralization, Trends Mol Med 19(4) (2013) 217-26.

[135] L.J. Schurgers, H.M. Spronk, J.N. Skepper, T.M. Hackeng, C.M. Shanahan, C. Vermeer, P.L. Weissberg, D. Proudfoot, Post-translational modifications regulate matrix Gla protein function: importance for inhibition of vascular smooth muscle cell calcification, J Thromb Haemost 5(12) (2007) 2503-11.

[136] R. Wallin, D. Cain, S.M. Hutson, D.C. Sane, R. Loeser, Modulation of the binding of matrix Gla protein (MGP) to bone morphogenetic protein-2 (BMP-2), Thromb Haemost 84(6) (2000) 1039-44.

[137] G. Luo, P. Ducy, M.D. McKee, G.J. Pinero, E. Loyer, R.R. Behringer, G. Karsenty, Spontaneous calcification of arteries and cartilage in mice lacking matrix GLA protein, Nature 386(6620) (1997) 78-81.

[138] M. Murshed, T. Schinke, M.D. McKee, G. Karsenty, Extracellular matrix mineralization is regulated locally; different roles of two gla-containing proteins, J Cell Biol 165(5) (2004) 625-30.

[139] P.A. Price, W.S. Chan, D.M. Jolson, M.K. Williamson, The elastic lamellae of devitalized arteries calcify when incubated in serum: evidence for a serum calcification factor, Arterioscler Thromb Vasc Biol 26(5) (2006) 1079-85.

[140] P.A. Price, S.A. Faus, M.K. Williamson, Warfarin causes rapid calcification of the elastic lamellae in rat arteries and heart valves, Arterioscler Thromb Vasc Biol 18(9) (1998) 1400-7.

[141] E. Tantisattamo, K.H. Han, W.C. O'Neill, Increased vascular calcification in patients receiving warfarin, Arterioscler Thromb Vasc Biol 35(1) (2015) 237-42.

[142] P.A. Price, G.R. Thomas, A.W. Pardini, W.F. Figueira, J.M. Caputo, M.K. Williamson, Discovery of a high molecular weight complex of calcium, phosphate, fetuin, and matrix gamma-carboxyglutamic acid protein in the serum of etidronate-treated rats, J Biol Chem 277(6) (2002) 3926-34.

[143] M.J. Shearer, Role of vitamin K and Gla proteins in the pathophysiology of osteoporosis and vascular calcification, Curr Opin Clin Nutr Metab Care 3(6) (2000) 433-8.

[144] J. O'Young, Y. Liao, Y. Xiao, J. Jalkanen, G. Lajoie, M. Karttunen, H.A. Goldberg, G.K. Hunter, Matrix Gla protein inhibits ectopic calcification by a direct interaction with hydroxyapatite crystals, J Am Chem Soc 133(45) (2011) 18406-12.

[145] N. Wajih, T. Borras, W. Xue, S.M. Hutson, R. Wallin, Processing and transport of matrix gamma-carboxyglutamic acid protein and bone morphogenetic protein-2 in cultured human vascular smooth muscle cells: evidence for an uptake mechanism for serum fetuin, J Biol Chem 279(41) (2004) 43052-60.

[146] A. Sweatt, D.C. Sane, S.M. Hutson, R. Wallin, Matrix Gla protein (MGP) and bone morphogenetic protein-2 in aortic calcified lesions of aging rats, J Thromb Haemost 1(1) (2003) 178-85.

[147] K. Mori, M. Emoto, M. Inaba, Fetuin-A: a multifunctional protein, Recent Pat Endocr Metab Immune Drug Discov 5(2) (2011) 124-46.

[148] W. Jahnen-Dechent, T. Schinke, A. Trindl, W. Muller-Esterl, F. Sablitzky, S. Kaiser, M. Blessing, Cloning and targeted deletion of the mouse fetuin gene, J Biol Chem 272(50) (1997) 31496-503.

[149] C. Schafer, A. Heiss, A. Schwarz, R. Westenfeld, M. Ketteler, J. Floege, W. Muller-Esterl, T. Schinke, W. Jahnen-Dechent, The serum protein alpha 2-Heremans-Schmid glycoprotein/fetuin-A is a systemically acting inhibitor of ectopic calcification, J Clin Invest 112(3) (2003) 357-66.

[150] A.M. Dabrowska, J.S. Tarach, B. Wojtysiak-Duma, D. Duma, Fetuin-A (AHSG) and its usefulness in clinical practice. Review of the literature, Biomed Pap Med Fac Univ Palacky Olomouc Czech Repub 159(3) (2015) 352-9.

[151] D.P. Lorant, M. Grujicic, C. Hoebaus, J.M. Brix, F. Hoellerl, G. Schernthaner, R. Koppensteiner, G.H. Schernthaner, Fetuin-A levels are increased in patients with type 2 diabetes and peripheral arterial disease, Diabetes Care 34(1) (2011) 156-61.

[152] A. Song, M. Xu, Y. Bi, Y. Xu, Y. Huang, M. Li, T. Wang, Y. Wu, Y. Liu, X. Li, Y. Chen, W. Wang, G. Ning, Serum fetuin-A associates with type 2 diabetes and insulin resistance in Chinese adults, PLoS One 6(4) (2011) e19228.

[153] Y. Yilmaz, O. Yonal, R. Kurt, F. Ari, A.Y. Oral, C.A. Celikel, S. Korkmaz, E. Ulukaya, O. Ozdogan, N. Imeryuz, E. Avsar, C. Kalayci, Serum fetuin A/alpha2HS-glycoprotein levels in patients with non-alcoholic fatty liver disease: relation with liver fibrosis, Ann Clin Biochem 47(Pt 6) (2010) 549-53.

[154] K. Voros, K. Cseh, L. Kalabay, The role of fetuin-A in cardiovascular diseases, Orv Hetil 155(1) (2014) 16-23.

[155] I.R. Orriss, T.R. Arnett, R.G. Russell, Pyrophosphate: a key inhibitor of mineralisation, Curr Opin Pharmacol 28 (2016) 57-68.

[156] R.G. Russell, L.B. Wadstrom, S. Lindstedt, A.D. Care, S. Bisaz, H. Fleisch, The origin of inorganic pyrophosphate in urine, Clin Sci 37(2) (1969) 419-29.

[157] H. Fleisch, S. Bisaz, Mechanism of calcification: inhibitory role of pyrophosphate, Nature 195 (1962) 911.

[158] H. Fleisch, R.G. Russell, F. Straumann, Effect of pyrophosphate on hydroxyapatite and its implications in calcium homeostasis, Nature 212(5065) (1966) 901-3.

[159] H. Fleisch, J. Maerki, R.G. Russell, Effect of pyrophosphate on dissolution of hydroxyapatite and its possible importance in calcium homeostasis, Proc Soc Exp Biol Med 122(2) (1966) 317-20.

[160] W.C. O'Neill, K.A. Lomashvili, H.H. Malluche, M.C. Faugere, B.L. Riser, Treatment with pyrophosphate inhibits uremic vascular calcification, Kidney Int 79(5) (2011) 512-7.

[161] V.P. Persy, M.D. McKee, Prevention of vascular calcification: is pyrophosphate therapy a solution?, Kidney Int 79(5) (2011) 490-3.

[162] R. Waksman, R. Pakala, P.K. Kuchulakanti, R. Baffour, D. Hellinga, R. Seabron, F.O. Tio, E. Wittchow, S. Hartwig, C. Harder, R. Rohde, B. Heublein, A. Andreae, K.H. Waldmann, A. Haverich, Safety and efficacy of bioabsorbable magnesium alloy stents in porcine coronary arteries, Catheter Cardiovasc Interv 68(4) (2006) 607-17; discussion 618-9.

[163] P.W. Serruys, D. Keane, The bailout stent. Is a friend in need always a friend indeed?, Circulation 88(5 Pt 1) (1993) 2455-7.

[164] G. Majno, I. Joris, From plasma calcium to apatite: some basic rules, Cells, Tissues, and Disease: Principles of General Pathology, Oxford University Press, New York, 2004, pp. 247-249.

[165] H.C. Anderson, Matrix vesicles and calcification, Curr Rheumatol Rep 5(3) (2003) 222-6.

[166] G. Schlieper, L. Schurgers, V. Brandenburg, C. Reutelingsperger, J. Floege, Vascular calcification in chronic kidney disease: an update, Nephrol Dial Transplant 31(1) (2016) 31-9.

[167] H.M. Spronk, B.A. Soute, L.J. Schurgers, J.P. Cleutjens, H.H. Thijssen, J.G. De Mey, C. Vermeer, Matrix Gla protein accumulates at the border of regions of calcification and normal tissue in the media of the arterial vessel wall, Biochem Biophys Res Commun 289(2) (2001) 485-90.

[168] T.M. Hackeng, J. Rosing, H.M. Spronk, C. Vermeer, Total chemical synthesis of human matrix Gla protein, Protein Sci 10(4) (2001) 864-70.

[169] D.L. Coutu, J.H. Wu, A. Monette, G.E. Rivard, M.D. Blostein, J. Galipeau, Periostin, a member of a novel family of vitamin K-dependent proteins, is expressed by mesenchymal stromal cells, J Biol Chem 283(26) (2008) 17991-8001.

[170] Y. Su, Y. Su, W. Zai, G. Li, C. Wen, In Vitro Degradation Behaviors of Manganese-Calcium Phosphate Coatings on an Mg-Ca-Zn Alloy, Scanning 2018 (2018) 6268579.

[171] J.E. Gray-Munro, C. Seguin, M. Strong, Influence of surface modification on the in vitro corrosion rate of magnesium alloy AZ31, J Biomed Mater Res A 91(1) (2009) 221-30.

[172] V. Wagener, S. Virtanen, Protective layer formation on magnesium in cell culture medium, Mater Sci Eng C Mater Biol Appl 63 (2016) 341-51.

[173] I. Johnson, W. Jiang, H. Liu, The Effects of Serum Proteins on Magnesium Alloy Degradation in Vitro, Sci Rep 7(1) (2017) 14335.

[174] A. Patil, O. Jackson, L. Fulton, D. Hong, P. Desai, S. Kelleher, D. Chou, S. Tan, P. Kumta, E. Beniash, Anticorrosive Self-Assembled Hybrid Alkylsilane Coatings for Resorbable Magnesium Metal Devices, ACS Biomaterials Science & Engineering 3(4) (2017) 518-529.

[175] A. Patil, S.H. Zaky, R. Chong, K. Verdelis, E. Beniash, In vivo study of self-assembled alkylsilane coated degradable magnesium devices, J Biomed Mater Res B Appl Biomater 107(2) (2019) 342-351.

[176] C. Helary, A. Abed, G. Mosser, L. Louedec, A. Meddahi-Pelle, M.M. Giraud-Guille, Synthesis and in vivo integration of improved concentrated collagen hydrogels, J Tissue Eng Regen Med 5(3) (2011) 248-52.

[177] S. Ramanujan, A. Pluen, T.D. McKee, E.B. Brown, Y. Boucher, R.K. Jain, Diffusion and convection in collagen gels: implications for transport in the tumor interstitium, Biophys J 83(3) (2002) 1650-60.

[178] B. Stevens, Y. Yang, A. Mohandas, B. Stucker, K. Nguyen, A review of materials, fabrication methods, and strategies used to enhance bone regeneration in engineered bone tissues, J Biomed Mater Res B Appl Biomater 85(2) (2008) 573–582.

[179] M.P. Staiger, A.M. Pietak, J. Huadmai, G. Dias, Magnesium and its alloys as orthopedic biomaterials: A review, Biomaterials 27(9) (2006) 1728-1734.

[180] A. Corces, M. Poduvalm, Metallic Alloys, 2018.

[181] M. Ball, I. Bonzani, M. Bovis, A. Williams, M. Stevens, Human periosteum is a source of cells for orthopaedic tissue engineering: A pilot study, Clin Orthop Relat Res 469 (2011) 3085-3093.

[182] J. Dwek, The periosteum: what is it, where is it, and what mimics it in its absence?, Skeletal Radiol 39 (2010) 319-323.

[183] J. Lu, X. Wang, C. Marin-Muller, C. Chen, Current advances in research and clinical applications of PLGA-based nanotechnology, Expert Rev Mol Diagn 9(4) (2009) 325-341.

[184] P. Gentile, V. Chiono, I. Carmagnola, P. Hatton, An overview of poly (lactic-co-glycolic) acid (PLGA)-based biomaterials for bone tissue engineering, Int J Mol Sci 15(3) (2014) 3640-3659.

[185] N. Bhardwaj, S. Kundu, Electrospinning: a fascinating fiber fabrication technique, Biotechnol Adv 28(3) (2010) 325-347.

[186] A. Sadeghi-Avalshahr, S. Nokhasteh, A. Molavi, M. Khorsand-Ghayeni, M. Mahdavi-Shahri, Synthesis and characterization of collagen/PLGA biodegradable skin scaffold fibers, Regen. Biomater. 4(5) (2017) 309-314.

[187] Y. Chen, S. Ye, H. Sato, Y. Zhu, V. Shanov, T. Tiasha, A. D'Amore, S. Luketich, G. Wan, W. Wagner, Hybrid scaffolds of Mg alloy mesh reinforced polymer / extracellular matrix composite for critical-sized calvarial defect reconstruction, J Tissue Eng Regen Med. 12(6) (2018) 1374-1388.

[188] C.S. Lin, Z.C. Xin, J. Dai, T.F. Lue, Commonly used mesenchymal stem cell markers and tracking labels: Limitations and challenges, Histol Histopathol 28(9) (2013) 1109-16.

[189] M. Dominici, K. Le Blanc, I. Mueller, I. Slaper-Cortenbach, F. Marini, D. Krause, R. Deans, A. Keating, D. Prockop, E. Horwitz, Minimal criteria for defining multipotent mesenchymal stromal cells. The International Society for Cellular Therapy position statement, Cytotherapy 8(4) (2006) 315-7.

[190] Y.K. Kim, H. Nakata, M. Yamamoto, M. Miyasaka, S. Kasugai, S. Kuroda, Osteogenic Potential of Mouse Periosteum-Derived Cells Sorted for CD90 In Vitro and In Vivo, Stem Cells Transl Med 5(2) (2016) 227-34.

[191] A. Patel, D. Taylor, C. Bartlett, T. Ichim, Mesenchymal Stem Cells, in: E. Perin, L. Miller, J. Willerson (Eds.), Stem Cell and Gene Therapy for Cardiovascular Disease, Academic Press2015, pp. 139-150.

[192] O. Duchamp de Lageneste, A. Julien, R. Abou-Khalil, G. Frangi, C. Carvalho, N. Cagnard, C. Cordier, S.J. Conway, C. Colnot, Periosteum contains skeletal stem cells with high bone regenerative potential controlled by Periostin, Nat Commun 9(1) (2018) 773.

[193] E. Golub, K. Boesze-Battaglia, The role of alkaline phosphatase in mineralization, Current Opinion in Orthopaedics 18(5) (2007) 444-448.

[194] A. Rutkovskiy, K. Stensløkken, I. Vaage, Osteoblast Differentiation at a Glance, Med Sci Monit Basic Res 22 (2016) 95-106.

[195] M. Bruderer, R.G. Richards, M. Alini, M.J. Stoddart, ROLE AND REGULATION OF RUNX2 IN OSTEOGENESIS, European Cells and Materials 28 (2014) 269-286.

[196] Y. Nishio, Y. Dong, M. Paris, R.J. O'Keefe, E.M. Schwarz, H. Drissi, Runx2-mediated regulation of the zinc finger Osterix/Sp7 gene, Gene 372 (2006) 62-70.

[197] K. Nakashima, X. Zhou, G. Kunkel, Z. Zhang, J. Deng, R. Behringer, B. de Crombrugghe, The novel zinc finger-containing transcription factor osterix is required for osteoblast differentiation and bone formation, Cell 108(1) (2002) 17-29.

[198] L. Malaval, D. Modrowski, A. Gupta, J. Aubin, Cellular expression of bone-related proteins during in vitro osteogenesis in rat bone marrow stromal cell cultures, Journal of Cellular Physiology 158(3) (1994) 555-572.

[199] L. Wang, X. Shi, R. Zhao, B.P. Halloran, D.J. Clark, C.R. Jacobs, W.S. Kingery, Calcitonin-gene-related peptide stimulates stromal cell osteogenic differentiation and inhibits RANKL induced NF-kappaB activation, osteoclastogenesis and bone resorption, Bone 46(5) (2010) 1369-79.

[200] X. Yu, S. Liu, H. Chen, X. Zhao, X. Chen, Y. Du, S. Li, CGRP gene-modified rBMSCs show better osteogenic differentiation capacity in vitro, J Mol Histol 49(4) (2018) 357-367.

[201] G. Karsenty, Minireview: Transcriptional Control of Osteoblast Differentiation, Endocrinology 142(7) (2001) 2731-2733.

[202] T. Komori, H. Yagi, S. Nomura, A. Yamaguchi, K. Sasaki, K. Deguchi, Y. Shimizu, R. Bronson, Y.-H. Gao, M. Inada, M. Sato, R. Okamoto, Y. Kitamura, S. Yoshiki, T. Kishimoto, Targeted Disruption of Cbfa1Results in a Complete Lack of Bone Formation owing to Maturational Arrest of Osteoblasts, Cell 89(5) (1997) 755-764.

[203] W. Tang, Y. Li, L. Osimiri, C. Zhang, Osteoblast-specific Transcription Factor Osterix (Osx) Is an Upstream Regulator of Satb2 during Bone Formation, The Journal of Biological Chemistry 286(38) (2011) 32995-33002.

[204] P. Bianco, L. Fisher, M. Young, J. Termine, P. Robey, Expression of bone sialoprotein (BSP) in developing human tissues, Calcif Tissue Int. 49(6) (1991) 421-426.

[205] M. Köllmer, J. Buhrman, Y. Zhang, R. Gemeinhart, Markers Are Shared Between Adipogenic and Osteogenic Differentiated Mesenchymal Stem Cells, J Dev Biol Tissue Eng 5(2) (2013) 18-25.

[206] T. Wang, X. Zhang, D.D. Bikle, Osteogenic Differentiation of Periosteal Cells During Fracture Healing, J Cell Physiol 232(5) (2017) 913-921.

[207] C. Colnot, X. Zhang, M.L. Knothe Tate, Current insights on the regenerative potential of the periosteum: molecular, cellular, and endogenous engineering approaches, J Orthop Res 30(12) (2012) 1869-78.

[208] M. Mehta, G.N. Duda, C. Perka, P. Strube, Influence of gender and fixation stability on bone defect healing in middle-aged rats: a pilot study, Clin Orthop Relat Res 469(11) (2011) 3102-10.

[209] U. Bilkay, C. Tokat, E. Helvaci, C. Ozek, O. Zekioglu, T. Onat, E. Songur, Osteogenic Capacities of Tibial and Cranial Periosteum: A Biochemical and Histologic Study, The Journal of Craniofacial Surgery 19(2) (2008) 453-458.